공학박사 학위논문

Microfluidic Platform for Quantitative Characterization of Biodiesel Formation in Microalgae

미세조류 내 바이오디젤 생산을 정량화하는

미세유체 플랫폼 개발

2015 년 2 월

서울대학교 대학원

기계항공공학부

박 재 우

Microfluidic Platform for Quantitative Characterization of Biodiesel Formation in Microalgae

지도 교수 전 누 리

이 논문을 공학박사 학위논문으로 제출함
2015 년 2 월

서울대학교 대학원
기계항공공학부
박 재 우

박재우의 박사 학위논문을 인준함
2015 년 2 월

위 원 장 김 호 영 (인)

부위원장 전 누 리 (인)

위 원 김 도 년 (인)

위 원 김 성 제 (인)

위 원 진 언 선 (인)

Abstract

Microfluidic Platform for Quantitative Characterization of Biodiesel Formation in Microalgae

Park, Jae Woo

School of Mechanical and Aerospace Engineering

The Graduate School

Seoul National University

Microfluidics always has been appealed to biologist because of the capability to control the cellular microenvironment in both a spatial and temporal manner. These system can generate a biological relevant stimulus including concentration gradient, nutrient conditions and physical and chemical stresses by taking advantage of basic characteristics of laminar flow and diffusion. Moreover, microfluidic techniques have been presented a novel paradigm for screening system with their small volume fractions and high-throughputs. Unfortunately, there are several considerable things for applying microalgae to microfluidic system. This research presents microalgae research into microfluidic platform by offering each solutions at every limiting steps. First, quantification of lipid droplet (LD) which is one of the major product of carbon conversion in microalgae is required for developing and optimizing microalgal bioprocess engineering. This report describes new fluorescence probes for LDs staining; Seoul-Fluor (SF) and JC-1 (5,5′,6,6′-Tetrachloro-1,1′,3,3′-tetraethyl-imidacarbocyanine iodide). We validated that lipophilic

fluorescence probe has a specific interaction with LDs and optimized staining conditions with each probes *via* systematic variations of physicochemical conditions. A protocol for quantitative measurement of accumulation kinetics of LDs in *Chlamydomonas reinhardtii* was developed using spectrofluorimeter and the accuracy of LD size measurement was confirmed by transmission electronmicroscopy (TEM). Second, unlike mammalian cells, investigation of microalgae in microfluidic system has been limited due to their small size and motility. Here, we present a simple surface immobilization method using gelatin coating as the "biological glue". We have continuously monitored single microalgal cells for up to 6 days. Surface immobilization allowed high-resolution, live-cell imaging of mitotic process in real time-which followed previously reported stages in mitosis and LDs accumulation of suspension cultured cells. Third, PDMS (polydimethylsiloxane), which is the main component of microfluidic system, is hard to observe and manipulate cellular behavior with adsorption of hydrophobic fluorescence probes. Here, we present a new simple method for preventing unwanted hydrophobic absorption on PDMS device using Teflon coating.

Throughout the clearing considered issues, we suggested a novel paradigm, never discussed, which could guarantee the most promising method for achieving economics of biodiesel. Based on miniaturized continuous culture system, we could generate various combinations of carbon and nitrogen source for measuring single cell behavior. This result indicate that single cell behavior under continuous culture system did not show similar result of conventional flask culture system. Throughput the result, cell size were affected by nitrogen concentration as well as intracellular lipid content were maximized by half deprivation of nitrogen. Especially, in mass (or continuous) culture system, it would be better to reduce only half of nitrogen source by considering economics of biodiesel. We hope that the applications of developed microfluidic platform become a useful tool for biodiesel research as well as

system biology by helping high-throughput screening and biological relevant stimulus.

This thesis also describes a new method for enhancing microalgal growth and intracellular lipid accumulation using vibration. As we previously mentioned, conventional microaglal biodiesel researches are only focused on the nutrient starvation that activates biosynthesis of lipid formation. However, these approaches slow down microalgal growth and development. Although these unfavorable conditions lead high lipid productivity at single cell level, their low growth rate are a major bottleneck considering commercial biodiesel production in the point of view at whole culture system. Due to this reason, we represent new concept for improving economics of biodiesel by realizing high growth rate and lipid productivity.

Chlamydomonas reinhardtii were treated in the presence of various frequencies under mechanical vibrations and sounds. Mechanical vibration enhanced proliferation and we assumed that the cell displacement is the crucial factor for maximizing growth and development. The most interest thing is mechanical vibration boosts proliferation *via* enhanced carbon conversion ability. Although mechanical vibration system cause stress on photosynthetic system, all frequencies enhances growth yield. In cases of sound, except for 1000 Hz, all frequencies boosts proliferation as well as lipid production. Our results presented here confirmed that vibration can be a new method not only for boosting intracellular lipid formation but also for enhancing cell proliferation in normal condition. We hope that these properties could be an applicable condition for algal cultivation during biodiesel production.

Keywords: Microalgae, Biodiesel, Microfluidics, High-throughput Screening, μ-chemostat, vibration
Student Number: 2009-31246

Contents

Chapter 1 Introduction 1

1.1 Microalgae as an alternative energy source 1
1.1.1 Recent energy crisis and global warming 1
1.1.2 Microalgae as a solution for current issues 2
1.2 Microfluidics for microalgal research 4
1.2.1 Issues on microalgae into microfluidics 4

Chapter 2 Quantitative measurement of lipid droplets with fluorescnce probe 8

2.1 Introduction 8
2.2 Materials and methods 11
2.2.1 Materials 11
2.2.2 Culture conditions 12
2.2.3 Visualization of LDs in *C. reinhardtii* 12
2.2.4 Optimization of SF44 and JC-1 staining 13
2.2.5 Viability assay 14
2.2.6 Liposome concentration measurement 14
2.2.7 Determination of LDs contents 15
2.2.8 LDs purification and size measurement 15
2.3 Results 16
2.3.1 Optimization of SF44 staining for microalgae 16
2.3.2 Quantification of lipid contents using SF44 21
2.3.3 Kinetics measurement of intracellular LDs using SF44 23
2.3.4 Optimization of JC-1 staining for microalgae 27
2.3.5 Quantification of lipid contents using JC-1 31
2.3.6 Kinetics measurement of intracellular LDs using JC-1 33

2.4 Conclusions 35

Chapter 3 Immobilization of microalgae 39

3.1 Introduction 39
3.2 Materials and methods 40
3.2.1 Materials 40
3.2.2 Culture conditions 40
3.2.3 Microfluidic device fabrication 41
3.2.4 Surface immobilization optimization 41
3.2.5 Patterned substrate preparation 42
3.2.6 Viability assay 42
3.2.7 Wall shear stress induced detachment assay 44
3.2.8 Live cell imaging of *C. reinhardtii* mitosis 44
3.2.9 Imaging and quantification of lipid accumulation in *C. reinhardtii* as single cell level 45
3.3 Results 45
3.3.1 Surface immobilization of *C. reinhardtii* using gelatin 46
3.3.2 Validation for microfluidic application 52
3.3.3 Live cell imaging of *C. reinhardtii* mitosis and lipid accumulation 55
3.4 Conclusions 60

Chapter 4 Preventing small hydrophobic molecule absorption on PDMS microchannel 63

4.1 Introduction 63
4.2 Materials and methods 64
4.2.1 Materials 64
4.2.2 Microfluidic device fabrication 65
4.2.3 Teflon coating method 65

4.2.4 Visualization of hydrophobic molecule absorption on PDMS microchannels 65
4.2.5 Measurement of gas permeability 67
3.2.6 Transparency measurement of PDMS 67
4.3 Results 68
4.3.1 PDMS microchannel that resist hydrophobic molecule absorption 68
4.3.2 Characteristics of Teflon coated PDMS microchannel 70
4.3.3 Cell imaging of *C. reinhardtii* on Teflon coated-PDMS microchannel 74
4.4 Conclusions 76

Chapter 5 Quantitative measurement of *Chlamydomonas reinhardtii* on gradient generation system 80
5.1 Introduction 80
5.2 Materials and methods 82
5.2.1 Materials 82
5.2.2 Culture conditions 83
5.2.3 Microfluidic device fabrication 83
5.2.4 Gradient generation with flow system 84
5.2.5 Visualization and quantification of *C. reinhardtii* 84
5.3 Results 85
5.3.1 Device design and validation for gradient generation 86
5.3.2 Carbon source dependent quantitative measurement 88
5.3.3 Nitrogen source dependent quantitative measurement 93
5.3.4 Combinations of carbon and nitrogen sources dependent quantitative measurement 95
5.4 Conclusions 97

Chapter 6 Effect of mechanical vibration and sound on *Chlamydomonas reinhardtii* 100
6.1 Introduction 100
6.2 Materials and methods 101
6.2.1 Materials 101
6.2.2 Culture conditions 101
6.2.3 Mechanical vibration generation system 101
6.2.4 Sound generation system 102
6.2.5 Measurement of growth for solid culture system 102
6.2.6 Measurement of growth kinetics for liquid culture system 102
6.2.7 F_v/F_m measurement 103
6.2.8 Measurement of intracellular lipid contents 103
6.3 Results 103
6.3.1 Mechanical vibration generation 103
6.3.2 Mechanical vibration effect on microlagal proliferation 106
6.3.3 Sound generation 110
6.3.4 Sound effect on microalgal proliferation and development 113
6.4 Conclusions 121
Chapter 7 Concluding remarks 123
Bibliography 127
Abstract 138

List of Figures

Figure 2.1 Schematic diagram of SF44 9
Figure 2.2 Schematic diagram of JC-1 10
Figure 2.3 Staining condition for SF44 18
Figure 2.4 Viability of *C. reinhardtii* with SF44 20
Figure 2.5 Micrograph of *C. reinhardtii* with SF44 22
Figure 2.6 Fluorescence characteristics of SF44 24
Figure 2.7 SF44 fluorescence intensity with PC liposome... 25
Figure 2.8 Accumulation kinetics of LD with SF44 26
Figure 2.9 Accumulation kinetics of LD with TEM..... 28
Figure 2.10 Accumulation kinetics of LD..... 29
Figure 2.11 Staining condition for JC-1..... 30
Figure 2.12 JC-1 fluorescence intensity with PC liposome. 32
Figure 2.13 Accumulation kinetic of LD with JC-1..... 34
Figure 2.14 Dual emission spectra of JC-1 36
Figure 3.1 Schematic diagram of gelatin coating process 43
Figure 3.2 Schematic diagram of gelatin coating..... 47
Figure 3.3 Optimized condition for gelatin coating 49
Figure 3.4 Effects of *C. reinhardtii* immobilization 50
Figure 3.5 Viability of *C. reinhardtiii* with immobilization . 53
Figure 3.6 Effect of shear stress..... 54
Figure 3.7 Singel cell time-lapse image for motosis 56

Figure 3.8 Time-lapse image and kinetics for intracellular lipid accumulation 58
Figure 4.1 Schematic diagram of Teflon coating process..... 66
Figure 4.2 Fluorescence profiles of PDMS with rhodamine 69
Figure 4.3 Fluorescence profiles of PDMS with BODIPY .. 71
Figure 4.4 Gas permeability of Teflon-coated PDMS 73
Figure 4.5 Transparency of Teflon-coated PDMS 75
Figure 4.6 Micrograph of *C. reinhardtii* 77
Figure 5.1 Microfluidic device 87
Figure 5.2 Validation for gradient generation..... 89
Figure 5.3 CFD result for split junction..... 90
Figure 5.4 Carbon dependent single cell measurement..... 92
Figure 5.5 Nitrogen dependent singel cell measurement 94
Figure 5.6 Carbon and nitrogen combination dependent single cell measurement..... 96
Figure 6.1 Mechanical vibration system and their acceleration profile 105
Figure 6.2 Mechanical vibration effect on *C. reinhardtii* ... 107
Figure 6.3 Displacement of cells on agar plate..... 109
Figure 6.4 Mechanical vibration effect on *C. reinhardtii* with minimal media.....111
Figure 6.5 F_v/F_m measurement..... 112

Figure 6.6 Sound system and their wave 114
Figure 6.7 Sound effect on *C. reinhardtii* 115
Figure 6.8 Displacement of cells on agar plate under sound system..... 117
Figure 6.9 Growth kinetics of *C. reinhardtii* 118
Figure 6.10 Quantitative measurement of lipid contents ... 120

Chapter 1. Introduction

1.1 Microalgae as an alternative energy source

1.1.1 Recent energy crisis and global warming

Since the industrial revolution, *Homo sapiens* have experienced an explosive growth of world population and global economy. These developments are based on energy consumption, which was increased more than 20-fold since the industrial revolution. [1] Among various sources of energy, petroleum-based fossil fuels have been used as a driving force for development of global economy. However, due to the increase of energy demand, the world is facing a risk of energy security. Especially, proven reserves of conventional oil are estimated remaining in the range of 40 to 45 years based on current consumption level. [2] Many governments, belonging in OECD, recognize this problem and try to reduce or maintain their energy consumption. [3] However, over the past years, economically emerged countries (especially, China and India) saw the world`s biggest increase in energy consumption with their rapid economic growth. Moreover, since 2008, non-OECD countries` energy consumption quantity was over OECD countries` and predicted doubled within 20 years based on current increasing rate. [2] Energy consumption also caused severe problems; global warming and climate change. There are numerous evidences global warming and climate change

caused by greenhouse gas emissions, especially CO_2. [4] CO_2 is a major byproduct from combustion of fossil fuels. Growth in CO_2 in the atmosphere has seen same trend with growth in fossil fuel consumption. It has been predicted that significant changes in climate leaded from anthropogenic CO_2 emission to atmosphere. [5] Over that past several decades, *Homo sapiens* already has been experienced the effects of climate change such as Arctic and Antarctic ice loss, sea level elevation and increased precipitation and warmth. Throughout these situation, numerous governmental and industrial efforts has been focused on reducing energy consumption through exploring alternative energy sources that are renewable and carbon neutral. [6]

1.1.2 Microalgae as a solution for current issues

Homo sapiens have tried to find solutions for alternative energy resources which satisfy renewable and carbon neutral. The first generation resources come from nature, such as hydropower, geothermal, wind, tide and sunlight. They only replaced limited fossil fuels` conventional usage such as electric generation and heating. [7] The limitations of the first generation resource is hard to replace transportable fuel, oil. This means that the first generation resources only take a role except for 25.92 % of energy demand. Nevertheless, many researchers have developed hybrid system based on the electrical energy storage technology such as lithium-ion battery to supplement internal combustion engine. [8] However, on the view of energy density, current battery storage is much smaller than liquid fuels by two orders of magnitude.

[9] Due to this reason, there needs to develop second generation alternative resources to directly replace transportable liquid fuels. Biodiesel, derived from crops including corn, soybean, canola, coconut and palm oils, is the most powerful candidate for alternative energy resources, as a transportable fuels. [10] They satisfied requirements as an alternative energy source; renewable, carbon neutral and transportable fuel. However, they cannot serve a promising replacement with their technological and ethical problems. Biodiesel derived from crops cannot entirely replace petroleum as transport fuels due to their relatively low oil yield (L/ha). [6] Moreover, main material, crops, with distorted agricultural market causes world food problem, especially famine in the Third world. [11]

Microalgae has been discussed as another alternative source of biodiesel for over 50 years. [12] Microalgae convert CO_2 and solar energy into biofuel[13-17], food[18], feed[19] and high-valuable molecules[20-25]. Compared with traditional crops, oil yield from microalgae can be up to 10^3 to 10^4 time higher. [6] In addition, microalgae can grow rapidly and require only 1 to 10 % of the cultivation area needed for most crops. Generally, the oil content of microalgae is 20 to 50 % by weight of dry biomass. [6] Moreover, microalgae is free from ethical problem. Biodiesel consist of mono-alkyl esters that are formed from triglycerides *via* transesterification. [26] In microalgae, triglycerides (TG) form lipid droplets (LDs), an intracellular organelle containing neutral lipids surrounded by a glycol- and phospho- lipid monolayer that are used for storing food energy. [27] Compared with crops, microalgae is promising renewable energy resource, but there still have considerable point,

economical problem. If biodiesel derived from microalgae can potentially replace liquid fuel, the price of biodiesel should be related to the price of crude oil, as follows:

$$\boldsymbol{C}_{\text{biodiesel}} = 6.9 \times 10^{-3}\, \boldsymbol{C}_{\text{petroleum}}$$

where $\boldsymbol{C}_{\text{biodiesel}}$ ($ per liter) is the price of biodiesel and $\boldsymbol{C}_{\text{petroleum}}$ is the price of crude oil ($ per barrel). [6] To improving economics of biodiesel from microalgae, there need to reduce cost of producing microalgal biodiesel by enhancing bio-refinery and photobioreactor process engineering and improving capabilities of microalgal biology. Especially, microalgal biology strategy can be used to potentially:

1. Increase photosynthetic efficiency
2. Enhance biomass growth rate
3. Increase oil content in biomass
4. Improve temperature tolerance
5. Reduce photo-inhibition and photo-oxidation
6. Identify biochemical and environmental trigger for LDs

1.2 Microfluidics for microalgal research

1.2.1 Issues on microalgae into microfluidics

Microfluidics-based experimental methods always have been appealed to biologist because of the capability to control the cellular microenvironment

in both spatial and temporal manner. Microfluidic-based experimental methods have expanded our knowledge of various microorganisms by offering well-controlled microenvironmental experimental conditions that could not be produced with conventional macroscale methods. [28] For example, yeast is a relevant biological system for investigating gene expression at the single cell level due to their rapid growth. Initially, applications of yeast into microfluidics were limited with their non-adherent characteristics. Moreover, continuous tracking of single cell is problematic for high-resolution microscopic imaging. Many researchers have tried to find solution for yeast applications into microfluidics, so they finally realize the applications of microfluidic platform to yeast based on the Tesla valve[29], trapping[30, 31] and immobilization[32, 33].

Similar to yeast, microalgae have non-adherent property, which limits microfluidic applications. Moreover, motile microalgae respond to light stimuli also known as phototaxis. [34] Due to their small size and motility, it is hard to capture on conventional physically modified microstructures as well as track single cellular behavior with conventional microscopic system. Given these properties, long-term continuous monitoring under different culture conditions has not been possible. Several approach have been explored to capture microalgae, micropillar-based cell trap [35] was successfully used to culture *Botryococcus braunii*. Cells trapped in a single device were exposed to different light conditions to examine their effect on biomass formation. However, *B. braunii* cells were captured at a single-colony resolution (> 50 μm, not as single-cell, cells). This system cannot be applied to other microalgal species

such as *Chlamydomonas reinhardtii*, most widely studied model microalgae whose genome is fully sequenced and annotated[36], as the vegetative cells of *C. reinhardtii* are much smaller in size (< 10 μm) and highly motile with two apical flagella. Digital microfluidics have been used study *C. reinhardtii* in droplets[37, 38] and microcapsules[39]. Unfortunately, *C. reinhardtii* move freely inside the droplets and microcapsule, making them difficult to image at single-cell level using high magnification objectives for observing single cell behavior and lipid droplet formation.

Microalgal lipid droplet (LDs) is typically used for precursor of commercially available biodiesel. Triglyceride (TG), major component of hydrophobic core of LDs, is converted into fatty acid methyl ester (FAME; biodiesel) *via* transesterification with methanol. [40] Therefore, measuring content of LDs is the important part for development of microalgal bioprocess engineering. The conventional LDs quantification methods have been developed in different ways; analytical instrument and fluorescence probe based detection. Analytical instruments including high pressure liquid chromatography (HPLC) and gas chromatography (GC) serve to identify quantity as well as quality of biodiesel. [41, 42] Recently, due to the development of microfluidics-based experiments, the concept of high-throughput screening (HTS) has been emerged to reduce time- and labor-intensive process of biodiesel process engineering. As a result, many researchers realized in situ measurement of lipid contents through fluorescence probes such as Nile Red[43] and BODIPY[44]. These probes have continuously been reported to enhance applications of HTS system.

However, most of the probes have a hydrophobic property, so it is easy to absorb or penetrate into PDMS (polydimethylsiloxane), which is the main component of microfluidic system. Due to the high permeability and hydrophobicity of PDMS[45], it is hard to observe and manipulate single cellular behavior with their unwanted absorption.

By considering current issues, previously presented, microalgae research using microfluidic platform should be proceeded by offering each solutions at every limiting steps; fluorescence probe, immobilization and absorption.

Chapter 2. Quantitative Measurement of Lipid Droplets with Fluorescence Probe

2.1 Introduction

For the biodiesel production through microalgae, there are some considerable factors containing technological and economic analysis. Quantification of LDs is one of the considerable factor for developing and optimizing bioprocess engineering. Due to the recent development of fluorescence probes, fluorescence based detection techniques were opened a new methodology for realizing time- and labor-free works; high-throughput screening (HTS). This chapter describes a new LD-specific fluorescence probe; SF44 (9-Aryl-1,2-dihydropyrrolo[3,4-*b*]indolizin-3-one) and JC-1 (5,5´,6,6´-Tetrachloro-1,1´,3,3´-tetraethyl-imidacarbocyanine iodide).

SF44 has a tunable and predictable fluorescence core skeleton. (Figure 2.1) SF44 and various analogues containing electron-donating amine moieties have been introduced as a LD-specific fluorescence probes in mammalian cells[46] and microorganisms[47]. SF44 has been successfully applied to the specific measurement of LD organelles using its fluorogenic properties under unique hydrophobic environment of LDs in cytosols. [46]

JC-1 is well-known probe for detecting early stage of apoptosis by measuring mitochondrial membrane potential.[48, 49] When excited at 490 nm, JC-1 emits green and red fluorescence at 540 nm and 600 nm, respectively.

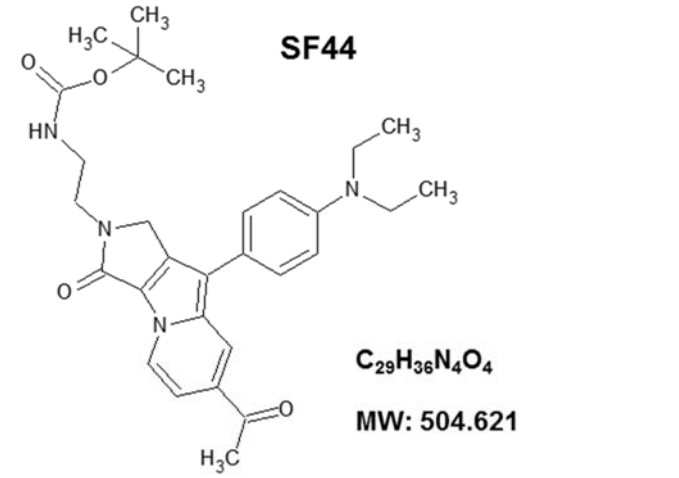

Figure 2.1. A schematic diagram showing the chemical structure of SF44. LDs and liposome specific fluorescence intensity was monitored at 540 nm with excitation at 450 nm.

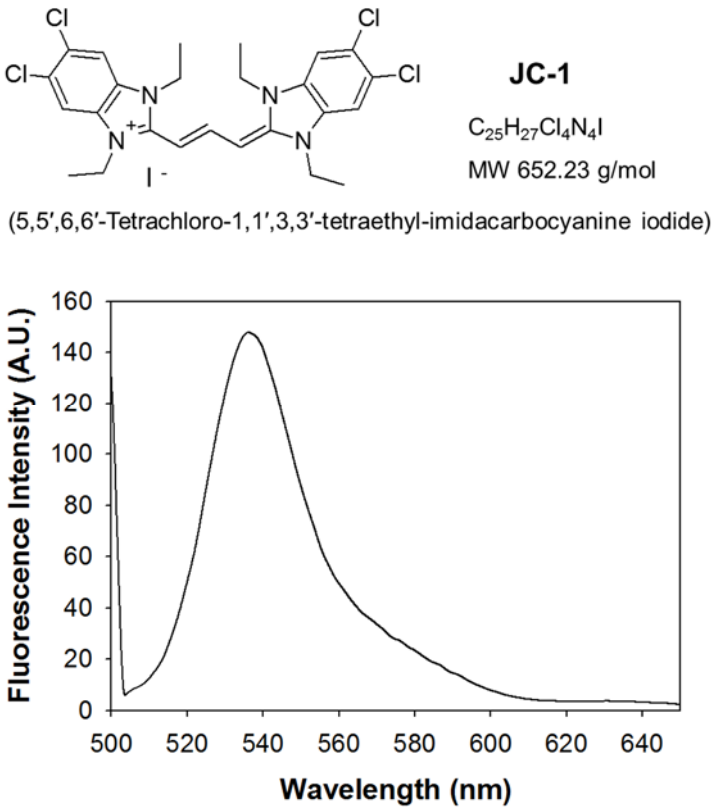

Figure 2.2. A schematic diagram showing the chemical structure of JC-1. LDs and liposome specific fluorescence intensity was monitored at 535 nm with excitation at 490 nm.

(Figure 2.2) Those of dual fluorescence properties were applicable to various physico-chemical phenomena including live cell assay and protein dynamics. [50] In the presence of artificial liposome, JC-1 emits only green fluorescence at 535 nm. It seems that monomers of JC-1 were clearly intercalated into lipids structures instead of forming J-aggregates which emits red fluorescence at 600 nm.

This chapter describes the demonstration of staining conditions using SF44 and JC-1 with *Chlamydomonas reinhardtii* (a species of microalgae widely used as a model organism). The optimized protocol is a sensitive and quantitative method for HTS of intracellular lipid accumulations of microalgae for biodiesel research.

2.2 Materials and methods

2.2.1 Materials

Chlamydomonas reinhardtii (CC-503; *cw92 mt+*) was purchased from the *Chlamydomonas* Resource Center at the University of Minnesota (St. Paul, MN, USA). SF44 was synthesized as described in a previous report[46] and provided by Prof. *Seung Bum Park*'s group (Department of Chemistry, SNU). JC-1 was purchased from Sigma-Aldrich Co. (St. Louis, MO, USA). EZ-Cytox kits were purchased from DoGen (Seoul, Korea). Other chemicals and reagents used in this study were purchased by Sigma-Aldrich Co. (St. Louis, MO, USA)

unless otherwise noted.

2.2.2 Culture conditions

C. reinhardtii in tris acetate phosphate (TAP) medium were cultured at 23 °C and 5% CO_2 while shaking on an orbital shaker at 125 rpm. The cultures were exposed to 12 h cycles of light (40 μmol/s/m^2) and dark. When the optical density (OD) of the culture (measured at 680 nm) was approximately 1.0 (early stationary phase), the cells were precipitated by centrifugation (1500 rpm, 3 min) in a test tube. After removal of the supernatant by vacuum aspiration, the pellet was re-suspended with TAP without a nitrogen source to induce accumulation of the LDs.

2.2.3 Visualization of LDs in *C. reinhardtii*

C. reinhardtii cells were washed with phosphate buffered saline (PBS) twice by centrifugation (1500 rpm, 3 min) and treated with probes. Cells were observed with an Olympus FV1000 confocal laser scanning microscope (Olympus, Tokyo, Japan) equipped with a multiline Ar laser (488 nm). The incubation chamber set was to 23 °C, 5 % CO_2. Micrographs were acquired with a ×60 oil objective and an appropriate excitation and emission filter set. Acquired fluorescence micrographs were processed with the Image software (NIH, Bethesda, MD, USA).

2.2.4 Optimization of SF44 and JC-1 staining

In cases of SF44, dye concentration, staining time, temperature, and pH were optimized. *C. reinhardtii* samples (198 μL, 2.4 × 10^6 cells/mL) were introduced into a test tube and treated with 2 μL of SF44 stock solution. Final concentrations of SF44 were 1 μM, 5 μM, and 50 μM. Test tubes were vortexed and incubated at 25 °C for 25 min. Microalgae cells were stained with 5 μM of SF44 in solutions of 2 % (*v/v*) DMSO. Staining times of 5, 25, and 60 min were evaluated. Staining temperatures was evaluated at 25 °C, 37 °C, and 40 °C and were optimized as described previously. Solution pH was evaluated at pH 6.0, 7.0, and 8.0. *C. reinhardtii* cells were washed with phosphate buffered saline (PBS) twice by centrifugation.

In cases of JC-1, dye concentration, staining time, solvent concentration and temperature were optimized. Fully starved *C. reinhardtii* (196 μL, 2.4 x 10^6 cells/ml) were introduced into a test tube and treated with 4 μL of JC-1 stock solution. Final concentrations of JC-1 ranged from 500 nM to 5 μM. Test tubes were vortexed and incubated at 40 °C for 5 min. Microalgae cells were stained with 2.5 μM of JC-1 in solutions of 2 % (*v/v*) DMSO. Staining times of 1, 3, 5 and 10 min were evaluated according to a previous procedure. DMSO concentrations ranged from 1 % to 10 % and were optimized as described previously. Staining temperatures ranged from room temperature (23 °C) to 40 °C and were evaluated according to a previously described procedure.

2.2.5 Viability assay

Cells were plated on 96-well plates at 2.4×10^6 cells/mL. After the early stationary phase (OD_{680} = 1.0), cells were treated with the fluorescence probe using the optimized methods. After treatment, 10 μL of EZ-Cytox solution was added to each well and the cells were incubated for 30 min at room temperature. Cell viability was monitored by measuring the solution absorbance at 450 nm. The assay solution containing the control was used as a blank.

2.2.6 Liposome concentration measurement

Phosphatidylcholine (PC; 1 mg/mL) from soybean was dissolved in hexane in a test tube. Hexane was evaporated away by gently blowing N_2 gas into the tube, which resulted in the formation of a thin lipid film on the surface of the tube. The tube was stored at −80 °C for 1 h and then moved to water bath of 60 °C to peel off lipid layer from wall. 1 ml of PBS with three glass bead was added to the tube and the mixture was vortexed vigorously. After removing the glass beads, the mixture was sonicated for 10 min in a bath sonicator. The suspension was extruded using Avanti® mini-extruder with 100 nm membrane (Mini-extruder, Avanti® Polar Lipids INC., Burnaby, Canada). Several concentrations of liposomes were prepared. Mixtures (196 μL) were stained with SF44 or JC-1 in DMSO (4 μL) to a final volume of 200 μL. Fluorescence intensity was measured at 540 nm with excitation at 450 nm (SF44) and 535

nm with excitation at 490 nm (JC-1) using a spectrofluorimeter (LS-55, Perkin-Elmer, Waltham, MA, USA).

2.2.7 Determination of LDs contents

Accumulation of intracellular LDs was tracked by monitoring SF44 fluorescence at 540 nm with excitation at 450 nm (SF44) and 535 nm with excitation at 490 nm (JC-1). During incubation, cells (196 μL) were combined with SF44 or JC-1 in DMSO (4 μL) to a final volume of 200 μL. Cells were collected by centrifugation (1500 rpm, 3 min) in a test tube. After removing the supernatant by vacuum aspiration, the pellet was re-suspended in PBS buffer.

2.2.8 LDs purification and size measurement

LDs were purified from N-source-starved *C. reinhardtii* with slight modifications of a previously reported procedure[51]. Cell samples were harvested by centrifugation (2000 rcf, 4 min) at 4 °C and re-suspended in a solution of ice-cold digitonin (5 mM potassium phosphate buffer, pH 6.5, containing 6% (*w/w*) polyethylene glycol 6000, and 0.004 % (*w/v*) digitonin). Cells were rapidly incubated at 30 °C for 7 min. After incubation, the solution was transferred to an ice bucket and harvested by centrifugation (2000 rcf, 4 min) at 4 °C. Cell pellets were re-suspended in cold osmotic lysis buffer (150 mM Tric-HCl, pH 7.5, containing 10 mM KCl, 1.5 mM EDTA, 0.1 mM $MgCl_2$, 15% (*w/v*) sucrose). Samples were immediately spun at 20,000 rcf for 45 min.

LDs were collected with a pipette after floating to the surface of the solution. For size measurement, micrographs of collected LDs were acquired with a transmission electron microscope (TEM, JEME 1010, JEOL, Tokyo, Japan). Aliquots (10 μL) of each sample were placed onto a carbon-coated copper grid (200 mesh) and incubated for 5 min to adsorb on carbon film. After the incubation, unadsorbed LDs and excessed solution were removed by wetting with a filter paper (Whatman™ Grade 1, GE Healthcare, Piscataway, NJ, USA). The samples were negative stained with 2 % uranyl acetate for 30 s and visualized with a TEM. All of the acquired micrographs were processed using Image J (NIH).

2.3 Results

2.3.1 Optimization of SF44 staining for microalgae

SF44 has been successfully used to stain LDs in mammalian cells such as 3T3-L1 murine adipose and HeLa cells. [46] Unlike mammalian cells, microalgae are surrounded by a dense, complex network of cell walls[52], therefore, additional physical and chemical factors need to be considered for staining *C. reinhardtii*. Moreover, we wanted to validate the possibility of *in situ* tracking of accumulations of LDs in *C. reinhardtii*, so we chose the optimal conditions for applicable live cell determination. Considered physico-chemical factors were dye concentration, staining time, temperature, pH, and solvent

concentration. (Figure 2.3) The fluorescence intensity of the *C. reinhardtii* stained with SF44 was affected by dye concentration. (Figure 2.3A) When SF44 concentration was increased from 1 μM to 5 μM, fluorescence intensity changed up to 5 μM. However, compared to 5 μM, no significant difference was observed at 50 μM of SF44. Similar to the optimal concentration used for LDs staining in mammalian cells[46], we identified 5 μM as the optimal concentration. Staining time is one of the critical factors for high-throughput screening determination. Figure 2.3B shows that staining efficiency of LDs in *C. reinhardtii* increased up to 60 min. Compared to 5 min, there was significant increase in fluorescence intensity at 25 min and 60 min. We considered the correlation between staining time and intensity as an optimization for in situ LD content determination. Although intensity of 25 min was 17 % less than intensity of 60 min, we settled on 25 min as an optimal time by trading off small gain in fluorescence intensity for reducing staining time more than 30 min.

For the measurement of LDs accumulation kinetics, real-time observation without additional processing is ideal. Moreover, conditions compatible with live-cell imaging considered as an important factors such as temperature, pH, and solvent concentration. As indicated in Figure 2.3C and D fluorescence intensity was influenced by the temperature and pH used during the staining process. In the case of temperature, intensity was increased with the staining temperature up to 37 °C, but decreased significantly at 40 °C. In case of pH, there was no significant difference between 6.0 and 7.0, but there was increase of fluorescence intensity at pH 8.0. Although fluorescence intensity at 25 °C and pH 7.0 were less than 37 °C and pH 8.0, we chose 25 °C

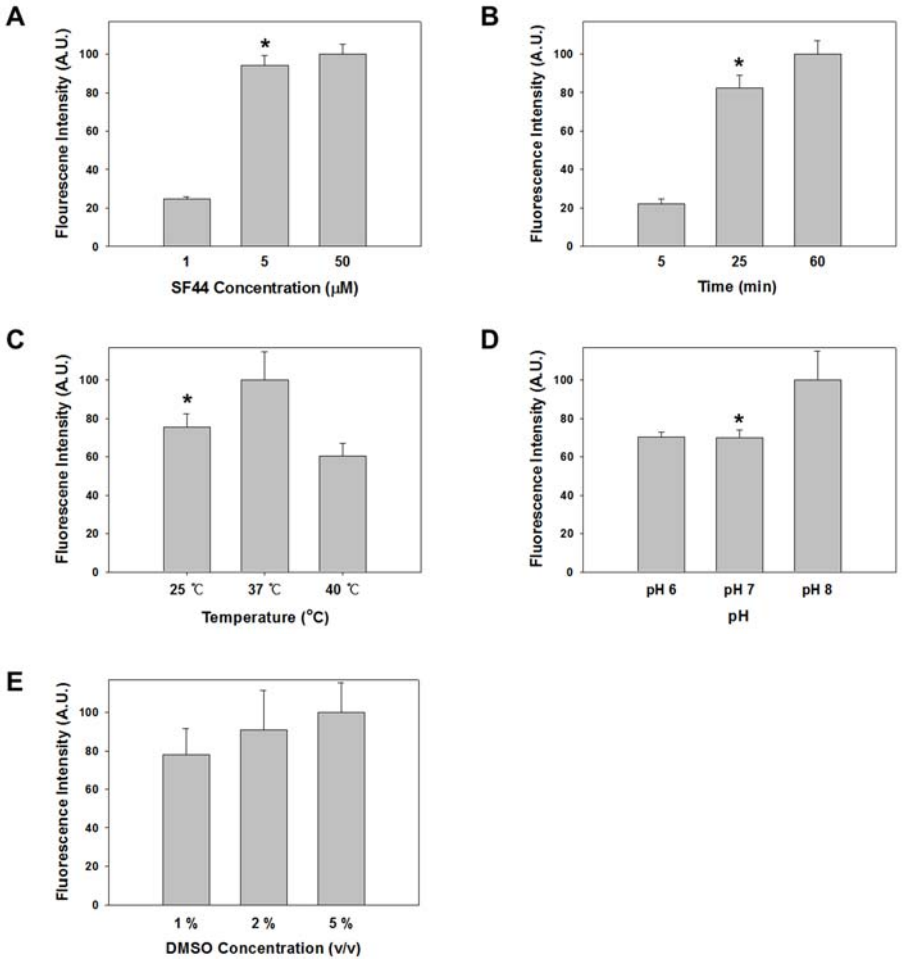

Figure 2.3. Effects of (A) dye concentration; (B) staining time; (C) temperature; (D) pH; and (E) DMSO concentration on the staining of *Chlamydomonas reinhardtii* cells are shown. The optical density of the cell suspensions was 1.0 (OD_{680}). All data are expressed as the mean of 30 replicates with a single standard deviation. Asterisk indicates the optimal condition for staining SF44.

and pH 7.0 as an optimal temperature and pH by considering the conventional freshwater *C. reinhardtii* culture system. In case of DMSO concentration, similar results were observed for different concentration from 1 % to 5 %. (Figure 2.3E) We identified 2 % of DMSO as an optimal concentration to minimize the amount of DMSO exposure to microalgal cells. The optimal condition for staining LDs in *C. reinhardtii* therefore involve using SF44 is 5 μM of SF44 dissolved in 2 % (*v/v*) DMSO (pH 7.0) and incubated at 25 °C for 25 min. That condition leads to capability for *in situ* tracking of LDs in *C. reinhardtii*.

Based on the above optimized condition, we performed cytotoxic assays for testing feasibility of live-cell continuous monitoring of LDs accumulation in microalgae. To determine cell viability, the aforementioned optimized staining methods for SF44 and previously reported method for Nile Red[53] were evaluated with EZ-Cytox assays over 2 days. (Figure 2.4) Compared to control, SF44 showed no significant cytotoxic effect, while Nile Red resulted in significant reduction in cell viability. Condition for Nile Red requires harsh conditions with high temperature (40 °C) in the presence of high concentration of DMSO (20 %), so this condition causes the significant decrease of cell viability. It seemed that condition for staining with SF44 is similar to conventional *C. reinhardtii* culture system, so these result shows that the optimal staining conditions determined herein for SF44 are sufficiently non-cytotoxic and can be used to monitor LDs accumulation kinetics while keeping the cells alive.

Throughout the optimization and cell viability test, we concluded that

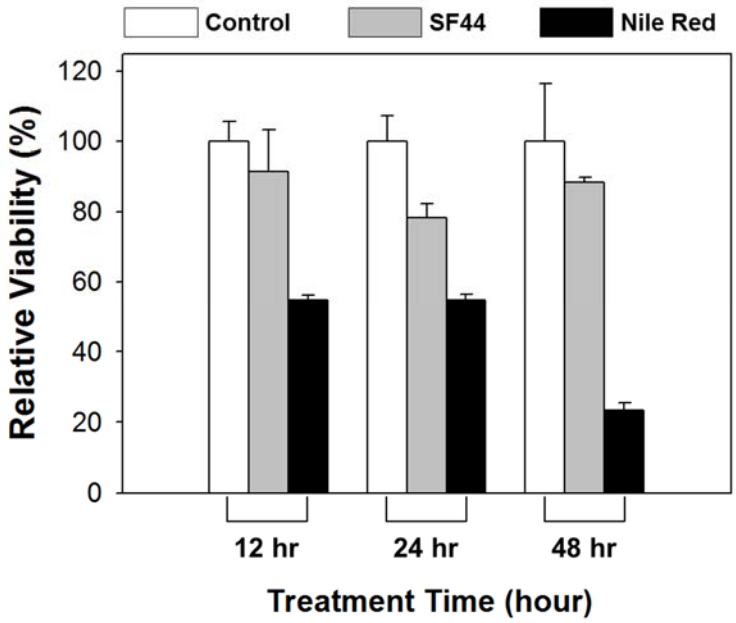

Figure 2.4. The viability of *C. reinhardtii* treated with SF44 (gray bar), Nile Red (black bar), and control (white bar) is shown with treatment of 12, 24, and 48 hours.

SF44 is suitable for *in situ* determination and real time live-cell monitoring for accumulations of LDs. To verify that SF44 based measurement of accumulation kinetics of LDs, we evaluated the possibility for quantification of lipid contents in *C. reinhardtii*.

2.3.2 Quantification of lipid contents using SF44

SF44 has been successfully used to visualize LDs in mammalian cells and microorganism. The validity of using SF44 as a LDs specific molecular probe was assessed by analyzing fluorescence micrographs. Figure 2.5 shows fluorescence micrographs of N-source-starved *C. reinhardtii* during 2 weeks. SF44 exhibited LDs specific staining properties with no overlapping fluorescence signals from chlorophyll, due to the different emission wavelength between SF44 (λ_{em} = 540 nm) and chlorophyll (λ_{em} = 600 nm). This result demonstrates that SF44 may be useful as a LDs specific probe. However, visualization of LDs stained with SF44 was not validated on initial stage of nitrogen starvation. (Initial stage from 1 day to 2 day, Data was not shown.) After 3 days of nitrogen starvation, LDs formed visible droplets when stained with SF44. It seems that resolution of conventional fluorescence microscope is not capable of resolving smaller size LDs before day 3. The resolution of conventional optical microscopes are limited to 180 nm in focal plane and 500 nm in optic axis. [54] The size of LDs at beginning microalgae is only a few tens of nanometers, therefore, microscopic imaging-based validation for LD accumulation, especially the early state, is not ideal for quantification of lipid

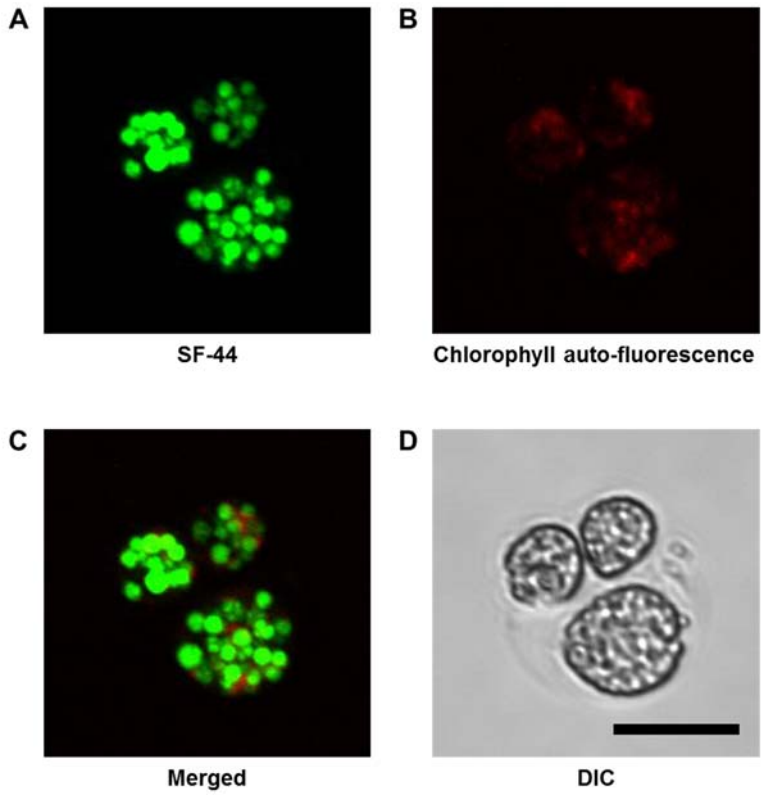

Figure 2.5. Micrographs showing (A) the fluorescence of LDs stained by SF44 (in green); (B) chlorophyll auto-fluorescence (in red); (C) the merged fluorescence SF44 and chlorophyll auto-fluorescence; and (D) a DIC image. All images were acquired through a confocal microscope (FV1000). The scale bar represents 10 μm.

content. There is a need for a quantitative measurement technique for early stage of LD formation.

As an alternative, we used a spectrofluorimeter to monitor SF44 stained LD quantitatively at 540 nm with excitation at 450 nm. (Figure 2.6) We prepared liposomes as model LDs using mechanical dispersion methods. Phosphatidylcholine (PC) liposomes were prepared at various concentrations ranging from 1 μg/mL to 100 μg/mL by diluting a stock solution. Fluorescence intensities were measured at each concentration. Figure 2.7 shows a linear (R^2 = 0.9944) standard curve acquired by plotting fluorescence intensity as a function of liposome concentration. This approach shows the possibility of indirect measurement for lipid content using a spectrofluorimeter.

Throughout the quantification of liposome, we concluded that SF44 is suitable for *in situ* determination for LDs content. So, we want to evaluate that SF44 based measurement of accumulation kinetics of LDs.

2.3.3 Kinetics measurement of intracellular LDs using SF44

Based on correlation between concentration of PC liposome and fluorescence intensity after SF44 staining, we confirmed that fluorescence intensity can be used to track the kinetics of intracellular lipid accumulation with N-source-starved *C. reinhardtii*. Figure 2.8 shows the fluorescence intensity associated with LD accumulation as a function of time. Fluorescence intensity was monitored at 540 nm with excitation at 450 nm. From the onset of the experiment to 60 h, the LDs concentration increased linearly as a function

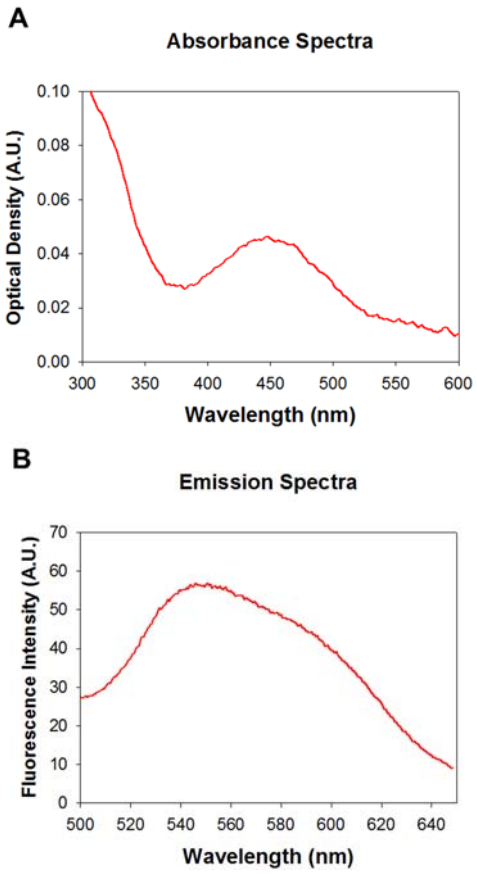

Figure 2.6. Fluorescence characteristics of SF44. (A) Absorbance and (B) emission spectra are shown for SF44 with 1 mg/mL of phosphatidylcholine (PC) liposome. Absorbance and emission wavelength were 450 nm and 540 nm, respectively.

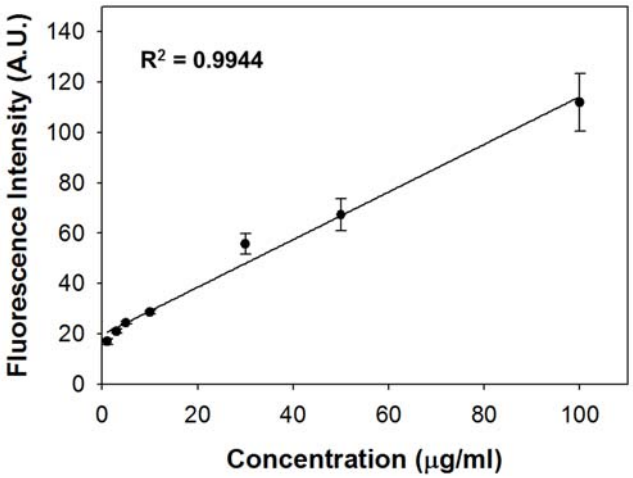

Figure 2.7. SF44 fluorescence intensity is shown with different concentrations of phosphatidylcholine (PC) liposome. All data are expressed as the mean of five replicates and a single standard deviation. ($R^2 = 0.9944$)

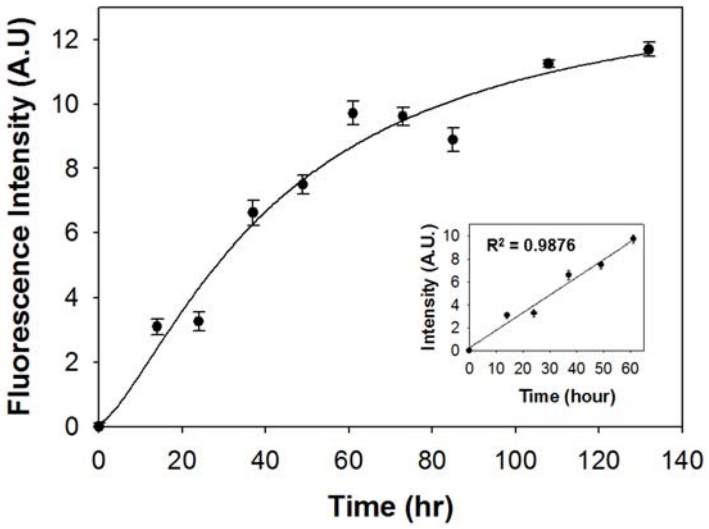

Figure 2.8. Accumulation kinetics of intracellular LDs. The fluorescence intensity of SF44 was monitored with a spectrofluorimeter. Regression result from initial to 60 h incubation is presented in insert. ($R^2 = 0.9876$) The sample contained C. reinhardtii in N-free TAP medium (pH 7.5) incubated at 25 °C, and 5 % CO_2 with continuous shaking at 125 rpm. All data are expressed as the mean of 5 replicates and a single standard deviation.

of time (R^2 = 0.9876). No further increase in LDs concentration was observed after 3 days of incubation.

To validate the fluorescence-based indirect measurement for LD accumulation, we measured the size of purified LDs and verified the kinetics. Figure 2.9 shows the size measurement (from TEM imaging of LD) associated with LDs accumulation. From the onset of the experiment to 48 h, the size of LDs increased linearly as a function of time (R^2 = 0.9982). Like with fluorescence-based indirect measurements, no further increase in size of LDs was observed after 3 days of incubation.

Both indirect and direct measurement methods show an increase until 3 days, then a steady state at the highest level. (Figure 2.10) This result indicates that SF44 can be used as a LD-specific probe for quantitatively tracking intracellular LD accumulation.

2.3.4 Optimization of JC-1 staining for microalgae

JC-1 is well-known probe for detecting early stage of apoptosis by measuring mitochondrial membrane potential. We validated that this well-known lipophilic fluorescence probe has a specific interaction with LDs. We optimized staining conditions with JC-1 *via* systematic variations of concentration, staining time, temperature and solvent concentration. (Figure 2.11) The fluorescence intensity of the *C. reinhardtii* stained with JC-1 was affected by dye concentration. When JC-1 concentration was increased from 0.5 μM to 2.5 μM, fluorescence intensity changed up to 2.5 μM. However,

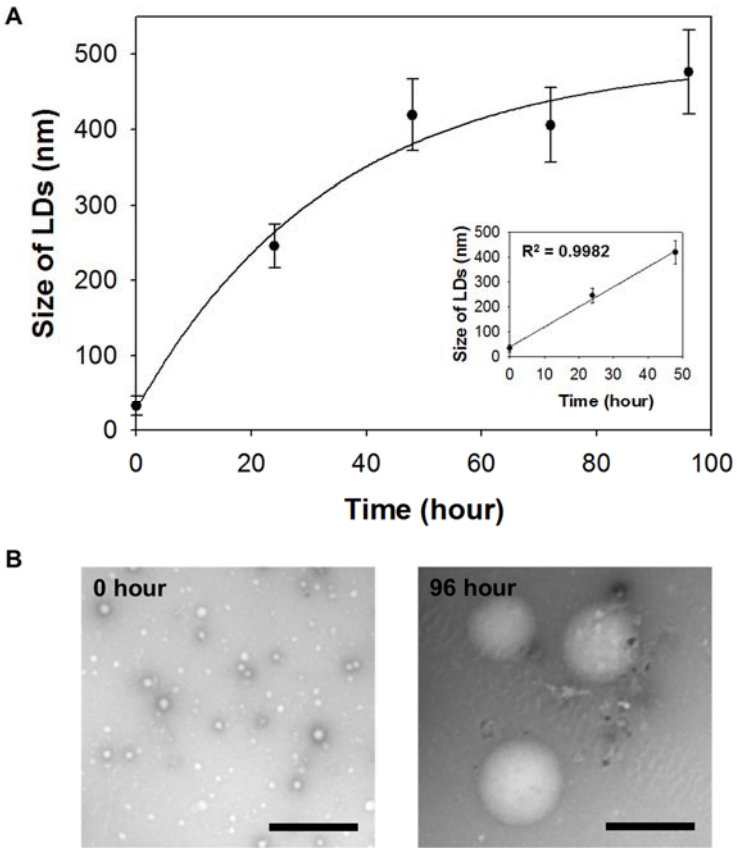

Figure 2.9. (A) Kinetics of size for intracellular LDs. The size of purified LDs was determined using TEM. Regression result from initial to 48 h incubation is presented in the insert (R^2 = 0.9982); (B) TEM micrographs at 0 h and 96 h incubation. The scale bar represents 500 nm. The sample contained *C. reinhardtii* in N-free TAP medium (pH 7.5) incubated at 25 °C, and 5 % CO2 with continuous shaking at 125 rpm. All data are expressed as the mean of 100 replicates and a single standard deviation.

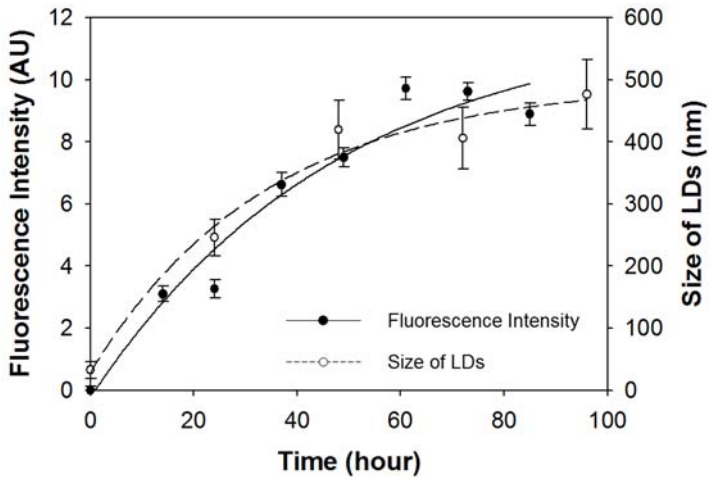

Figure 2.10. Accumulation kinetics of intracellular LDs. The fluorescence intensity of SF44 was monitored with a spectrofluorimeter. (closed dot and line) The size of purified LDs was determined using TEM micrograph. (open dot and dashed line)

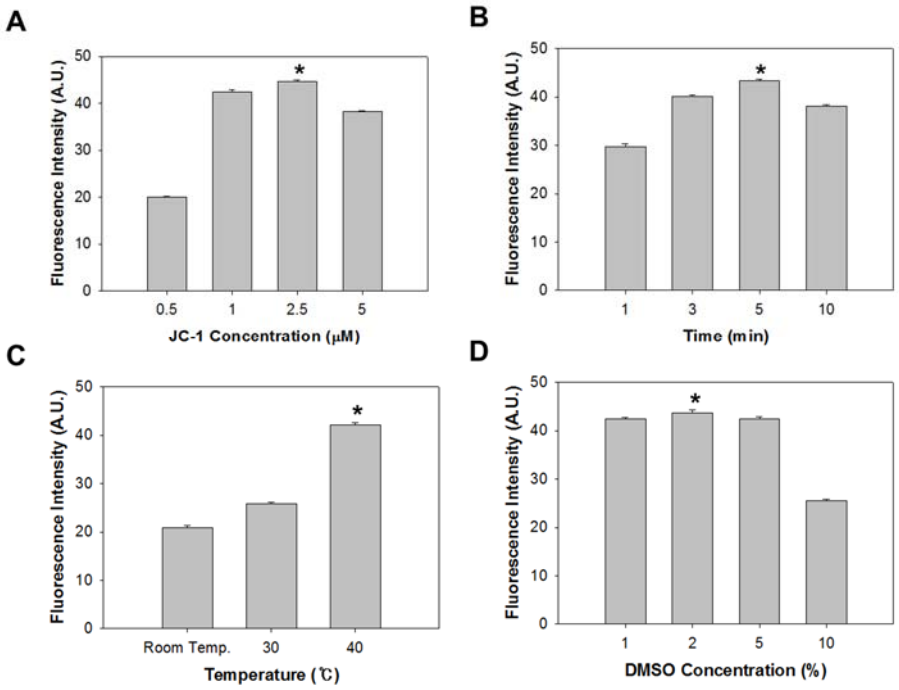

Figure 2.11. Effects of (A) dye concentration; (B) staining time; (C) temperature and (D) DMSO concentration on the staining of *C. reinhardtii* cells are shown. The optical density of the cell suspensions was 1.0 (OD_{680}). All data are expressed as the mean of 30 replicates with a single standard deviation. Asterisk indicates the optimal condition for staining JC-1.

compared to 2.5 μM, fluorescence intensity was decreased at 5 μM of JC-1. We identified 2.5 μM as the optimal concentration. Figure 2.11B shows that staining efficiency of JC-1 in *C. reinhardtii* increased up to 5 min. Similar to concentration result, sustainable treatment was not guaranteed increased fluorescence intensity. As indicated in Figure 2.11C fluorescence intensity was influenced by the temperature used during the staining process. In the case of temperature, intensity was increased with the staining temperature up to 40 °C, fluorescence intensity was doubled at 40 °C. In case of solvent concentration, there was no significant difference between 1 % and 5 %. (Figure 2.11D)

The optimal condition for staining LDs in *C. reinhardtii* therefore involve using JC-1 is 2.5 μM of JC-1 dissolved in 2 % (*v/v*) DMSO and incubated at 40 °C for 5 min. That condition leads to capability for *in situ* tracking of LDs in *C. reinhardtii*.

2.3.5 Quantification of lipid contents using JC-1

Similar to the SF44, we used a spectrofluorimeter to monitor JC-1 stained LD quantitatively at 535 nm with excitation at 490 nm. We prepared liposomes as model LDs using mechanical dispersion methods. Phosphatidylcholine (PC) liposomes were prepared at various concentrations ranging from 1 μg/mL to 100 μg/mL by diluting a stock solution. Fluorescence intensities were measured at each concentration. Figure 2.12 shows a linear (R^2 = 0.9979) standard curve acquired by plotting fluorescence intensity as a function of liposome concentration. This approach shows the possibility of

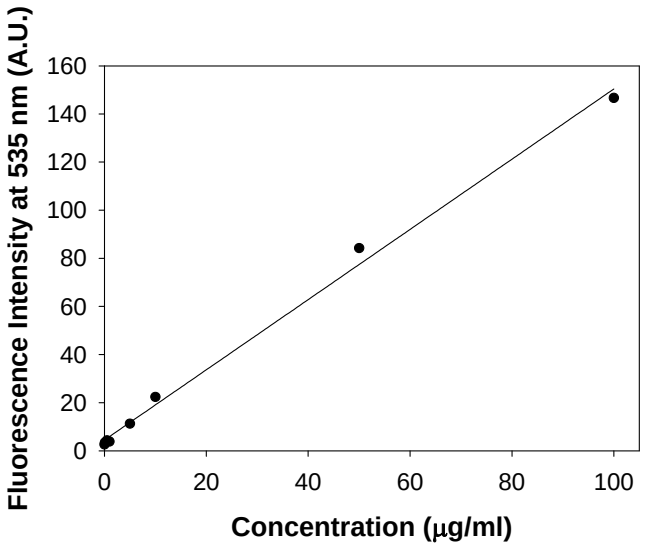

Figure 2.12. JC-1 fluorescence intensity is shown with different concentrations of phosphatidylcholine (PC) liposome. All data are expressed as the mean of five replicates and a single standard deviation. ($R^2 = 0.9979$)

indirect measurement for lipid content using a spectrofluorimeter.

Throughout the quantification of liposome, we concluded that JC-1 is suitable for *in situ* determination for LDs content. So, we want to evaluate that JC-1 based measurement of accumulation kinetics of LDs.

2.3.6 Kinetics measurement of intracellular LDs using JC-1

Based on correlation between concentration of PC liposome and fluorescence intensity after JC-1 staining, we confirmed that fluorescence intensity can be used to track the kinetics of intracellular lipid accumulation with N-source-starved *C. reinhardtii*. Figure 2.13 shows the fluorescence intensity associated with LD accumulation as a function of time. Fluorescence intensity was monitored at 535 nm with excitation at 490 nm. We validate the JC-1 based indirect measurement for LD accumulation with size measurement of LDs. Both of these data sets indicated that similar kinetic trends were observed between two methods.

When we measured kinetics of intracellular LDs accumulation, there was considerable result from fluorescence characteristics of JC-1. JC-1 emits green and red fluorescence at 535 nm and 600 nm with excitation at 490 nm, respectively. In the presence of artificial liposome, JC-1 only emits green fluorescence at 535 nm. It seems that monomers of JC-1 were clearly intercalated into inside of hydrophobic lipid structures instead of forming J-aggregates which emits red fluorescence at 600 nm. However, when we measured kinetics of intracellular LDs, JC-1 emits red fluorescence, which

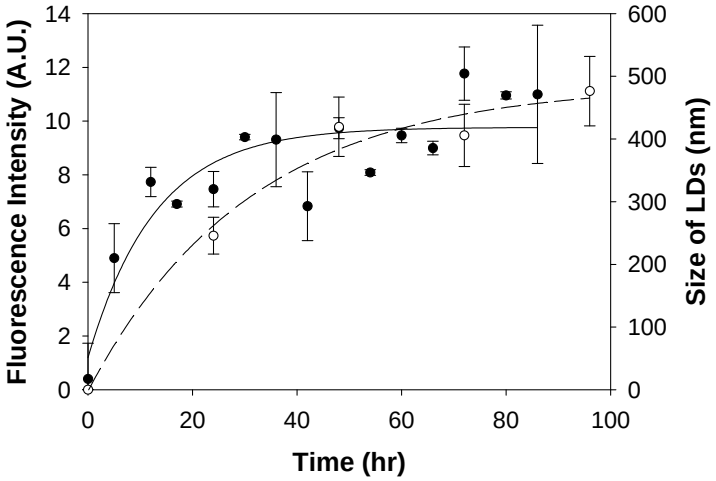

Figure 2.13. Accumulation kinetics of intracellular LDs. The fluorescence intensity of JC-1 was monitored with a spectrofluorimeter. (closed dot and line) The size of purified LDs was determined using TEM micrograph. (open dot and dashed line) The sample contained *C. reinhardtii* in N-free TAP medium (pH 7.5) incubated at 25 °C, and 5 % CO_2 with continuous shaking at 125 rpm. All data are expressed as the mean of 5 replicates and a single standard deviation.

could not be disregarded. Compared with initial stage of *C. reinhardtii*, fully starved state show increased green and decreased red fluorescence, respectively. (Figure 2.14) It seems that red fluorescence indicates small sizes of LDs (a few nanometers), which dimension is similar to J-aggregates. As time goes by, small size LDs accumulates large state, so it is enough to emit green fluorescence signals.

2.4 Conclusions

In this chapter, SF44, a tunable and hydrophobic organelle specific fluorescence probe, and JC-1, lipophilic fluorescence probe, was used to monitor LD accumulation in live *C. reinhardtii* cells. Optimal staining conditions for SF44 and JC-1 in *C. reinhardtii* were identified with regard to dye concentration, staining time, temperature, pH and solvent concentration. However, as Nile Red has emerged as an industrial standard through application on numerous microalgal species of various classes, optimized staining process for SF44 and JC-1 must also be verified in other species. Moreover, microalgal lipid productivity is commonly affected by their surrounding environmental stresses and culture conditions such as nutrient, light, gas concentration, temperature and pH. Especially, pH (about 10.0)-induced LD accumulation is the best conditions in green algae for application in industrial systems. For the advanced applications of SF44 and JC-1 in industrial systems, methodology should be considered as a “tailor-made” system and reconstructed with their

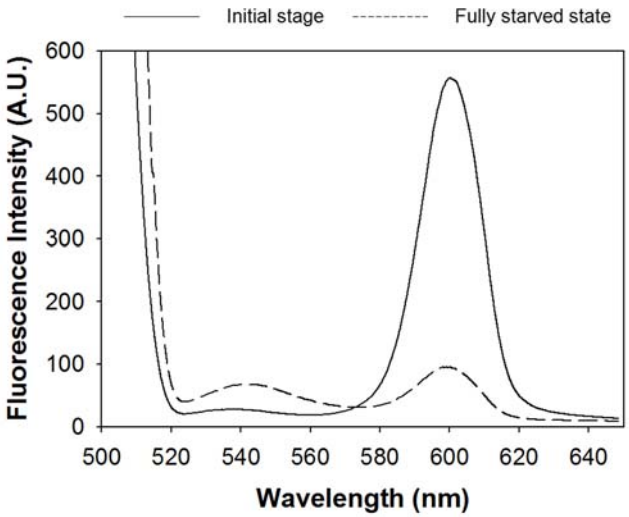

Figure 2.14. Emission spectra of JC-1 with initial (line) and fully starved state (dashed line) of *C. reinhardtii*. The sample contained *C. reinhardtii* in N-free TAP medium (pH 7.5) incubated at 25 °C, and 5 % CO_2 with continuous shaking at 125 rpm.

optimized conditions. In this chapter, our optimization was only for conventional culture system, so it needs to be re-optimized with specific experimental conditions.

The feasibility of measuring the kinetics of intracellular LDs accumulation *via* SF44 staining was also demonstrated. Kinetic parameters were also determined by measuring the size of purified LDs using TEM. Both of these data sets indicated that LD accumulation was linear for 3 days before reaching a steady state. At the end point of linear growth (3 day), fluorescence intensity and size showed 88% and 84% of maximum level, respectively. Moreover, the kinetics were well fitted by the same nonlinear regression equation and showed similar R^2 values. (0.9955 and 0.9884, respectively) This result indicated that similar kinetic trends were observed between two methods. Therefore, SF44 provides a simple means of tracking intracellular LDs. This approach allows not only indirect measurement but also tracking for initial stage of LDs accumulation which is impossible to validate their fluorescence intensity through microscopic image analysis with their low resolution.

The tracking of intracellular LDs in microalgae is essential for high-throughput screening of samples for determining their biodiesel potential. Conventional chromatographic methods involve several sample preparation steps and are not always suitable for in situ measurements. To overcome the limitations of chromatographic methods, fluorescence probes have emerged as a rapid and reliable means of acquiring in situ data on LDs accumulation and LDs content of a sample. [53] This study shows that SF44 is a powerful, LDs specific fluorescence probe, that is suitable for use in multi well plate based

read-out systems and high-throughput screening of intracellular LDs accumulation.

Although JC-1 cannot be used to monitor live kinetics of LDs accumulation due to their harsh staining condition, JC-1 with their dual fluorescence properties can be the most powerful tool for analyzing whole process of lipid dynamics such as formation, growth and generation by tracing green and red fluorescence.

Chapter 3. Immobilization of Microalgae

3.1 Introduction

Conventional agar plate and batch culture system typically observed cells on agar plate and microscope coverslip which is limited to acquire the quality of long-term continuous monitoring, as cells trend to grow and migrate out of the focal plane of microscope. Microfluidics based experimental method have expanded our knowledge of various microorganisms by offering well-controlled microenvironmental experimental conditions that could not be manipulate with conventional macroscale methods. [28] Microfluidic platforms can generate precise spatially and temporally controlled microenvironments at single cell level. Understanding the mechanism of lipid droplet formation, optimization of culture conditions and screening new strains that have high lipid productivity would benefit greatly from implementation of microfluidic techniques.

Here, we presented surface immobilization techniques for *C. reinhardtii* in a microfluidic platform using gelatin coating. The vegetative cell wall of *C. reinhardtii* is composed entirely of glycoproteins rich in *O*-glycosylated hydroxyproline (Hyp) - up to 85 % in total weight. [55] To immobilize *C. reinhardtii* on a glass substrate that has been coated with gelatin, a Hyp-rich material. Gelatin is derived from collagen and widely used for gelatin in food, drugs and cosmetics. It contains a large amount of Hyp

(12 %)[56], therefore, we used it as an attachment complex to glycoproteins on the *C. reinhardtii* cell wall using non-covalent bonding interactions. Prior to developing a detailed quantitative analysis of cellular lipid droplet accumulation, here we show the first demonstration of single cell imaging and characterization of lipid droplet accumulation in *C. reinhardtii* in a microfluidic platform. The application of microfluidics with surface immobilization method can become a useful tool for biodiesel research by helping high-throughput screening of new algal strains and rapid optimization of culture conditions.

3.2 Materials and methods

3.2.1 Materials

Chlamydomonas reinhardtii (CC-125; wild type mt+ and CC-503; wall-deficient mutant mt-) was obtained from the *Chlamydomonas* Resource Center at the University of Minnesota (St. Paul, MN). Polydimethylsiloxane (PDMS), Sylgard 184, was purchased from Dow Corning (Midland, MI). SU-8 negative photoresist was purchased from Micro-Chem Corp. (Newton, MA). Gelatin from bovine skin was purchased from Sigma–Aldrich (St. Louis, MO). All other chemicals and reagents used in this study were purchased from Sigma–Aldrich unless otherwise mentioned.

3.2.2 Culture conditions

C. reinhardtii cells in Tris-acetate-phosphate (TAP) medium were cultured at 23 °C, 5 % CO_2 with shaking on an orbital shaker at 125 rpm. Light conditions were maintained 12 h of light (40 μmol/s/m^2) and 12 h of darkness cycles. When the optical density (O.D.) at 680 nm was approximately 1.0 (early stationary phase), the cells were removed from the flask and used for attachment on the gelatin-coated substrates.

3.2.3 Microfluidic device fabrication

Devices were fabricated by soft lithography. Photolithography using SU-8 negative photoresist was used to generate a master mould on a Si wafer. PDMS device was fabricated by casting and curing Sylgard 184 mixture of oligomer and curing agent (10:1, *w/w*) at 95 °C. After curing, the PDMS device was separated from the master mould and cut to obtain individual devices.

3.2.4 Surface immobilization optimization

Glass coverslips were placed in plasma cleaner (Femto Science, Seoul, Korea) for 1 min (50 W) to generate a hydrophilic surface. Moulded PDMS piece was immediately placed on the clean glass coverslips to form the microchannel. Gelatin solution was introduced into the microchannels incubated for a set time at 37 °C. After the coating step, the microchannels were washed with TAP media for three times. *C. reinhardtii* cells were introduced

and allowed to settle and attach to the gelatin substrate and the number of remaining cells (within 200 μm × 200 μm area, five different regions) after gentle wash at 0.25 dyne/cm^2 was counted. Unattached cells were removed by gentle washing with TAP media. Gelatin solutions at pH 6.0, 7.0, and 8.0 were tested. Gelatin solution concentration tested ranged from 1 to 10 mg/mL. The immobilization time ranged from 0 to 6 h and was optimized as described previously.

3.2.5 Patterned substrate preparation

Clean glass coverslip was coated with gelatin with optimized procedure described earlier. Gelatin coated coverslip was washed with PBS for three times and air-dried. A micro-pillar patterned PDMS stamp was placed over the gelatin coated coverslip and exposed to plasma etching for 1min. To block the surface from microalgae attachment, 3 % BSA (*w/v*) in PBS was used to cover etched areas except for micro-pillar contact region and resulting in gelatin coated circular patterns. (Figure 3.1)

3.2.6 Viability assay

C. reinhardtii viability after surface immobilization was tested using EZ-Cytox with cells immobilized on glass bottom 96-well plates. After the immobilization and incubation, 10 mL of EZ-Cytox solution was added to each well and the cells were incubated for 30 min in an incubator. Cell viability was

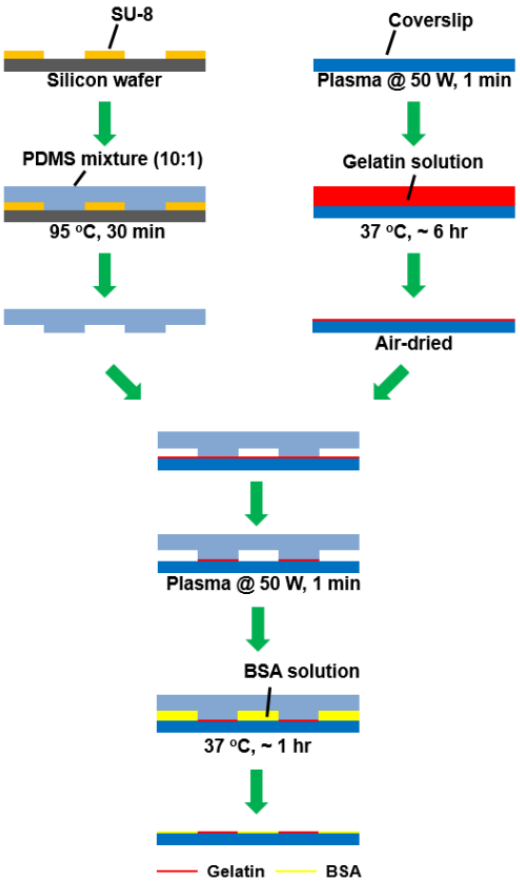

Figure 3.1. A schematic diagram showing the whole process of gelatin patterned substrate preparation.

obtained by measuring absorbance at 450 nm.

3.2.7 Wall shear stress induced detachment assay

C. reinhardtii cells were immobilized inside the microfluidic device (900 μm wide and 100 μm high) and subjected to fluid flow. Flow was generated using gastight syringe (500 mL, Hamilton, NV) and a syringe pump (Harvard Apparatus PHD2000, MA).Wall shear stress was adjusted by controlling the flow rate. Wall shear stress was calculated using the following equation,

$$\tau = \frac{6\mu Q}{wh^2}$$

where μ, w, h, and Q are viscosity, chamber width and height, and flow rate, respectively.

3.2.8 Live cell imaging of *C. reinhardtii* mitosis

Live cell imaging was performed with an inverted microscope (Olympus IX81, Tokyo, Japan) fitted with an environmentally controlled imaging chamber (Live Cell Instrument, Seoul, Korea). The chamber was maintained at 23 °C and 5 % CO_2. All images were processed with ImageJ (NIH, Bethesda, MD, USA). To observe *C. reinhardtii* mitotic process, cells were first immobilized on the glass surface within a microfluidic device (gelatin solution, pH 8.0 at 1 mg/mL, coated for 6 h and cells attached for 1 h). DIC Images were

acquired at 30 min intervals for up to 12 h.

3.2.9 Imaging and quantification of lipid accumulation in *C. reinhardtii* as single cell level

Immobilized *C. reinhardtii* cells were treated with 1 μM BODIPY for 10 min. After the staining, cells were washed with fresh medium. Cells were observed with an inverted fluorescence microscope (Olympus IX81, Tokyo, Japan) equipped with a LED light source (CoolLED pE-1, NY, USA). Fluorescence images were acquired in 24 h intervals for 6 days. All acquired images were processed with ImageJ (NIH, Bethesda, MD, USA).

3.3 Results

The main goal of this chapter is to monitor microalgae, as *C. reinhardtii*, model microalgae that are genetically well characterized and a *C. reinhardtii* is fixed inside microfluidic device while exposed to combination culture conditions.

When immobilizing yeast on surfaces, Concanavalin A (ConA), a lectin (carbohydrate-binding protein) is widely used. Yeast cell wall is composed of polysaccharides that interact with ConA *via* non-covalent bonding (*i.e.* hydrogen bonding and electrostatic interaction). To use similar approach, we first analyzed the composition of microalgal cell wall and considered

surface molecules that can be used for surface immobilization. *C. reinhardtii* cell wall is made up of Hyp-bound *O*-glycans. [57] *Weibel et. al.* had utilized Hyp residue coated polystyrene beads to attach microalgae to the microbeads. [58] To take advantage of large number of Hyp residues and use them for immobilizing microalgae on surfaces, we chose gelatin as the counterpart and thus function as a "biochemical glue".

3.3.1 Surface immobilization of *C. reinhardtii* using gelatin

Figure 3.2A shows the schematic showing the composition of microalgae cell wall and gelatin. Like plants, microalgae have cell walls that contain either polysaccharides or a variety of glycoproteins. The cell wall is located outside the cell membrane and provides these cells with structural support and protection. *C. reinhardtii* is a single cellular green microalgae about 5 μm in diameter that is surrounded by an extracellular coat composed of hydroxyproline-rich glycoproteins. [55] Gelatin is derived from collagen and contains a large amount of Hyp residues due to their repeat tripeptide unit, Gly-Pro-Hyp (12%). [56] Gelatin has exposed Hyp residues as the subunits that make collagen triple helix are disassembled during hydrolyzation process. As shown in the schematic figure 3.2A, Hyp-Hyp non-covalent interaction is utilized for *C. reinhardtii* surface immobilization on gelatin coated surfaces.

Figure 3.2B shows the DIC and fluorescence (chlorophyll auto-fluorescence) photographs of immobilized microalgae on surface that has been patterned with gelatin. We first used plasma-based dry patterning method [59]

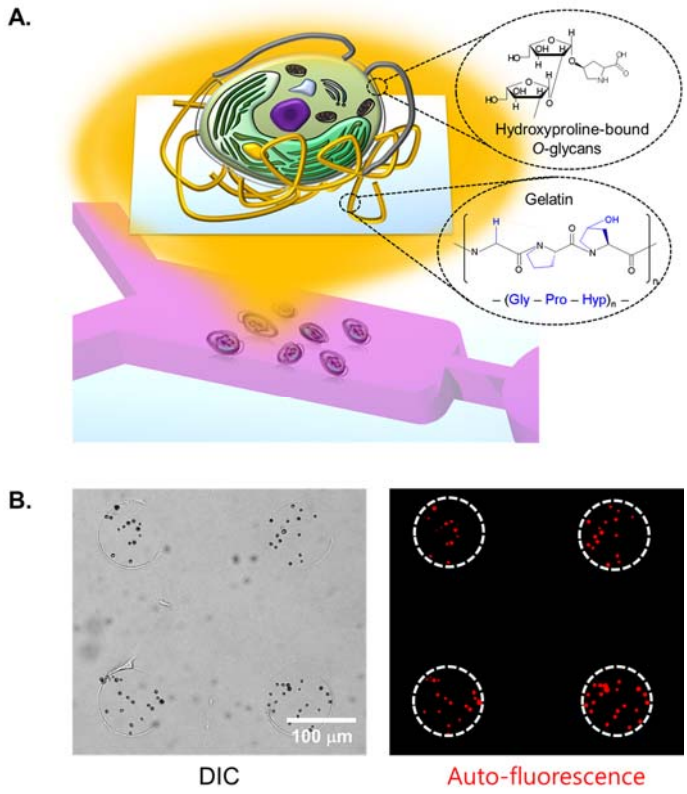

Figure 3.2. (A) Schematic diagram of *Chlamydomonas reinhardtii* attached on gelatin coated surface. Gelatin contains repeating glycine-proline-hydroxyproline (Hyp) sequence while *C. reinhardtii* cell wall is composed of Hyp-bound *O*-glycans. (B) Micrographs showing DIC and fluorescence (chlorophyll auto-fluorescence) images of microalgae that are attached on patterned gelatin islands. Gelatin pattern (white dotted circle) is confined to its circle shapes. The scale bar represents 100 μm.

to generate gelatin island patterns (r = 50 μm) on the glass substrate. (Figure 3.1) Areas outside the gelatin were covered with bovine serum albumin (BSA) to deter microalgae attachment. When *C. reinhardtii* cells were placed into the microchannel, they selectively attached on gelatin patterns but not on BSA covered regions.

Effectiveness of non-covalent interactions can be influenced by experimental conditions such as pH, temperature, concentration and time. Clean glass substrates were first coated with gelatin (1 mg/ml at pH 8.0, 37 °C) for 6 hours. After incubation, the glass substrate was washed three times with TAP media. Microalgae was allowed to settle down and kept in dark condition (25 °C) for another hour for optimal cell attachment. Figure 3.3 shows the effect of various experimental conditions on surface immobilization. Microalgae that have not attached firmly can be simply washed away with gentle flow. After the wash, the cells continue to remain firmly attach even at significantly higher flow rate (0.2 dyne/cm^2), as discussed later in Figure 3.6.

To understand the mechanism for immobilization and to confirm that large number Hyp residues on gelatin is responsible for capturing microalgae, we tested different surface coatings. Figure 3.4A shows the effect of various surface coating on number of immobilized *C. reinhardtii* inside the microfluidic channel. Gelatin coated surface shows significantly higher number of attached microalgae compared to control glass surface, BSA, and collagen coated surfaces. Although uncoated glass and BSA show few numbers of attached cells, BSA coated surface exhibited the lowest value. BSA is widely used as a blocking agent for unwanted adsorption of proteins and mammalian cells and

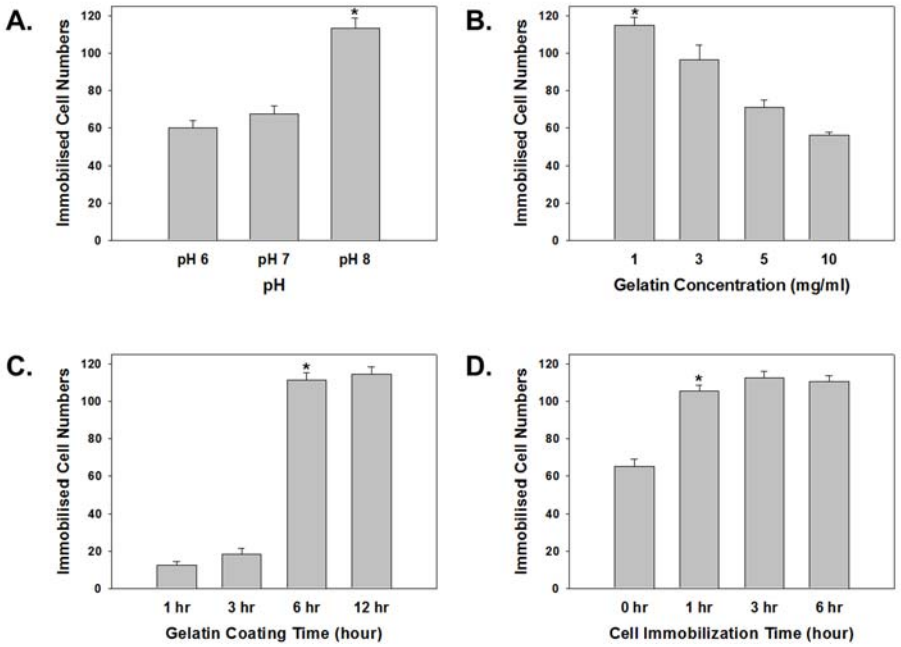

Figure 3.3. Optimization gelatin surface coating conditions for *C. reinhardtii* immobilization as a function of (A) pH, (B) concentration, (C) coating time and (D) immobilization time. All data are expressed as the mean of five replicates with a single standard deviation. Asterisks indicate the best condition for immobilization.

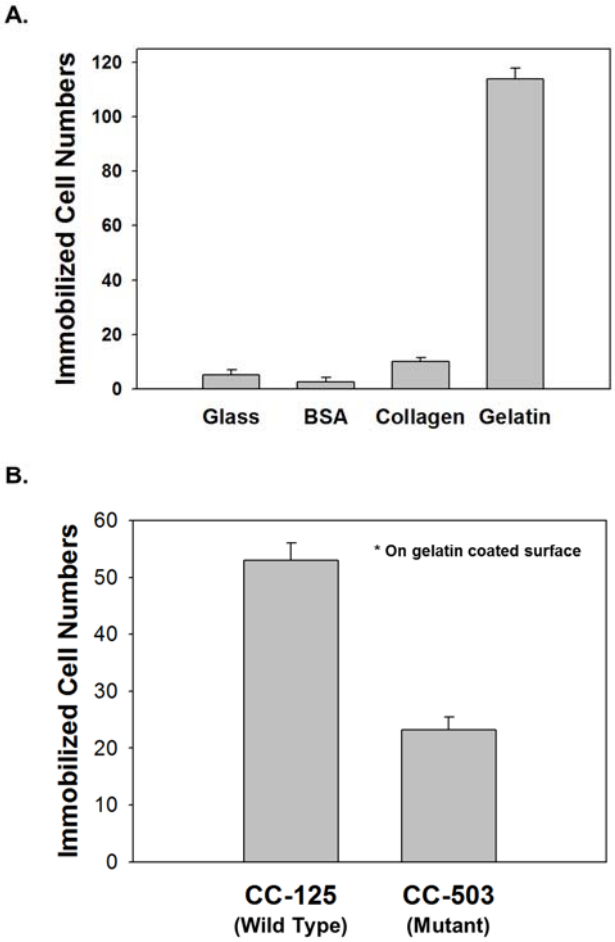

Figure 3.4. (A) Effect of various surface coatings on *C. reinhardtii* immobilization. (B) Comparison of wild type (CC-125) and cell wall deficient mutant (CC-503) immobilization on gelatin surface. All data are expressed as the mean of five replicates and a single standard deviation.

it seems to function in similar way for microalgae.

Gelatin is derived from collagen and hence they are identical in chemical composition. However, their hierarchical structure is significantly different because gelatin is prepared by hydrolyzation process of collagen. Collagen has high number of Hyp residues but they are not available for interacting with Hyp residues on microalgae cell wall. The Hyp residues are buried inside the 3D structure used for forming and stabilizing triple helix structure. [60] Markedly increased number of attached microalgae on gelatin coated surface (~ 12x compared to collagen) indicates that Hyp is a key molecule for capturing microalgae.

To test the importance of Hyp decorated cell wall, we compared wild type *C. reinhardtii* (CC-125, with intact cell wall) with a mutant *C. reinhardtii* (CC-503, cell wall deficient) for immobilization on gelatin coated surface. CC-503 is a very clean wall-deficient strain derived from wild type CC-125. [61] The results shown in Figure 3.4B shows that the cell-wall deficient CC-503 cells significantly less adhere to the gelatin coats than the wild type cells; however, the wall deficient cells still exhibit the same preferential immobilization on the gelatin over the other coats. The results clearly indicate that cell wall plays a major role in adhesion to Hyp. In addition, CC-503`s affinity to the gelatin surface shows that the interaction between CC-503`s plasma membrane (such as glycolipids) with gelatin likely involves other forces such as electrostatic and van der waals interactions. Above two results support that gelatin coat can be a universal platform for immobilizing microalgae with or without cell walls.

3.3.2 Validation for microfluidic application

For real-time imaging applications inside microfluidic devices, cell viability should not be affected while they are immobilized over long periods. We used EZ-Cytox assay on immobilized samples to determine the effect of gelatin-based immobilization on viability. (Figure 3.5) Over the experimental period, with the samples obtained in 1 day intervals, when compared with flask cultured control cells, immobilized cells showed no difference in viability. This means that gelatin-based immobilization does not cause aberrant effects to microalgae cells and it can be safely used for long-term live cell manipulations in a microfluidic system.

Since the microalgae may be cultured under constant flow conditions inside the microfluidic channels, we investigated the effect of wall shear stress on microalgal attachment. The usual range of wall shear stress used in typical microfluidic experiments is from 0.01 to 0.2 dyne/cm^2 (7 μl/h to 140 μl/h for a channel with 100 μm × 1 mm [height × width]).

Figure 3.6 shows the effect of wall shear stress on *C. reinhardtii* attachment. We wanted to confirm that cells remain attached in typical microfluidic experimental conditions. Wall shear stress was increased from 0.015 to 8.2 dyne/cm^2 in step-wise fashion. Constant wall shear stress was applied for 10 min and a photograph was taken to count the number of cells remaining in 200 μm × 200 μm area. For each sample, 5 different images were taken at different positions and the number of attached cells was averaged.

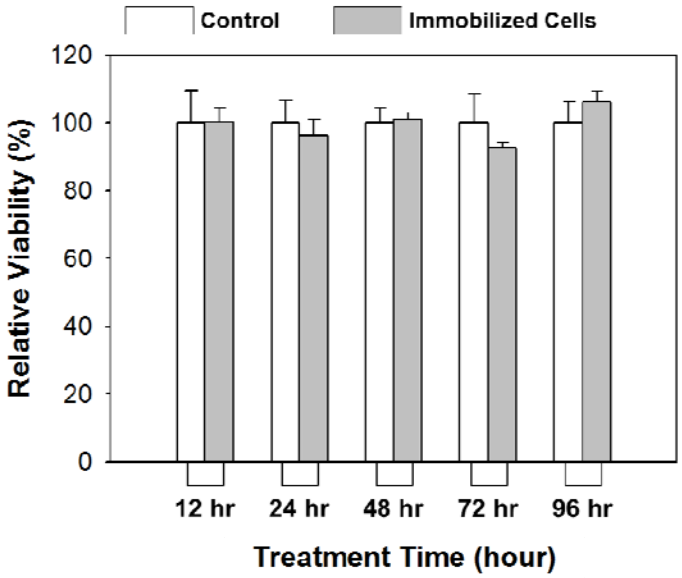

Figure 3.5. Viability of bulk suspension cultured (white bar) and immobilized (gray bar) *C. reinhardtii* is shown after 12, 24, 48, 72 and 96 h culture.

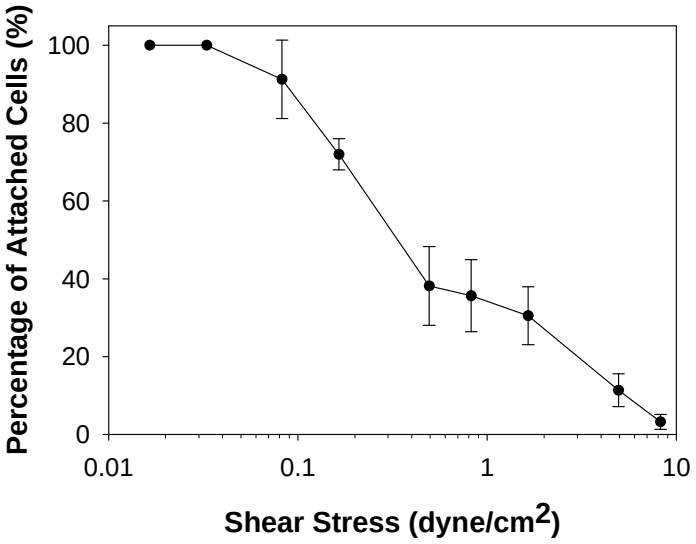

Figure 3.6. Percentage of attached cells as a function of increasing wall shear stress. The number of cells remaining attached in 200 x 200 μm area were counted after 10 min application of increasing wall shear stress at each condition from 0.015 to 8.2 dyne/cm^2. All data are expressed as the mean of five replicates and a single standard deviation.

Below 0.1 dyne/cm^2, most of the cells remain attached (very small error bar). Few weakly adhered microalgae, around 10 - 20 percent of the cells, detach from the surface as the flow is increased. In most microfluidics experiments, an upper limit of flow rate used generates wall shear stress value of 0.1 dyne/cm^2. Even when the wall shear stress was increased to 0.5 dyne/cm^2, 40 % of immobilized cells still remained attached. At maximum wall shear stress of 8.2 dyne/cm^2, all cells were washed off from the surface. Conventional microfluidic perfusion culture system operates over wide range of flow (with wall shear stress) conditions depending on specific experiment and cell types. For typical experiments using gradient generation devices[62], less than 0.2 dyne/cm^2 of wall shear stress is used. When microalgae are immobilized using gelatin, it is compatible with most of the microfluidic experiments.

3.3.3 Live cell imaging of *C. reinhardtii* mitosis and lipid accumulation

Figure 3.7 shows time-lapse images of immobilized *C. reinhardtii* undergoing mitosis over 7 hour time period. We successfully observed 3 distinct stages of cell cycle including shrinking (0 to 1 h), rotation (1 to 3 h) and mitosis (3 to 5 h)[63]. This result shows that immobilization techniques can be used to follow dynamic processes and observe natural physiological processes such as cell division and growth under well-controlled conditions.

The advantage of live cell imaging compatible immobilization method is that we can continuously monitor the changes in size and shape of

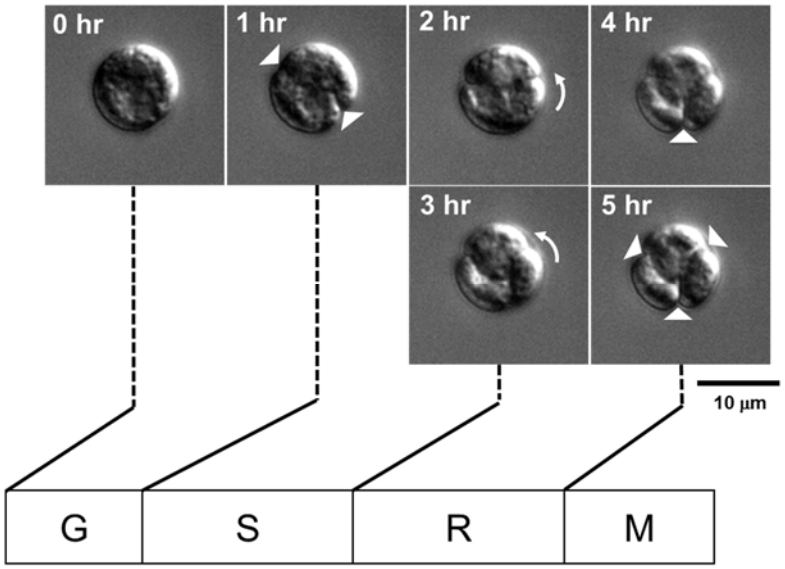

Figure 3.7. Single-cell time-lapse images of *C. reinhardtii* mitosis. Images were acquired at 30 min interval for 12 h under dark conditions. The scale bar represents 10 μm.

cell over the entire cell cycle. Conventionally, live cell imaging has not been available in agar plate culture system due to large groups of cells tend to grow as a clump so it is hard to visualize on microscope. Matsumura's work[63] on microalgae time-lapse images was obtained by manually finding and focusing on each sample because the cells could not be immobilized. They had to look around the culture chamber to identify and photograph the same cell at every time-point. Acquisition of images with confocal laser scanning microscope (CLSM) or coherent anti-stokes raman scattering (CARS) microscope (image lipids without fluorescence probe) takes few minutes to obtain the 3D images. However, after one around of mitosis, hatched cells do not immobilize on surface anymore, since only mother cell wall adhere on the gelatin surface. Instead, released daughter cells were immobilized other region or washed away on a case by case. By considering microfluidic device design and flow rate, it will be possible to continuously track cells throughout their whole life span with enhanced immobilization method.

An important area in biodiesel research is the accumulation of intracellular lipid droplet in microalgae. Single-cellular lipid accumulation kinetics in microalgae has been difficult to visualize. Due in part to small size of lipid droplets (20 – 400 nm), any movement result in blurred faint images that is difficult to use for quantitative analysis. With gelatin-based immobilization, cells remain stationary during image acquisition and clearly focused 3D images can be obtained.

Figure 3.8 shows time-lapse images of intracellular lipid accumulation in *C. reinhardtii* cultured under nitrogen deprivation condition

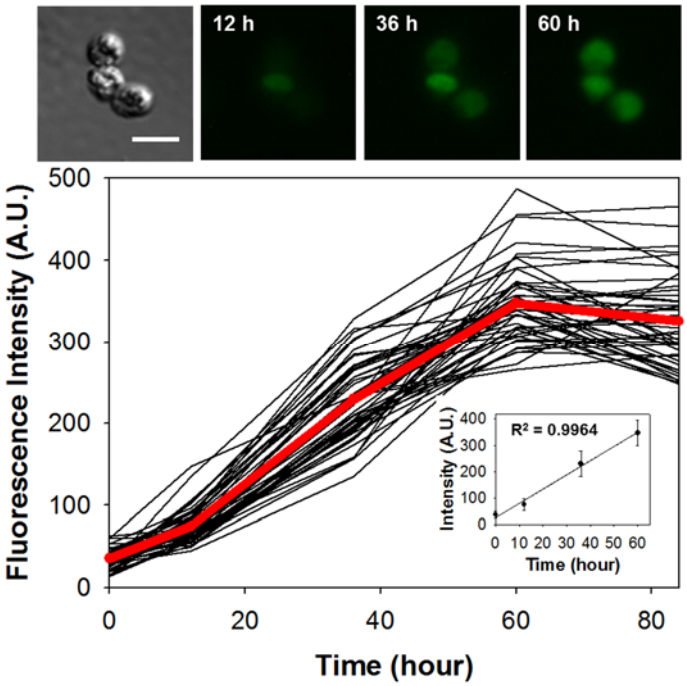

Figure 3.8. Time-lapse images of intracellular lipid accumulation under TAP without nitrogen source. Images were acquired at 24 h interval for 84 h. The scale bar represents 10 μm. Accumulation kinetics of the intracellular lipid. Insert show the regression result from initial to 60 h nitrogen starvation (R^2 = 0.9964). All data are expressed as the fifty single cells (black line) and their mean (red line) and a single standard deviation.

by imaging intracellular lipids stained fluorescence probe, BODIPY. BODIPY is intrinsically lipophilic molecular probe and exhibits intracellular lipids specific staining properties. This staining method enables dynamic process of lipids to be followed using time-lapse imaging. [64] Time-lapse images show that the fluorescence intensity associated with lipid droplets increase as a function of time as they are cultured in nitrogen deprivation condition. From the onset of starvation to 60 hours, the intensity increased linearly as a function of time (R^2 = 0.9964). After 60 hours the lipid accumulation plateaus and the fluorescence intensity does not increase further, in agreement with our previous report (Chapter 2) on lipid droplet growth in suspension cultured microalgae. The kinetics of lipid accumulation can be fitted by same non-linear regression and showed similar R^2 values from simple linear regression (0.9964 for microfluidic culture and 0.9876 for bulk suspension culture, respectively). This result indicates that similar trends are observed for two very different types of culture conditions and further indicate that the microalgae are not adversely affected by surface immobilization.

Although our results demonstrate qualitative trend of intracellular lipid accumulation kinetics based on semi-quantitative measurement, we are confident that when higher resolution 3D microscopy methods (*i.e.* super resolution microscopy) are used on immobilized microalgae, an accurate and detailed quantitative measurement of lipid droplet formation can be obtained.

Microalgal lipid are used as a feedstock for the production of biodiesel but the exact mechanism for lipid synthesis is still unknown. Only limited details on lipid droplets have been reported, in the beginning of starvation culture

condition, lipid droplets size starts at around 20 nm and grows to 400 nm near the end. We believe that our immobilization method will serve as a useful platform for understanding lipid droplet biogenesis, maturation as well as for optimization of culture conditions in high-throughput manner.

3.4 Conclusions

This chapter describes a simple surface immobilization approach for continuous live-cell imaging of *C. reinhardtii*, a model microalgae. Although gelatin has been already used for mammalian cell attachment, to the best our knowledge, it is the first application in microalgae. Instead of using physical traps or droplets, we took advantage of high number of *O*-glycosylated Hyp residues present in microalgal cell walls to engage in non-covalent interaction with gelatin coated surface (also with high number of Hyp residues) to capture and immobilize them. Viability and behavior of the immobilized cells were shown to be similar to suspension-cultured controls. Microalgae could be cultured for upto 6 days allowing time-lapse observation of the entire mitotic process. The cells remain immobilized under hydrodynamic shear conditions (upto 0.2 dynes/cm^2) and accumulate lipid droplets in nitrogen deprivation condition. This work represents the first demonstration of single cell imaging and quantitative analysis of lipid droplet accumulation in *C. reinhardtii* in a microfluidic platform.

Applying for a microalgal biodiesel research, it needs to verify optimal

condition for surface immobilization using various microalgal species. The present method should be considered as a “tuning” system and reconstructed with specifically optimized conditions for individual microalgal species. However, we convince that gelatin will be still valid to various microalgal species, since it confers stable affinity to both high Hyp cell wall strain and naked cell wall deficient strain. Moreover, the critical process consist of simple gelatin coating step, so it can be more convenient in time consumption with covalent bonding methods with functionalised glass substrate (*i.e.* amino, carboxyl and epoxy group) and protein coupling agents (*i.e. N*-Hydroxysuccinimide [NHS] and ethyl[dimethylaminopropyl] carbodiimide [EDC]).

Since the microfluidic technique has emerged in the past several decades, it opened a new paradigm in biological research. Microfluidic technique has appealed to biologist by overcoming limitations of conventional petri dish-based culture systems. Many researchers determined exact mechanisms of biological phenomena in mammalian cells as well as microbes due to potential application of microfluidic techniques for a more accurate spatiotemporal design of cues delivered to cells. Unlike mammalian cells, microbes are difficult to observe and perfuse in microfluidic platform due to their non-adherent property. In case of yeast, there were some solutions such as Tesla valve[29], trapping[30, 31, 33] and immobilization[32, 65] for a critical problem to study yeast in microfluidic platforms. They accelerate intensive researches to investigate single cellular responses such as signaling pathway, gene expression and phenotypic changes. Similar to the yeast, our

immobilization method will open a new era for both fundamental and applied microalgal research for biodiesel.

Combination of surface immobilization with imaging will lead to better methods to quantify and monitor lipid accumulation and open many possibilities for microfluidics based biodiesel research. High-throughput screening system for selecting better microalgae strain that produce higher lipid content can be developed. Furthermore, real-time monitoring and analysis of lipid accumulation using single cell imaging will allow rapid optimization of microalgae culture conditions to maximize lipid production. We believe that microfluidics will play an important role in future fundamental and applied microalgal biodiesel researches.

Chapter 4. Preventing small hydrophobic molecule absorption on PDMS microchannel

4.1 Introduction

Microfluidics is well defined techniques to provide opportunity for taking a benefit to system biological experimentation. [66] Microfluidics technique has always appealed to biologist due to their capability of manipulating extracellular environments and controlling single cell level treatment using biochemical cues. As a result, many researchers have enhanced understandings of biological phenomena through precise spatially and temporally controlled microenvironments in an *in vitro* system. [66, 67, 68]

To investigate single cell analysis that serves accurate understandings of biological phenomena, there needs various types of fluorescence probes and biochemical cues. Most of the probes and cues have a hydrophobic property, so it is easy to absorb or penetrate into PDMS, which is the main component of microfluidic system. Due to high permeability and hydrophobicity of PDMS[45], it is hard to observe and manipulate single cellular behavior with their unwanted absorption. To solve the problem given these properties, several approaches have been explored to prevent unwanted small hydrophobic molecule absorption though coating with parylene[69], paraffin wax[70] and poly(vinylmrthylsiloxane) (PVMS)[71].

Here, we present a new simple method for preventing unwanted

hydrophobic molecule absorption on PDMS device using Teflon coating. Teflon is the best-known material developed by DuPont Company. Teflon has been already used in a wide range of areas (*i.e.* optical materials, semiconductor, fibre optics and biomedical materials) due to its optical transparency, thermal stability, biocompatibility, high gas permeability and solvent resistance properties[72]. The major advantage of Teflon is "non-stick" property, so it is often used to a coating material for cooking ware like frying pans. Given its non-adherent property, we assumed that Teflon-coating method is applicable to inhibit unwanted absorption in microfluidic system same as previously developed other methods. We believe that our new method will take a role for accurate quantitative analytical solution for microfluidic system with fluorescence probes and biochemical cues. Especially, this method will serve more powerful tool for high-throughput screening systems and single cellular level dynamics of lipid accumulations in the field of biodiesel research by measuring lipid content of microalgae.

4.2 Materials and methods

4.2.1 Materials

Polydimethylsiloxane (PDMS), Sylgard 184, was purchased from Dow Corning (Midland, MI). SU-8 negative photoresist was purchased from Micro-Chem Corp. (Newton, MA). Teflon® AF solution was purchased from

DuPont™ (Wilmington, DE). All other chemicals and reagents used in this study were purchased from Sigma–Aldrich unless otherwise mentioned.

4.2.2 Microfluidic device fabrication

Devices were fabricated by soft lithography. Photolithography using SU-8 negative photoresist was used to generate a master mould on a Si wafer. PDMS device was fabricated by casting and curing Sylgard 184 mixture of oligomer and curing agent (10:1, *w/w*) at 95 °C. After curing, the PDMS device was separated from the master mould and cut to obtain individual devices.

4.2.3 Teflon coating method

PDMS piece and glass coverslip were placed in plasma cleaner (Femto Science, Seoul, Korea) for 1 min (50 W), then moulded PDMS device was immediately placed on the coverslip to form a microchannel. After the bonding step, Teflon solution, which was diluted with FC-40 (3%, v/v), was introduced into the microchannel and incubated at 80 °C dry oven to generate adherence to the PDMS surfaces. When solutions were fully vaporized, PDMS device were successfully coated with Teflon. (Figure 4.1)

4.2.4 Visualization of hydrophobic molecule absorption on PDMS microchannel

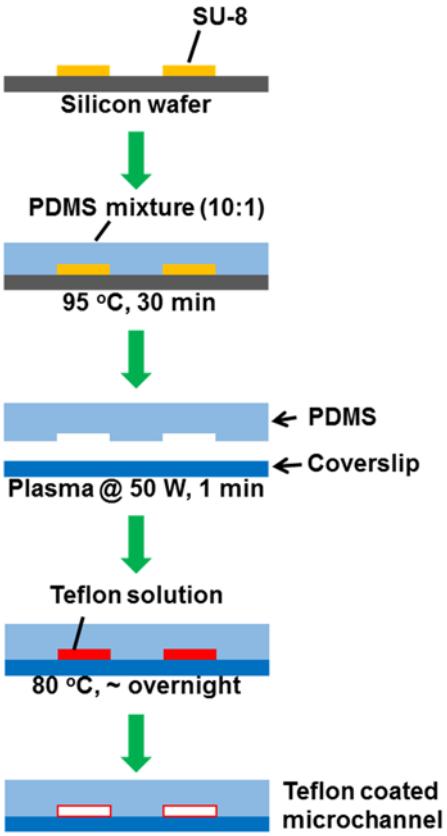

Figure 4.1. A schematic diagram showing the whole process of Teflon coating method.

Rhodmamine (500 μg/mL) and BODIPY fatty acid (1 μM) were used as indicators for demonstrating small molecule absorption on PDMS microchannels. Channels were observed with an inverted fluorescence microscope (Olympus IX81, Tokyo, Japan) equipped with a LED light source (CoolLED pE-1, NY, USA). Fluorescence images were acquired during 3 h. All acquired images were processed with ImageJ (NIH, Bethesda, MD, USA).

4.2.5 Measurement of gas permeability

We prepared a microfluidic device with a PDMS membrane and microchannels with modified monolithic fabrication method of *Quake`s* group. [73] Bottom layer contains phosphate buffer saline (PBS, pH 7.0) and dissolved oxygen (DO) level indicator, ruthenium tris(2,2'-dipyridyl) dichloride hexahydrate (RTDP), which represents DO-dependent fluorescence intensity. We continuously injected 1 M sodium sulfite (Na_2SO_3) as an oxygen scavenger into a top channel and measured fluorescence profile of bottom channel during 6 hours with an inverted fluorescence microscope (Olympus IX81, Tokyo, Japan) equipped with a LED light source (CoolLED pE-1, NY, USA). All acquired images were processed with ImageJ (NIH, Bethesda, MD, USA).

4.2.6 Transparent measurement of PDMS

Transparency of Teflon coated and bare PDMS were measure with UV-VIS spectrometer (GeneQuant 1300, GE Healthcare). All spectra were

measured by wavelength scan mode (280 to 900 nm).

4.3 Results

The main goal of this chapter is to generate PDMS microchannel that resist small hydrophobic molecule absorption. All of the fluorescence probe for detecting intracellular lipid droplets are based on their small molecular size and hydrophobic property, so it is easy to penetrate into PDMS.

Here, we presents a solution for one of drawbacks of PDMS; small molecules absorption. This chapter describes a simple method for preventing unwanted absorption of small molecules on microfluidic platforms.

4.3.1 PDMS microchannel that resist hydrophobic molecule absorption

We prepared Teflon-coated PDMS microchannel by deposition method as shown in figure 4.1. We sought to validate some of the advantages of Teflon-coated PDMS device. We demonstrated that Teflon-coating resists small molecule absorption though rhodamine (500 μg/ml). Figure 4.2 shows the compared result between bare and Teflon-coated PDMS microchannel. After 3 hours of exposure, rhodamine filed in PDMS channel shows a significant smear of rhodamine to sidewalls of microchannel. (Figure 4.2A) However, Teflon-coated microchannel shows non-absorption of rhodamine.

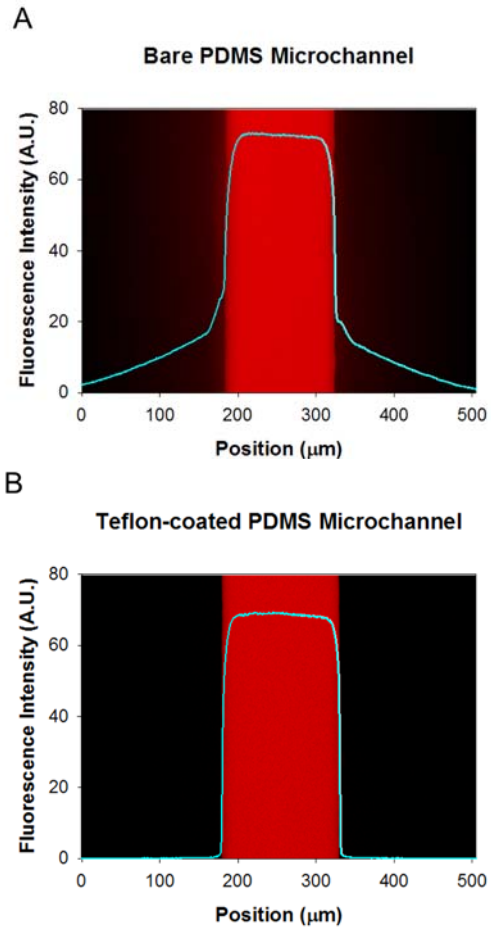

Figure 4.2. Fluorescence micrographs and fluorescence intensity profiles of PDMS microchannels with rhodamine (500 μg/ml). The channel was 140 μm in width and 100 μm in height. Fluorescence signal of (A) bare PDMS and (B) Teflon coated microchannels exposed to rhodamine dye for 3 hours.

(Figure 4.2B) As shown in the cross sectional profile of rhodamine fluorescence intensities, the profile of Teflon-coated microchannel shows well-matched physical geometry of microchannel. However, bare PDMS microchannel shows significant increase of fluorescence intensity with top and sidewalls of microchannel. Markedly enhanced non-smear effect for rhodamine indicates that we successfully realised small molecule resist PDMS *vi*a Teflon treatment.

As we already know, Teflon shows both oleophobic and hydrophobic property, we also validated that Teflon-coating resist hydrophobic molecule absorption through representative hydrophobic fluorescence probe, BODIPY. BODIPY has widely used to visualize intracellular lipid droplets due to their high sensitivity and easy to use. [74] However, it is easy to penetrate into PDMS and to represent fluorescence signal, so it is hard to observe intracellular lipid droplets with their own fluorescence signals. We tested that 0.5 % of Teflon-coating resists BODIPY absorption using PDMS micropillars. Figure4.3 shows the result between bare and Teflon-coated micropillars. As shown in compared fluorescence intensities, Teflon-coating reduces fluorescence intensities of both micropillar and microchannel. Especially, intensity of Teflon-coated PDMS shows 10-fold lower than bare PDMS. Throughout the results from rhodamine and BODIPY prevention, the proper characteristics of Teflon, hydrophobicity and oleophobicity, take a fundamental role to inhibit unwanted absorption.

4.3.2 Characteristics of Teflon coated PDMS microchannel

The main component of microfluidic platform, PDMS, has been

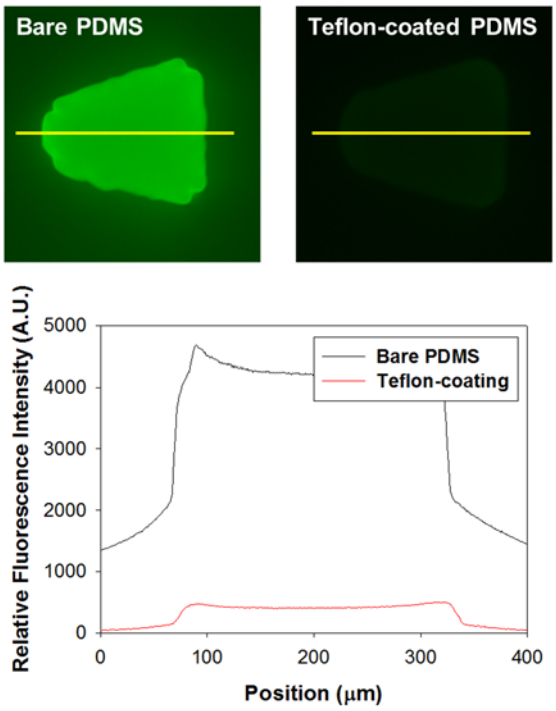

Figure 4.3. Fluorescence micrographs and fluorescence intensity profiles of PDMS micropillar with 1 μM of BODIPY-fatty acid. The cross sectional profiles represents yellow lines of micropillar.

wildly used on the field of biological micro-electro-mechanical systems (bioMEMS) due to its optical transparency, thermal stability, biocompatibility and gas permeability. [75] As we mentioned previously, Teflon also known to have a same properties like PDMS. Gas permeability is the most important criteria for applying to biological researches, so that is the reason why silicon and glass were replaced with PDMS for culturing cells[76]. Due to this reason, we validated gas permeability of modified microchannel with O_2. We prepared a microfluidic device with a PDMS membrane and microchannels with modified monolithic fabrication method of *Quake*`s group. [73] (Figure 4.4A) Bottom layer contains phosphate buffer saline (PBS, pH 7.0) and dissolved oxygen (DO) level indicator, ruthenium tris(2,2'-dipyridyl) dichloride hexahydrate (RTDP), which represents DO-dependent fluorescence intensity. We continuously injected 1 M sodium sulfite (Na_2SO_3) as an oxygen scavenger into a top channel and measured fluorescence profile of bottom channel during 6 hours. (Figure 4.4B) Teflon coated PDMS membrane shows about 80 % of oxygen transfer rate than bare PDMS. Nevertheless, modified PDMS membrane still has gas permeability, so it is enough to apply on the biological researches.

Another important criterion for applying biological research is the transparency. The most of microfluidic system is conventionally applied to quantification assays with fluorescence probe. Fluorescence is the emission of light from absorbed appropriate excitation of wavelengths for molecular probes. Therefore, transparency of microchannel is important to validate right application of quantitative measurement. Due to these reasons, we validated

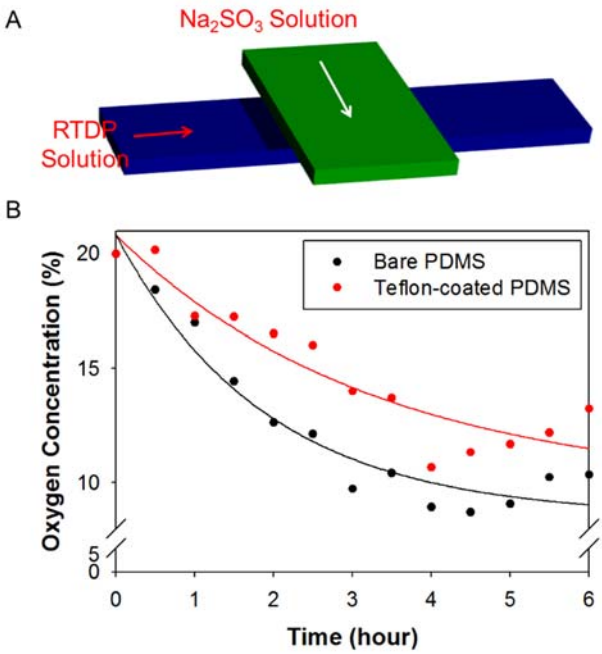

Figure 4.4. Gas permeability of Teflon-coated PDMS membrane. (A) The device is composed of two layers of microchannels. The bottom layer is for measuring dissolved oxygen level with RTDP and top layer flows oxygen scavenger solution. (B) DO level profile of bare and Teflon treated PDMS membrane. DO levels were converted from RTDP fluorescence intensities.

transparency of Teflon coated PDMS. Figure 4.5 shows the absorbance spectra of bare and Teflon treated PDMS. This result indicates that there is no significant difference between bare and Teflon treated PDMS. Especially, the most of fluorescence probes have an excitation of visible light (380 – 750 nm), so from the onset of the wavelength of visible range, each samples are well matched.

4.3.3 Cell imaging of *C. reinhardtii* on Teflon coated PDMS microchannel

Throughout the previously mentioned results, we validated that this method can be applied into a biological research. Our target application is biological lipids research. Biological lipids are recently regarded as important biomolecules with their biological functions and mechanisms. Lipids are commonly used storage of energy by transforming various classes of fatty acids. Another usage of lipids in biological system is the central architecture of biological membranes by phospholipid and glycolipids. Moreover, some classes of lipids play crucial roles in metabolic events as signals, cofactors and pigments.

Lipid droplet (LD) is one of unique organelle in eukaryotic cells that contains many species of lipid components including phospholipids, sterol esters and triacylglycerols. Recently, LDs have been recognized as a crucial organelle due to their participation in biogenesis, catabolism and functional activities in cell system. [77] The knowledge of LDs have an implications for

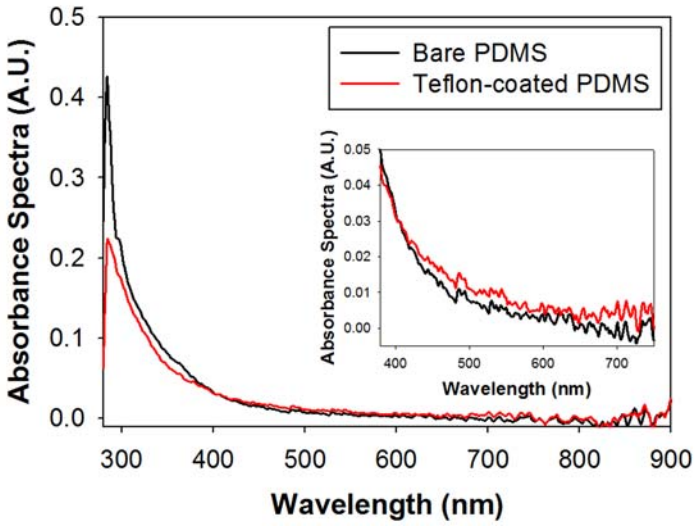

Figure 4.5. Transparency of bare and Teflon-coated PDMS. The absorbance spectra were monitored with 280 to 900 nm by taking empty cuvette as a blank.

other field of biology including human disease and biodiesel production. [27] However, still we could not get an exact answer about basal backgrounds like biogenesis and dynamics of LDs.

Based on previous results, we validate that the modified PDMS can be used to visualize microalgal intracellular LDs; *Chlamydomonas reinhardtii*. Microalgae are recently emerged microorganism as a source of biodiesel with their high lipid content. Microalgal intracellular LDs are a primary source of triacylgriceride (TAG), a crude oil for biodiesel. Previously mentioned LDs specific fluorescence probe, BODIPY-fatty acid, was tested to visualize intracellular LDs with modified and bare PDMS microchannels. Figure 4.6 shows that micrograph of N-source starved *C. reinhardtii* (CC-503; *mt*+) stained with 1 μM of BODIPY-fatty acid. As shown in bare PDMS microchannel, it is hard to visualize intracellular lipids due to their high background signal. Moreover, fluorescence intensities of cells are lower than background, so intracellular LDs are shown in dark. However, compared with bare PDMS, Teflon coating method successfully visualizes intracellular lipids. This result indicate that Teflon coating method inhibits absorption and smear of lipophilic fluorescence probe, BODIPY and further indicate that expansion of microfluidics into microalgal biodiesel research with intracellular LDs formation.

4.4 Conclusions

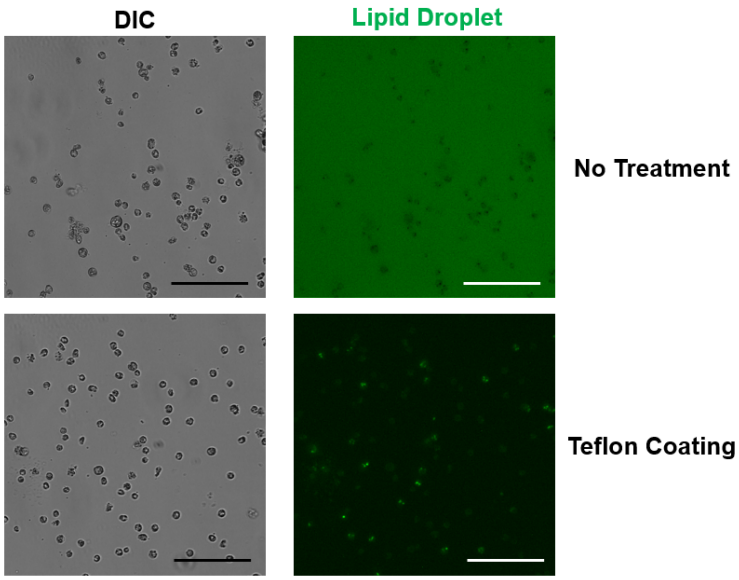

Figure 4.6. Micrographs showing a DIC image and the fluorescence of lipid droplets stained by BODIPY (in green) on bare and Teflon-coated PDMS microchannels. A microalgae, *Chlamydomonas reinhardtii* (CC-503), was incubated under nitrogen deprived condition during 5 days. The scale bar represents 100 μm.

This chapter describes an easy way to prevent unwanted small hydrophobic molecule absorption on PMDS microchannel. Conventionally, biologists have widely used polystyrene based culture platforms such as petri dishes, culture flasks and micro-well plates. Unless polystyrene based platforms do not have any smear effect for fluorescence probes, these platforms are considerably more challenging than microfluidic platforms. In the conventional cell culture system, cells are randomly seeded and their cellular responses also randomly depend on proximity and distribution. Moreover, cells are cultured in static condition, making it difficult to demonstrate spatially localized focal stimulation of signals. Microfluidics technique has appealed to biologist due to their capability of manipulating extracellular environments and controlling single cell level treatment using biochemical cues. PDMS as a material for microfluidic platform enables rapid prototyping with its low cost, easy to fabricate. As a result, microfluidics has emerged as the most rapidly advanced technologies and opened a new standard in biological researches. Nevertheless, there have been some limitations that concerns about PDMS as an appropriate material for biological researches.

Here, we presents a solution for one of drawbacks of PDMS; small molecules absorption. This paper describes a simple method for preventing unwanted absorption of small molecules on microfluidic platforms. We took advantage of oleophobic and hydrophobic properties of Teflon to prevent unwanted absorption of small molecules. We successfully demonstrated that small molecules resist PDMS *via* Teflon-coating. Teflon-coating method also does not show any significant effects on transparency and gas permeability of

PDMS.

Based on our simple method, imaging of lipid droplets in microfluidic platform will lead to better method to quantify and monitor lipid dynamics. We also convince that this method will open many possibilities for microfluidics based biological lipid researches including human disease and biodiesel production. Especially, it serves for high-throughput screening system for selecting better microalgae strain that produces high lipid contents. Furthermore, real-time monitoring and analysis of lipid accumulation will allow rapid and precise optimization of culture conditions to maximize bio-products. We believe that our method will play an important role in fundamental and applied microalgae based biodiesel researches.

Chapter 5. Quantitative measurement of *Chlamydomonas reinhardtii* on gradient generation system

5.1 Introduction

As we previously mentioned, microalgae always have not served promising future for substitution of liquid fuels. Especially, estimated cost of producing a kilogram of biodiesel from microalgae is higher than crude oil. [78] Therefore, improvement of economics of biodiesel should be proceeded for complete replace of petroleum. Many researchers have improved economics of microalgal biofuel through enhancing large-scale production has been developed improving capabilities of microalgae by bioprocess engineering such as race way ponds[79] and tubular photobioreactors[80-82]. Another strategy for improving economics of biodiesel is enhancing microalgal biology through genetically and metabolically modified microalgae. [83-85] Many researchers have been developed genetic and metabolic engineering technologies for increasing photosynthetic efficiency, growth rate, oil content and temperature tolerance. [6] Developed microalgae are also need to be recognized possible biochemical cues and environmental factors that enhance accumulation of oil contents. Many microalgae commonly produce neutral lipid (mainly triacylglyceride, TAG) under unfavorable and stressed conditions such as

nutrient starvation, temperature shift, heavy metals, change in salinity and pH, and light and UV irradiation. [86]

The lipid accumulation state can be more enhanced by combinations of different induction type and intensities. The exact combination for the best lipid productivity should be referred as a “tailor made” system on numerous microalgal species of various classes in large-scale commercial cultivation systems. However, screening for exact combinations of conditions using conventional flask scale batch culture system is both time- and labour-intensive works.

Microfluidic devices offer an excellent experimental system to investigate the biological phenomena. They can generate a biological relevant stimulus including concentration gradient, nutrient conditions and physical and chemical stresses by taking advantage of basic characteristics of laminar flow and diffusion. Moreover, microfluidic techniques have been presented a novel paradigm for screening system with their small volume fractions and high throughputs. Recently, screening system can generate more complex combinations of biochemical cues including chemicals and gas components. [87, 88]

Here, we presented a new method - single cellular imaging based quantitative measurement for *C. reinhardtii* using gradient generation system. This method can estimate single cell behaviour (*i.e.* cell size and carbon conversion; lipid droplet) under various culture conditions. Microfluidic gradient generation system is slightly modified *Jeon`s* gradient generation device (as known as *Christmas Tree device*) [89] by connecting both sides of

inlets. We have used this platform to generate stable combinations of two different nutrients with 3-inlets. These combinations were produced by controlled diffusive mixing of nutrients that flow inside a network of microchannels under conditions of low Reynolds number. We adapted previously developed technologies (*i.e.* fluorescence probe, immobilization and absorption) with microfluidic device to study single cellular microalgal behaviour by generating major nutrients combination such as carbon and nitrogen.

The application of developed microfluidic device become a useful tool for biodiesel research by helping high-throughput screening of new algal strains and rapid optimization of culture conditions.

5.2 Materials and methods

5.2.1 Materials

Chlamydomonas reinhardtii (CC-125; wild type mt+) was obtained from the *Chlamydomonas* Resource Center at the University of Minnesota (St. Paul, MN). Polydimethylsiloxane (PDMS), Sylgard 184, was purchased from Dow Corning (Midland, MI). SU-8 negative photoresist was purchased from Micro-Chem Corp. (Newton, MA). All other chemicals and reagents used in this study were purchased from Sigma–Aldrich unless otherwise mentioned.

5.2.2 Culture conditions

C. reinhardtii cells in Tris-acetate-phosphate (TAP) medium were cultured at 23 °C, 5 % CO_2 with shaking on an orbital shaker at 125 rpm. Light conditions were maintained 12 h of light (40 μmol/s/m^2) and 12 h of darkness cycles. When the optical density (O.D.) at 680 nm was approximately 1.0 (early stationary phase), the cells were removed from the flask and transferred into microfluidic device. Microfluidic device was cultured at photo-incubator as same condition with shaking incubator system.

5.2.3 Microfluidic device fabrication

Device was fabricated by soft lithography. Photolithography using SU-8 negative photoresist was used to generate a master mould on a Si wafer. PDMS device was fabricated by casting and curing Sylgard 184 mixture of oligomer and curing agent (10:1, *w/w*) at 95 °C. After curing, the PDMS device was separated from the master mould and cut to obtain individual devices. Glass coverslips were placed in plasma cleaner (Femto Science, Seoul, Korea) for 1 min (50 W) to generate a hydrophilic surface. Moulded PDMS piece was immediately placed on the clean glass coverslips to form the microchannel. Surface treatment and PDMS coating process refers to chapter 3 and 4. (Note that instead of gelatin, poly-lysine also used for immobilization and instead of Teflon coating, intensive plasma treatment also used for preventing absorption)

5.2.4 Gradient generation with flow system

Flow was generated using gastight syringe (Hamilton, NV) and a syringe pump (Harvard Apparatus PHD2000, MA). To monitor the nutrient combinations at each culture chamber, fluorescein isothiocyanate (FITC) was used to validate device characterization. Fluorescence micrographs were obtained with an inverted fluorescence microscope (Olympus IX81, Tokyo, Japan) equipped with a LED light source (CoolLED pE-1, NY, USA). All acquired images were processed with ImageJ (NIH, Bethesda, MD, USA).

5.2.5 Visualization and quantification of *C. reinhardtii*

Intracellular lipid droplet in *C. reinhardtii* were treated with 1 μM BODIPY (or Nile Red) for 10 min. After the staining, cells were washed with fresh medium. Cells were observed with an inverted fluorescence microscope (Olympus IX81, Tokyo, Japan) equipped with a LED light source (CoolLED pE-1, NY, USA). All acquired images were processed with ImageJ (NIH, Bethesda, MD, USA). Acquired micrographs were converted into binary image by application of the threshold function to ensure single cell segmentation.

5.3 Results

Microalgae is the unicellular species, which exist individually. Unlike higher plants, microalgae do not have roots and leaves. However, same with higher plants, they have a chlorophyll that performs photosynthesis to produce O_2 by consuming CO_2. Due to this reason, their growth and development are affected by nutrients like higher plants such as C, H, O, N, P, K, S, Ca, Mg, Fe and other micronutrients. Conventionally, optimal growth condition for microalgae leads large amount of biomass with relatively low lipid droplet contents. As we previously mentioned, to improving economics of biodiesel, many researchers considered increase lipid droplet contents through the inductions of lipid biosynthesis by environmental stresses. [86] There are several methods for lipid inducing stress conditions such as nutrient starvation, temperature stress, osmolality and pH change and light or UV irradiation. However, those methods are only focused on the single cellular lipid contents, not considering whole mass of total system with their relatively low growth yields. Moreover, the most of experimental results are based on the flask scaled culture system (or batch culture system). When we apply those results for mass culture system (or continuous culture system), it does not guarantee the promising result for enhancing economics of biodiesel with their different culture system.

Microfluidic system, we called it as a "μ-chemostat", is similar with continuous culture system with continuously perfused fresh medium. [90] By taking advantages of basic characteristics of laminar flow and diffusion, we

developed microfluidic based screening platform for optimal growth and lipid accumulation with different nutrient combinations. The main goal of this chapter is finding optimal condition for maximizing economics of biodiesel.

5.3.1 Device design and validation for gradient generation

Figure 5.1A shows an actual microfluidic device with food dye (red, blue and yellow). Microfluidic gradient generation system is composed of a piece of PDMS with an embedded network of microchannels enclosed with a glass coverslip (75 × 55 mm). Device is functionally composed of a single layer with a disk shaped arrangement of the components, which include a microchannel network (100 μm width × 50 μm height), twelve cell culture chambers (2.2 mm width × 3.5 mm length × 50 μm height) and three inlets and twelve outlets. The channel network structure was considered to generate linear gradient at each chambers. Inlets were arranged into the device with a first-circle outline for the sufficient diffusive mixing of each solutions under conditions of low Reynolds number. Six hemisphere shaped serpentine channels were connected in the second-circle outline with twelve intersections. As flow streams infused the network, they were repeatedly split, mixed. After two generations of branched systems, each branch generated 12 different combinations of chemical concentrations.

The analysis of the splitting of flow can be understood as following infused flow rates. When infuse rate bellows about 200 μL/hr, the Reynolds number is low, *i.e.* $Re << 1$. In this case, the inertial forces are assumed to be

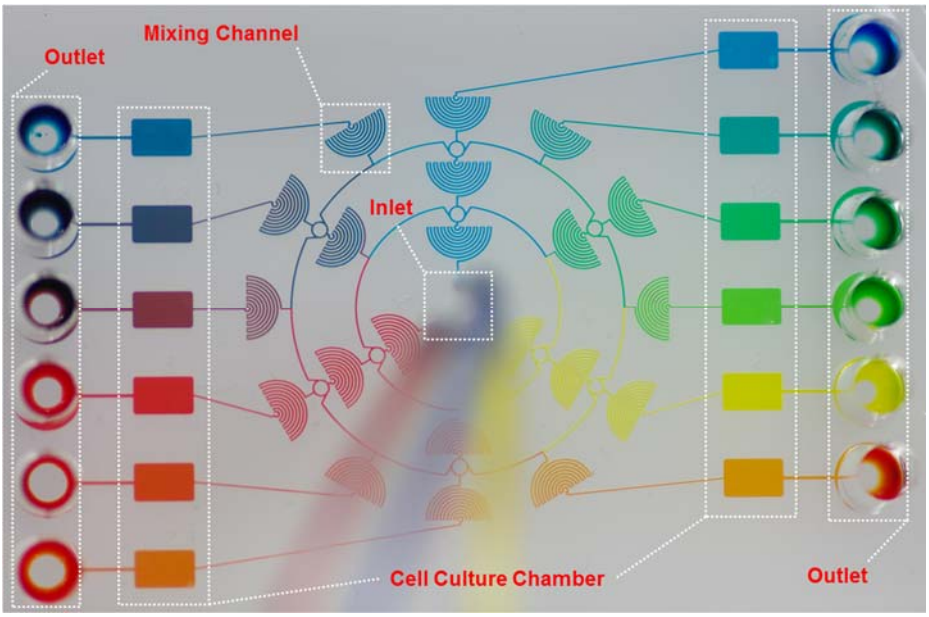

Figure 5.1. Microfluidic gradient generation device. The actual microfluidic gradient combinations marked with food dyes (blue, red and yellow).

negligible compared with the viscous force of Navier-Stokes equation, we called it as a Stokes flow. We considered that the splitting of flow ratio is converged to 1:2:1. As shown in Figure 5.2A, we generated linear concentration gradients calculated fluorescence intensity from fluorescein isothiocyanate (FITC) with various flow rates. The simulated result with computational fluid dynamics (CFD) also well matched with experimental result. (Figure 5.2B)

Considering flow rates for applying microalgal research, $Re << 1$ is sufficiently useful to investigate typical experiments using gradient generation system as previously mentioned at chapter 3. Nevertheless, if there need a use of higher flow rate, $Re > 1$, we need to consider the splitting of flow due to resistance differences between horizontal and vertical channels. Conventionally, the resistance in microchannel is affected by flow scales linearly with length of the channel in Hagen-Poiseuille flow. In this platform, we adapted rotary shaped split system to maintain splitting of flow ratio as converged into 1:2:1. When we applied high flow rate ($Re > 1$) on CFD simulation, rotary shaped split system shows similar flow rates on first circle outline as converged into 1:2:1 ratio on junctions. (Figure 5.3)

5.3.2 Carbon source dependent quantitative measurement

Nutrients are significantly impact on growth and development of microalgae. When nutrients are limited, microalgal cell division rate is steadily decreasing. In this situation, there is no requirements for the synthesis of new

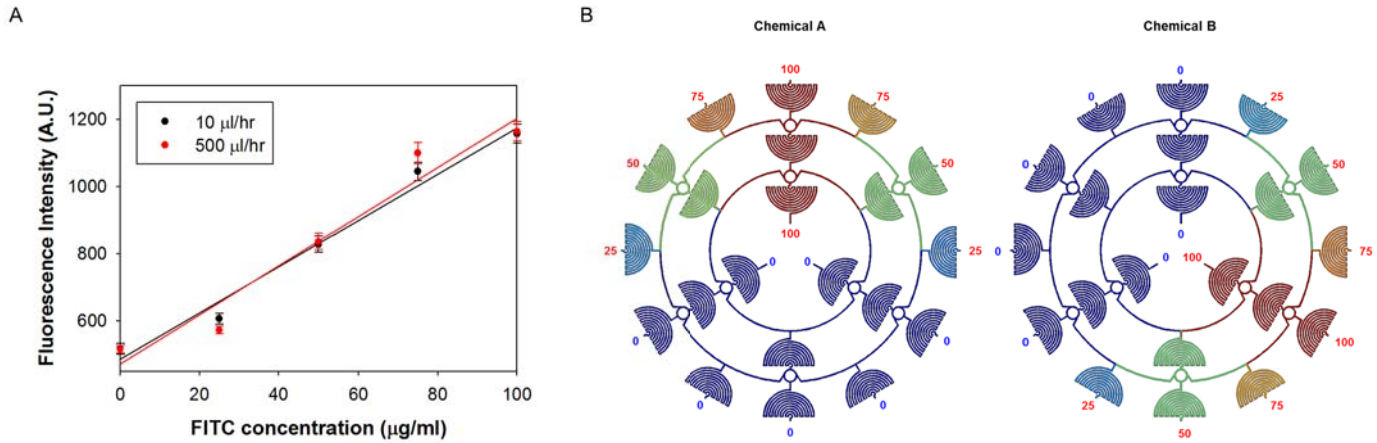

Figure 5.2. Validation for gradient generation. (A) The calculated concentration profiles of FITC in each chamber at various flow rates of 10 and 500 μl/hr. (B) Simulated image of the gradient combination profile in the microchannels.

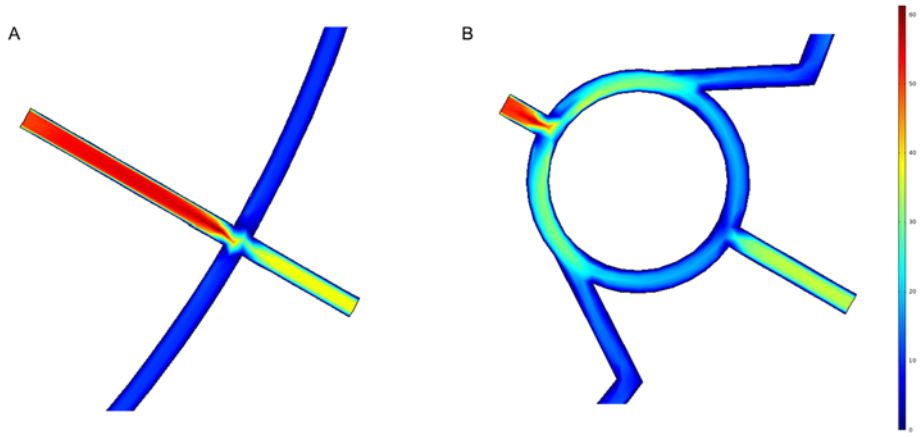

Figure 5.3. CFD simulation result of flow split system. Simulated image of (A) cross-shaped and (B) rotary shaped split system under Re > 1 (flow velocity was 0.1 m/s).

membrane, so the cells deposits fatty acids in to TAG for serving a protective mechanism.

In this section, we measured carbon concentration dependent cell size and intracellular lipid content by analyzing microscopic micrographs. As we previously mentioned, carbon is the most important nutrient for microalgae, so the first experimental target is carbon concentration dependent single cell measurement. Figure 5.4A shows the correlation of single cell between cell size and lipid contents. This results indicate that cell size and lipid contents are linearly correlated at every concentrations. As shown in figure 5.4B, average cell size were increased as decreasing carbon concentrations. Especially, just started reducing 25 % of carbon source, cell sizes were increased about 36.3 % (from 34.1 to 46.5 μm^2). Below 75 % of normal culture condition, there were quite similar cell sizes under each conditions. Figure 5.4C also indicates that different carbon concentrations influences the intracellular lipid contents. As reducing carbon source, average lipid contents were slightly increased from 2.8 to 4.8 %. From overall effects from carbon source, cell size were extensively affected by carbon source, but lipid contents were not. This means that carbon is the major source for cell growth and division. As previous researches indicated[91], minimal medium (by omitting carbon source, acetate, form TAP medium) have been used for synchronizing growth of *C. reinhardtii*. They indicated that cells are continuously increased their cell size without entering G1 phase at conventional flask (batch) culture system. However, in μ-chemostat, only reducing 25 % of carbon source, cells perceive minimal condition to divide under continuous culture system. By considering entire relation between

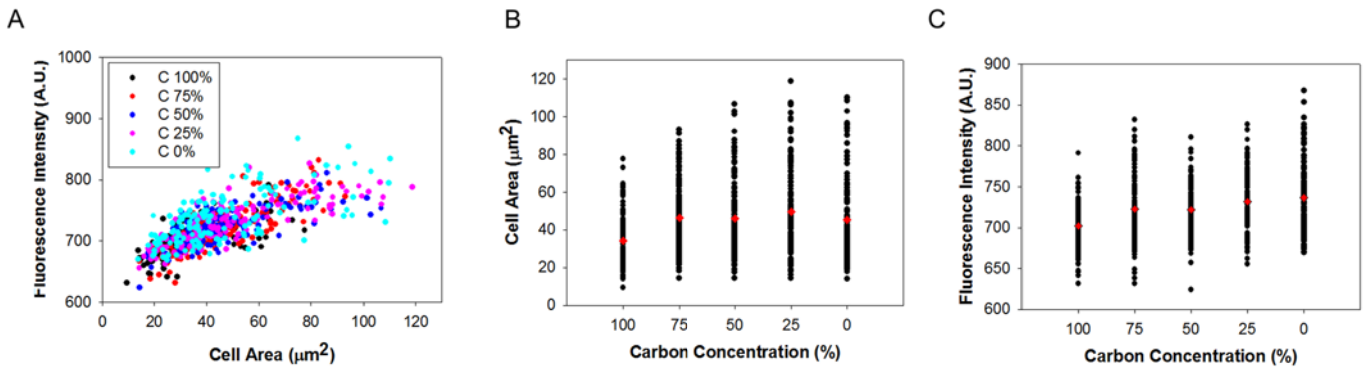

Figure 5.4. Carbon source dependent single cell measurements. (A) Correlation between cell size and lipid contents at every concentrations. (B) Carbon dependent cell size and (C) lipid contents of each cells. Red diamond (◆) indicates that average size and lipid contents at every concentrations. All data are expressed as the 150 single cells (dot) and their mean (diamond).

cell size and carbon source, μ-chemostat is sufficiently available to understand single cellular behavior under definitive condition, which could not be available under conventional culture system with concentration change as time goes by.

5.3.3 Nitrogen source dependent quantitative measurement

Nitrogen is one of the most critical nutrient affecting lipid metabolism in microalgae. Many researches revealed that nitrogen limitation alter microalgal biosynthetic metabolic pathway toward the formation and accumulation of intracellular lipid contents. [86] Based on previous researches, it is true that among the all nutrient deprivation approaches, nitrogen deprivation technique is most widely used to consider production of biodiesel.

As same with carbon dependent quantification, in this section, we measured nitrogen concentration dependent cell size and intracellular lipid content by analyzing microscopic micrographs. Figure 5.5A shows the correlation of single cell between cell size and lipid contents. This result shows that cell size and lipid contents are linearly correlated at every concentrations as same with carbon source. As shown in figure 5.5B, average cell size were linearly increased as a function of concentration from 100 to 25 %. Especially, by reducing 75 % of nitrogen source, cell size were maximized about 69.1 % (from 34.1 to 57.7 μm^2). No further size increase was observed after 75 % of deprivation. Figure 5.5C also indicates that different nitrogen concentrations influences intracellular lipid contents. As depriving nitrogen source, average lipid contents were increased at overall deprived conditions. The most

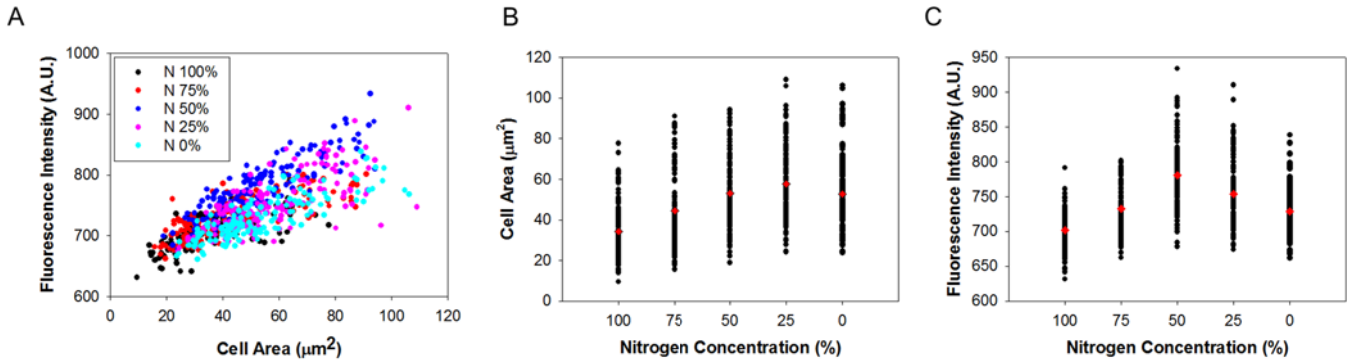

Figure 5.5. Nitrogen source dependent single cell measurements. (A) Correlation between cell size and lipid contents at every concentrations. (B) Nitrogen dependent cell size and (C) lipid contents of each cells. Red diamond (◆) indicates that average size and lipid contents at every concentrations. All data are expressed as the 150 single cells (dot) and their mean (diamond).

interesting thing is maximized lipid content was observed at 50 % of deprivation (11.2 % of increase), not 100 % of deprivation (3.8 % of increase). This result reveals that fully deprived nitrogen source could not serve a promising results under continuous culture system. Previously reported conventional nitrogen based lipid induction [86] was only focused "fully" deprived nitrogen source for maximizing intracellular lipid contents under batch culture system. However, those methods are only focused on the single cellular lipid contents, not considering whole mass of total system with their relatively low growth yields. When scaled up those results for mass culture system (or continuous culture system), it does not guarantee the promising result for enhancing economics of biodiesel. Based on our results, in continuous culture system, it would be better to reduce only half of nitrogen source by considering economics of biodiesel with mass culture system.

5.3.4 Combinations of carbon and nitrogen sources dependent quantitative measurement

Including previous sections, many researches only focused on single nutrient deprivation effect on biodiesel production using all the microalgae species. Our developed gradient generation system validates not only single nutrient effect but also combinatory effect of two different nutrients at single platform.

In this section, we measured combinatory effect of carbon and nitrogen ratio by analyzing microscopic micrographs. Figure 5.6A shows the

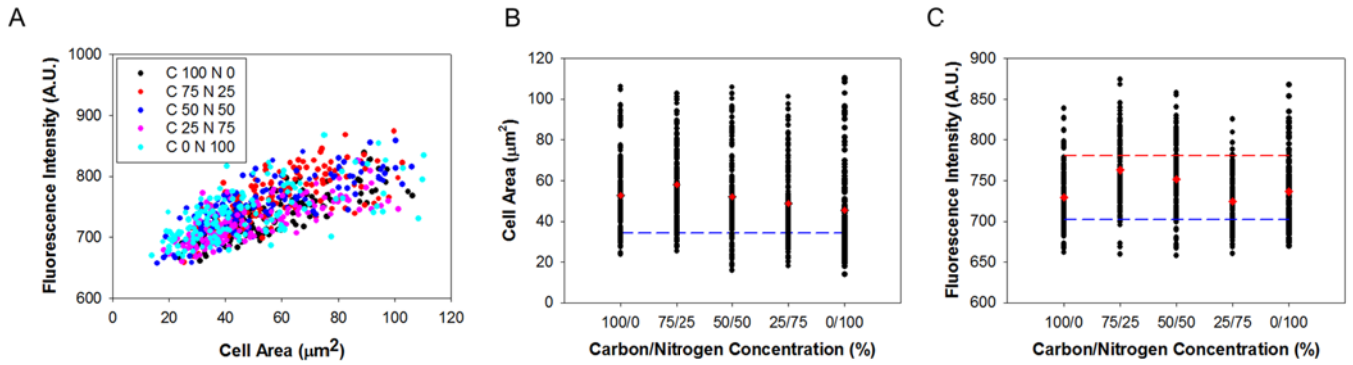

Figure 5.6. Carbon and nitrogen sources combination dependent single cell measurements. (A) Correlation between cell size and lipid contents at every combinations. (B) Cell size and (C) lipid contents of each cells. Red diamond (◆) indicates that average size and lipid contents at every concentrations. Blue dashed line (- - -) indicates average cell size and lipid contents at optimal cell culture condition (100 % of C and N). Red dashed line (- - -) indicates maximized lipid contents at 50 % of nitrogen deprived condition. All data are expressed as the 150 single cells (dot) and their mean (diamond).

correlation between cell size and lipid content under combinations of carbon and nitrogen. This result also shows that cell size and lipid contents are linearly correlated at every combinations as same with carbon and nitrogen sources. As shown in figure 5.6B, compared with optimal culture condition (100 % of carbon and nitrogen), average cell size were increased at all combinations. Combination of 75 and 25 % (carbon and nitrogen, respectively) shows the largest cell increase (70.1 %) as similar with 25 % of nitrogen concentration (69.1 % of increase). Moreover, under the different combinations, trend of cell size was almost same with nitrogen effect. Their trends were well fitted by regression (R^2 = 0.9465). This result indicate that increase of cell size is only depends on nitrogen concentrations. Figure 5.6C also indicates that different combinations influences intracellular lipid contents. Compared with optimal culture condition, intracellular lipid contents were increased at all combinations. Unlike with cell size, lipid contents did not show any similar trend with carbon and nitrogen effects, respectively. The optimal combination for maximizing lipid content (75 and 25 % of C and N) could not reach to 50 % of nitrogen deprivation. We assumed that molecular pathway of lipid accumulation is depended on various synthesis mechanisms such as fatty acid synthesis and Calvin`s cycle[85], so nitrogen effect was diminished or boosted by different carbon concentrations at each points.

5.4 Conclusion

To realize economics of biodiesel production, the exact culture condition for the best intracellular lipid productivity should be referred as a "tailor made" system in large-scale continuous culture system. However, previous researches only focused on flask (batch) culture system for enhancing lipid productivity. Moreover, they only focused on the single cellular lipid contents, instead of considering whole product of total culture system with their relatively low growth yield. Due to these reasons, previous results could not guarantee the promising strategy for achieving economics of biodiesel with their different system and point of view.

This chapter describes a new method – single cellular imaging based quantitative measurement for *C. reinhardtii* using gradient generation system. Throughout clearing considered issues, represented at previous chapters, we suggested a novel paradigm, never discussed, which could guarantee the most promising method for economics of biodiesel. This method could estimate single cellular behavior such as cell size and lipid contents under various combinations of nutrients under miniaturized continuous culture system, we called it as a μ-chemostat. In this system, we validated that single cellular behavior under continuous culture did not show similar results of conventional flask (batch culture). Fully deprived nitrogen source shows the best condition for maximizing lipid contents under the batch culture, but rather half of deprivation is the best under the continuous culture. Moreover, half of deprivation does not show significant inhibition for cell growth and development. The point of view at whole culture system, half deprivation could serve a promising method for achieving economics of biodiesel. This platform

also takes a role for serving an exact way to understand intracellular molecular pathway for investigating system biology.

In this chapter, we just started the first step toward biodiesel research which have not tried. The applications of developed platform become a useful tool for biodiesel research as well as microalgal system biology by helping high-throughput screening and biological relevant stimulus.

Chapter 6. Effect of mechanical vibration and sound on *Chlamydomonas reinhardtii*

6.1 Introduction

Mechanotransduction is defined as a cellular response that converts mechanical stimuli into biochemical signals. [92] Cells are sensitive and responsive to their physical surroundings such as external force and tension. However, there have been intensive researches for understanding mechanotransduction during past decades; many researchers are still finding the answer for molecular basis. Nevertheless, it seems that recognition and response to mechanical stimuli have an effect on the growth and functions of cells. [93] Mechanical stimulus has been used to promote differentiation of mammalian cells. One of the most commonly used mechanical stimuli is cyclic strain through tensile stress. [94-98] Previous reports revealed the positive effect of mechanical stimuli as a clinical treatments in the field of tissue engineering and stem cell therapy. [99-103]

Here, we describe a new method for enhancing growth rate and lipid accumulation through mechanical stimulus using vibration and sound system. Although microalgal system were so complicated to understand entire biological pathway, we investigated the biological effect of microalgae using mechanical vibration and sound.

6.2 Materials and methods

6.2.1 Materials

Chlamydomonas reinhardtii (CC-125; wild type mt+) was obtained from the *Chlamydomonas* Resource Center at the University of Minnesota (St. Paul, MN). Other chemicals and reagents used in this study were purchased from Sigma–Aldrich unless otherwise mentioned.

6.2.2 Culture conditions

C. reinhardtii (CC-125) were cultured on 1 % of agar plate (*w/v*) with TAP (Tris acetate phosphate) medium at 23 ^{o}C. The cultures were exposed to 12 hour cycles of light (40 μmol/s/m^2) and dark. Each plates were cultured at various frequencies.

6.2.3 Mechanical vibration generation system

Mechanical vibration generation system was provided from Turbosonic apparatus (Turbosonic Korea, Seoul, Korea). The device generates horizontal vibration *via* different frequencies of 10, 30, 50 and 100 Hz at the same maximum acceleration (0.3 G). Each frequency was controlled by applied voltage from amplifier for making a same maximum acceleration. All

acceleration profile was measured by gravity sensor (G-MEN DR20, Nagano, Japan).

6.2.4 Sound generation system

Sound were generated from commercially available speaker (Wallsound, Seoul, Korea). The speaker generates acoustic wave *via* different frequencies of 10, 100, 1000 and 10000 Hz at the same sound pressure level (65 dB). Each frequencies were generated by sine wave function with MATLAB program.

6.2.5 Measurement of growth for solid culture system

Colony growth and development was monitored with an inverted microscope (Olympus IX71, Tokyo, Japan). All acquired images were processed with ImageJ (NIH, Bethesda, MD, USA). Acquired micrographs were converted into binary image by application of the threshold function to ensure single cell segmentation.

6.2.6 Measurement of growth kinetics for liquid culture system

Growth kinetics was monitored with optical density (O.D.) at 750 nm. During the incubation, each tube was measured with a UV/VIS spectrometer (GeneQuant 1300, GE Healthcare Life Sciences).

6.2.7 F_v/F_m measurement

F_v/F_m was measured with a Walz PAM imaging system (Imaging PAM M-Series, Effeltrich, Germany). Cultured cells on agar plate were dark-adapted for a 10 min before measurement.

6.2.8 Measurement of intracellular lipid contents

Intracellular lipid contents was measured by SF44 fluorescence at 540 nm with excitation at 450 nm. Cells (198 μL) were combined with 100 μM of SF44 in DMSO (2 μL) to a final volume of 200 μL. Fluorescence was measured with a luminescence spectrometer (LS-55, Perkin-Elmer).

6.3 Results

6.3.1 Mechanical vibration generation

Mechanical vibration is defined as a motion of oscillations. Mechanical vibration system generates horizontal vibration *via* different frequencies. (Figure 6.1A) Frequencies were controlled by applied voltage from amplifier for making a simple harmonic oscillation. Simple harmonic motion is the motion that a displacement exhibits when under the influence of an external force of the form represented by *Hooke`s law*. The oscillation describes as a sine wave function.

$$x(t) = A\sin(wt) = A\sin(2\pi ft) \quad - \quad (1)$$

Here, x is the phase of displacement, w is called the angular velocity of the oscillation and A is called the amplitude of the oscillation. Note that angular velocity is normally converted to frequency ($w = 2\pi f$). f is called frequency which describes how cycles of oscillation per second and measured in units of hertz (Hz). From the wave function of displacement *Eq. (1)*, we find the velocity of the oscillation at any time t.

$$v(t) = \frac{d\,x(t)}{dt} = wA\cos(wt) \quad - \quad (2)$$

Further, it is also shown that the acceleration at any time t is

$$a(t) = \frac{d\,v(t)}{dt} = -w^2A\sin(wt) = -w^2x(t) \quad - \quad (3)$$

Multiplying *Eq. (3)* by the mass m, we find the net force on oscillation system represented by *Newton`s second law*.

$$F(x) = ma(t) = -mw^2x(t) \quad - \quad (4)$$

Our goal is to validate mechanical vibration effect on microalgal proliferation and development at different frequencies. We want to focus on effect of vibration frequency on microalgae. We adjusted same maximum acceleration value for making a same maximum external force from *Eq. (4)*.

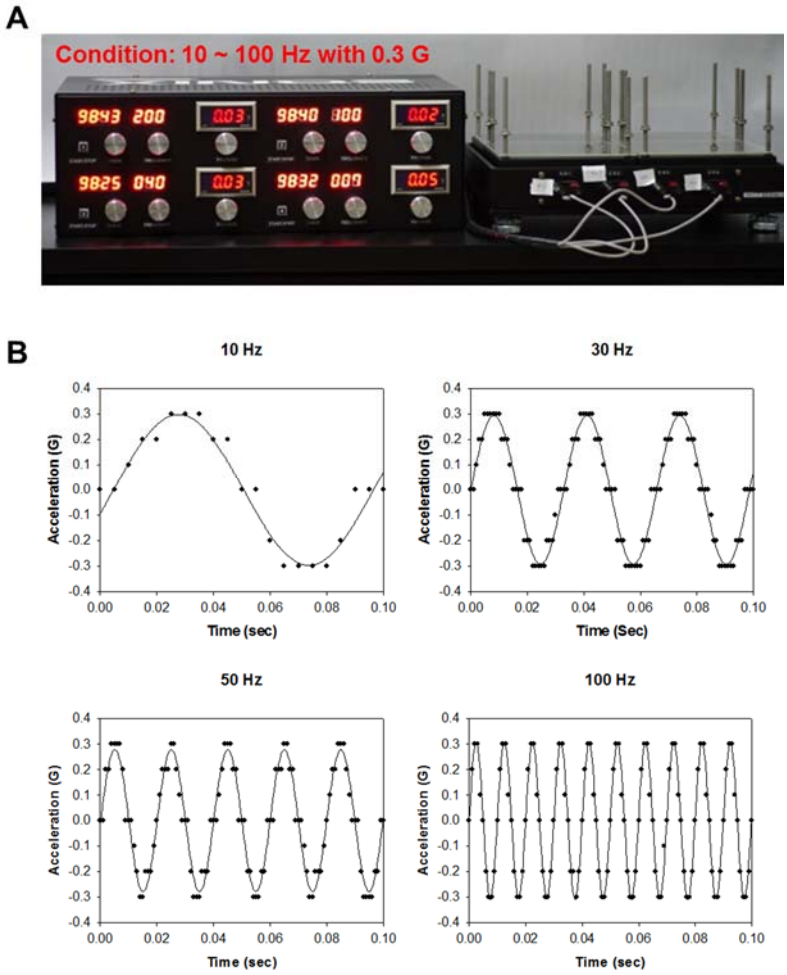

Figure 6.1. Mechanical vibration generation system. (A) System configuration and (B) their acceleration profile measured with gravity sensor at each frequencies.

Figure 6.1B shows validated acceleration profile measured with gravity sensor at different frequencies. Mechanical vibration system generates ideal simple harmonic oscillation motion at all frequencies. Their maximum acceleration is adjusted on 0.3 G (2.97 m/s^2) and frequency was validated from period T ($f = 1/T$).

6.3.2 Mechanical vibration effect on microalgal proliferation

Our goal is to validate mechanical vibration effect on proliferation and development of *Chlamydomonas reinhardtii*, as a model organism of microalgae. Solid culture system (agar plate) is advantageous because cultured cells will proliferate in the spot where they were inoculated, giving an information to observe their distinctive proliferation and development. Especially, compared with liquid culture system, it is relatively easy to analyze vibration effect on cells by simple mass-spring-damper model.

C. reinhardtii was cultured on 1.0 % of agar plate with TAP medium under 10, 30, 50 and 100 Hz of frequencies. Figure 6.2A shows the micrograph of colonies at each conditions after 3 days of inoculation. We measured colony size and their intensity to analyze vibration effect for proliferation and development. Figure 6.2B shows the correlation of colony size and their intensity under different frequencies. This result indicate that colony size and intensity are linearly correlated as following increase of frequency. Compared with control (0 Hz), proliferation was increased with the frequency up to 50 Hz, but decreased at 100 Hz. Based on the proliferation results, we analyzed

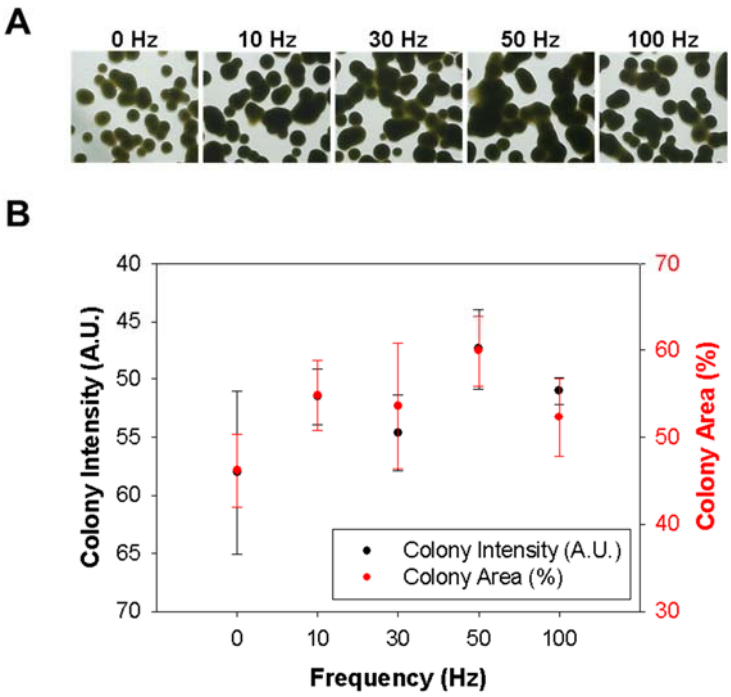

Figure 6.2. Mechanical vibration effect on *C. reinhardtii*. (A) Micrograph of colonies and (B) correlation of colony intensity (black) and their relative area (red) under different frequencies. All cells were cultured on 1.0 % of agar plate with TAP media. All data are expressed as the mean of 8 replicates and a single standard deviation.

why 50 Hz shows maximized proliferation ability by simple mass-spring-damper model. The conventional forced vibration system is represented by following equation.

$$F = m\ddot{x} + c\dot{x} + kx \quad - \quad (5)$$

Here, $F, m, c, k, \ddot{x}, \dot{x}$ and x are external force, mass, damping coefficient, stiffness, acceleration, velocity and displacement of vibration. The result from acceleration profile as shown in figure 6.1B, we know the function of external force F. When we assume that solid culture system does not have any damping system, so *Eq. (5)* is represented by following equation.

$$F = m\ddot{x} + kx \quad - \quad (6)$$

From the measured acceleration profile and stiffness, the solution of *Eq. (6)* is describes the displacement of cells in form of *Eq. (1)*. Figure 6.3 shows calculated displacement of the cells at each frequencies. It seems that tens of micrometer displacement (10 times higher than conventional cell size, 4 to 7 μm) enhances maximized proliferation ability. Although above and below ranges of tens of micrometer displacement show relatively low proliferation ability, they still show enhanced proliferation than control.

As same with higher plants, microalgal growth and development are affected by nutrient such as C, H, O, N, P, K, S, Ca, Mg, Fe and other micronutrients. C is the most important nutrient for microalgal growth. Conventional culture system, C source is supplied from TAP media in forms of acetate. When they exposed minimal media which does not contains acetate, their growth is entirely depends on their carbon conversion ability by using CO_2 in the air. Due to this reason, we want to validate mechanical vibration is

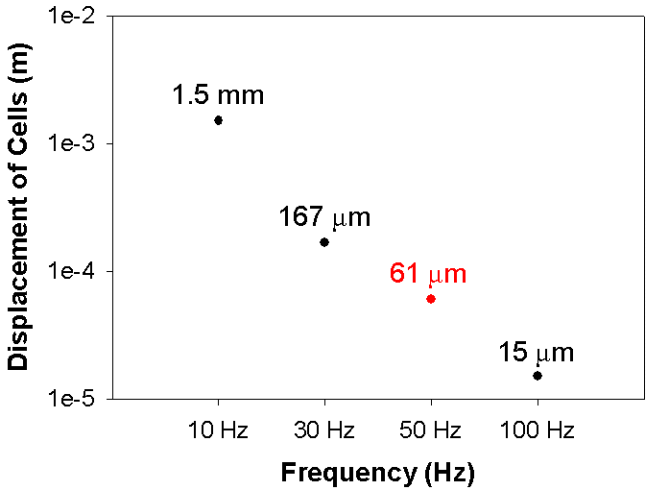

Figure 6.3. Displacement of cells on agar plate under mechanical vibration. Note that displacement of cells were calculated by simple mass-spring-damper model.

effect on proliferation and development of *Chlamydomonas reinhardtii* under minimal growth condition. Figure 6.4A shows the micrograph of colonies at each conditions after 4 days of inoculation. We measured colony size and their intensity to analyze vibration effect on growth under C source deprivation. Figure 6.4B shows the correlation of colony size and their intensity under different frequencies. This result indicate that colony size and intensity are linearly correlated as following increase of frequency (except for 30 Hz). Although all frequencies show enhanced proliferation than control, 30 Hz shows relatively low proliferation ability. Based on the proliferation results under C deprivation, we analyzed why 30 Hz shows relatively low proliferation ability by measuring F_v/F_m ratio. F_v/F_m ratio is the most wildly used test for measuring stress on photosynthetic system of chlorophyll. Figure 6.5 shows the result of F_v/F_m ratio at each frequencies. Surprisingly, 30 Hz shows small difference compared with 0 Hz (3.2 % of reduction). Other frequencies shows 8 to 16 % of reduction. It seems that mechanical vibration (except for 30 Hz) may cause the stresses on photosynthetic system, so it boosts their growth ability. On the other hand, 30 Hz of mechanical vibration causes relatively low stresses on photosynthetic system, but it still boosts growth ability compared with 0 Hz.

6.3.3 Sound generation

Previously described mechanical vibration system only generates low frequencies (below hundreds of Hz) of vibration. When we validate the effect

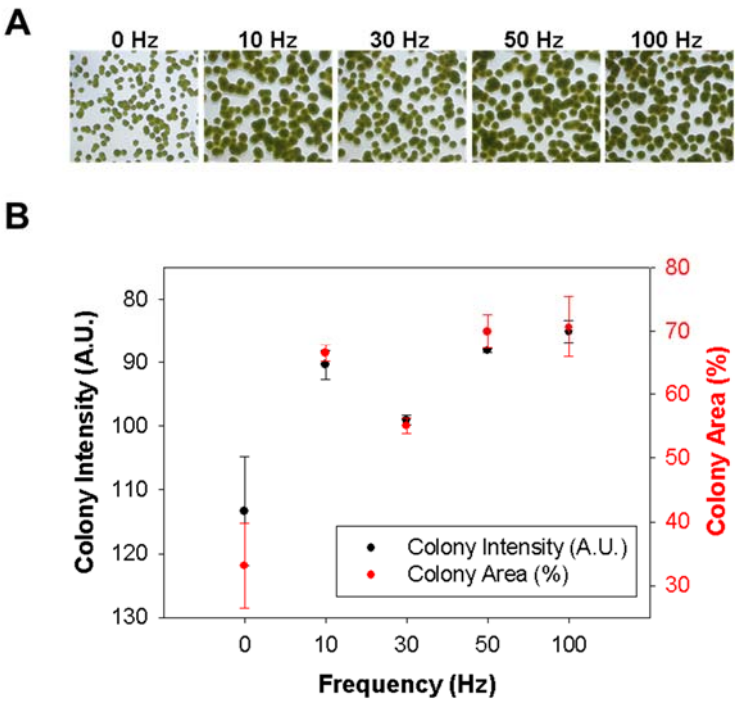

Figure 6.4. Mechanical vibration effect on carbon conversion of *C. reinhardtii*. (A) Micrograph of colonies and (B) correlation of colony intensity (black dot) and their relative area (red dot) under different frequencies. All cells were cultured on 1.0 % of agar plate with minimal media (TAP without acetate). All data are expressed as the mean of 8 replicates and a single standard deviation.

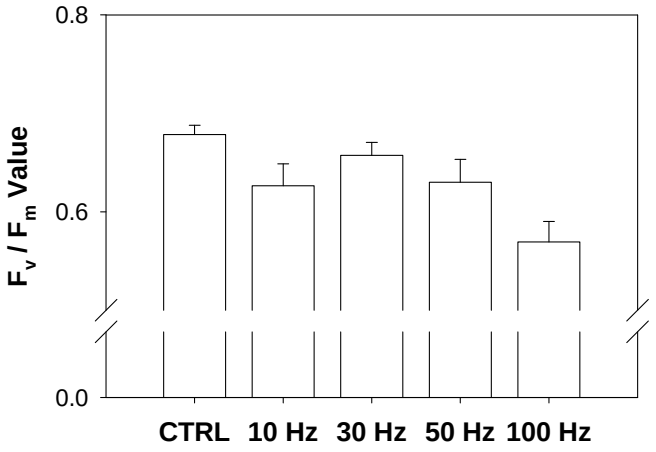

Figure 6.5. Mechanical vibration effect on F_v/F_m ratio. All data are expressed as the mean of 8 replicates and a single standard deviation.

of high frequency (more than hundreds of Hz) on microalgal proliferation and development, there need another strategy to generate higher frequencies which could not generate at mechanical vibration system. Instead of contact-based mechanical vibration, we focused on non-contact-based acoustic vibration system. The sound is a vibration that propagates wave of pressure through a medium such as air and water, so it is easy to generate high frequency of vibration. Using commercially available speaker system (Figure 6.6A), we generated acoustic wave *via* different frequencies of 10, 100, 1000 and 10000 Hz. All sound was generated by simple sine wave function from *Eq. (1)* using MATLAB program. Note that amplitude A is adjusted to each frequencies by considering same acceleration functions. The acceleration value is proportional to f^2 from *Eq. (3)*, so A is decreased as following in squire of frequencies. Figure 6.6B shows created wave sound. Their sound pressure level is adjusted on 65 dB and frequency was validated from period T $(f = 1/T)$.

6.3.4 Sound effect on microalgal proliferation and development

As same with the mechanical vibration system, we validated effect of high frequency on proliferation and development of microalgae. *C. reinhardtii* was cultured on 1.0 % of agar plate with TAP medium under 10, 100, 1000 and 10000 Hz of frequencies. Figure 6.7A shows the micrograph of colonies at each conditions after 3 days of inoculation. We measured colony size and their intensity to analyze vibration effect for proliferation. Figure 6.7B shows the correlation of colony size and their intensity under different frequencies. This

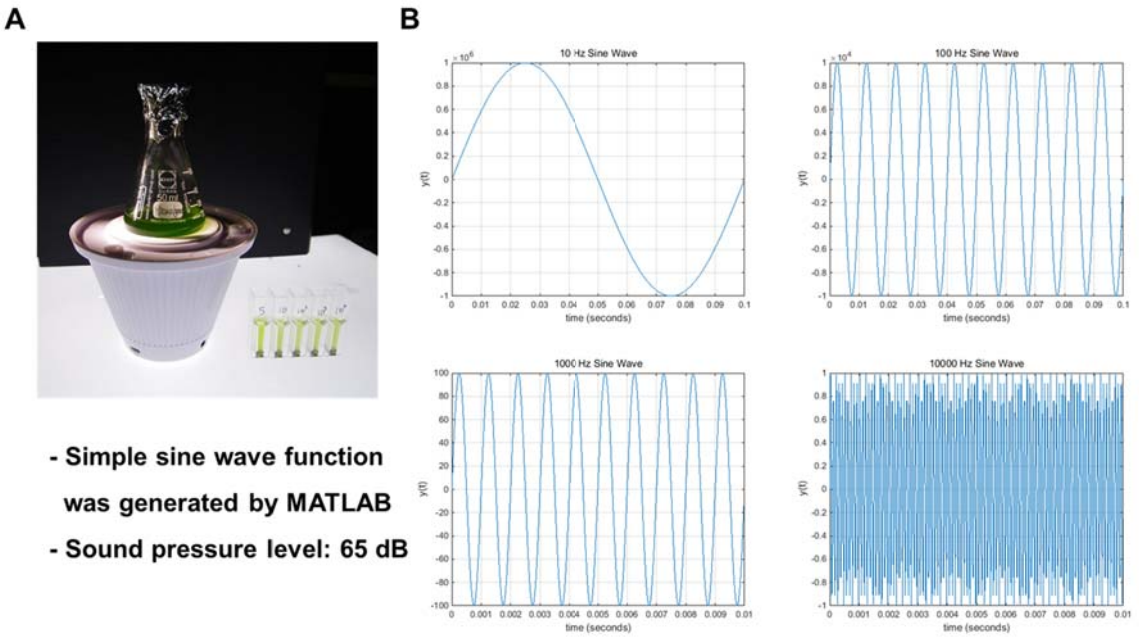

Figure 6.6. Sound generation system. (A) System configuration and (B) their sine wave profile created with MATLAB program.

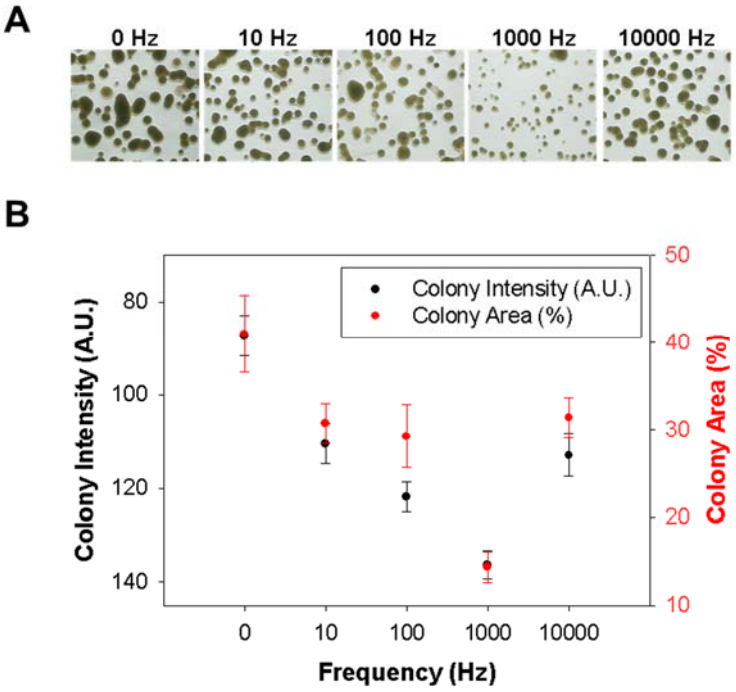

Figure 6.7. Sound effect on *C. reinhardtii*. (A) Micrograph of colonies and (B) correlation of colony intensity (black dot) and their relative area (red dot) under different frequencies. All cells were cultured on 1.0 % of agar plate with TAP media. All data are expressed as the mean of 8 replicates and a single standard deviation.

result indicate that colony size and intensity are not linearly correlated as following increase of frequency. Compared with control (0 Hz), proliferations under all frequencies were decreased with the frequency up to 1000 Hz, but 10000 Hz showed similar proliferation trend of 10 Hz. Based on the proliferation results, we also analyzed why acoustic vibration shows reduced proliferation ability by simple mass-spring-damper model. As same with mechanical vibration, the solution of *Eq. (6)* is describes the displacement of cells in form of *Eq. (1)*. Note that adjusted sound pressure level (64 dB) was converted to acceleration value 5.62e-4 m/s^2. Figure 6.8 shows calculated displacement of the cells at each frequencies. Unlike with mechanical vibration system, displacement of all frequencies are much smaller than cell size (10^{-1} to 10^{-7}), so it does not show enhanced proliferation ability than control.

Conventionally, characteristics of sound such as physical properties and speed are depend on their ambient conditions. Especially, the medium is the most critical factor for affecting on the speed of acoustic sound. For example, in the air, the speed of sound is approximately 343 m/s and in the water, it is approximately 4.3 times faster than the air (1,482 m/s). Due to this reason, we assumed that water can be a more effective medium for propagating acoustic wave effect on microalgae. Although liquid culture system is too complex to analyze physical parameters with their non-immobilized system, we want to validate effect of high frequency on microalgal proliferation and develpoement. *C. reinhardtii* was cultured on TAP medium under 10, 100, 1000 and 10000 Hz of frequencies. Figure 6.9 shows growth kinetics and their specific growth rate of *C. reinhardtii* under 10, 100, 1000 and 10000 Hz of frequencies and control

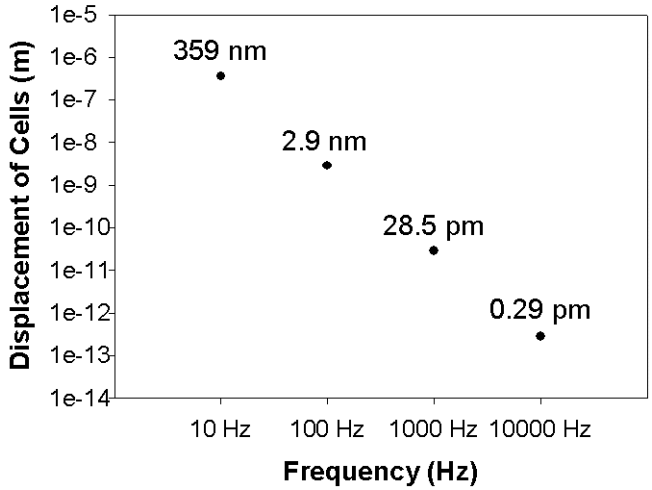

Figure 6.8. Displacement of cells on agar plate under sound system. Note that displacement of cells were calculated by simple mass-spring-damper model.

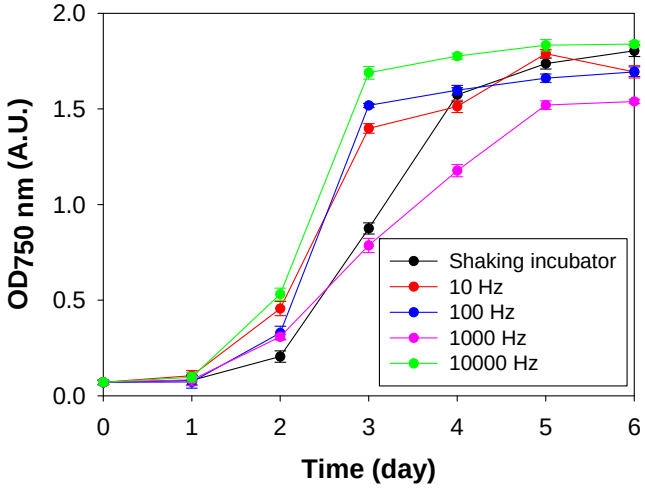

Figure 6.9. Growth kinetics of *C. reinhardtii* under sound system. All cells were cultured on TAP media and measured with $OD_{750\,nm}$. All data are expressed as the mean of 5 replicates and a single standard deviation.

(conventional shaking incubation). The result indicate that acoustic sound enhance proliferation ability compared with shaking incubation (except for 1000 Hz). After 3 days of incubation, 10, 100 and 10000 Hz of frequencies show great increase of proliferation and enter the stationary state after 5 days of incubation. However, 1000 Hz of frequency shows inhibitory effect on proliferation of *C. reinhardtii* as same with solid culture system (in figure 6.7). It seems that unlike with low frequencies with mechanical vibration, all of high frequencies with acoustic vibration does not show a promising enhancement of proliferation on microalgae. Nevertheless, except for 1000 Hz, other ranges of frequencies still show positive effect on proliferation

When we cultured on liquid culture system under acoustic vibration, the most interesting phenomena was observed. Figure 6.10A shows the micrograph of cultured flasks after 6 days of incubation. When we measured each flasks of optical density at 750 nm, their values are almost similar. However, as shown in figure 6.10A, the colors of cultured cells are quite different. Flasks exposed acoustic vibration appear yellow green color than shaking incubation. Due to this reason, we want to validate what was happened on microalgal cells under sound. We measured intracellular lipid contents using SF44, which is the fluorescence-based molecular probe for analyzing lipid contents with fluorescence spectrometer. Surprisingly, sound boosts intracellular lipid accumulation with their fast proliferation. All ranges of frequencies shows 1.5 to 3.1 times enhanced lipid production after 6 days of incubation (steady state). Especially, 100 Hz shows maximized lipid contents under non-nutrient deprived condition. This results indicates that vibration

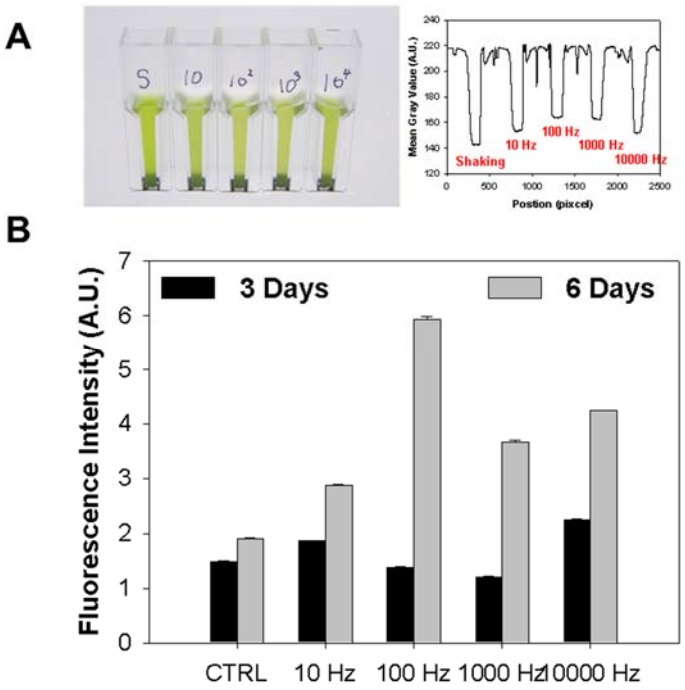

Figure 6.10. Sound effect on intracellular lipid accumulation of *C. reinhardtii*. (A) Micrograph of cultured media and their intensity profile. (B) Quantitative measurement of intracellular lipid contents. The fluorescence intensity of SF44 was monitored with a luminescence spectrometer. All data are expressed as the mean of 5 replicates and a single standard deviation.

boosts proliferation as well as lipid accumulation without any inhibition for growth yield. Conventional strategy for enhancing lipid content in microalgae is only focused on nutrient deprivations. However, they do not consider whole mass of total system with their relative low growth yields. Based on our result, it can serve a new paradigm for dual positive effect on microalgal biodiesel research by considering economics of biodiesel.

6.4 Conclusion

Here we described a vibration effect on *C. reinhardtii*, never discussed. Mechanical vibration enhanced proliferation and we assumed that the cell displacement is the crucial factor for maximizing growth and development. The most interest thing is mechanical vibration boosts proliferation *via* enhanced carbon conversion ability. Although mechanical vibration system cause stress on photosynthetic system, all frequencies enhances growth yield. In cases of sound system, except for 1000 Hz, all frequencies boosts proliferation as well as lipid production.

In this report, we focused and explained cellular responses *via* vibration dynamics. Although we still have a long journey to explore intracellular signal pathway to get an exact mechanism what involves in, we initiate the first step toward realizing economics of biodiesel. Our results presented here confirmed that vibration can be a new method not only for boosting intracellular lipid formation but also for enhancing cell proliferation

in normal condition. To the best our knowledge, it has been never discussed concept for acquiring economics of biodiesel. We hope that our new experimental technique will opened a new paradigm in microalgal biodiesel research. In this report, we only focused *C. reinhardtii*, the most widely studied model microalgae. For the advanced applications of vibration in industrial system, we should explore other green microalgae species to identify their optimal condition for achieving economics of biodiesel.

Chapter 7. Concluding remarks

This thesis describes a whole process for developing microfluidic based microalgal carbon conversion research. The research presents microalgae into microfluidic platform by offering solutions at every limiting steps. First, quantification of lipid contents is required for developing and optimizing microalgal bioprocess engineering. Second, surface immobilization of microalgae is essential for applying microfluidic system. Third, prevention of small hydrophobic molecule absorption on PDMS is necessary for observing intracellular lipid contents at microfluidic system. At the first limiting step, we introduced new fluorescence probes, SF44 and JC-1, for quantifying lipid contents. Each probes allow not only indirect measurement but also tracking for initial stage of lipid accumulation which is impossible to validate their fluorescence intensity. Throughout the result, each probes are sufficiently suitable for applying high-throughput screening system to determine lipid contents. At the second limiting step, we developed a new surface immobilization method for continuous monitoring of microalgae in microfluidic system. Instead of using physical traps or droplets, we took an advantage of high number of Hyp residues present in microalgal cell walls to engage in non-covalent interaction by gelatin coated surface. Throughout the result, immobilization technique with imaging based quantification will allow to better method for opening many possibilities for biodiesel researches. At the

final limiting step, we presented a solution for drawback of PDMS, small molecular absorption, with Teflon coating treatment. We took an advantage of "non-stick" property of Teflon to prevent unwanted absorption of small molecules especially, fluorescence probe. Based on our simple method, imaging of lipid contents in microfluidic platform will lead better method to quantify and monitor lipid content.

Throughout clearing considered limiting issues, we developed a novel microfluidic platform for single cellular imaging based quantitative measurement of *C. reinhardtii*. This platform applied single cell behavior such as cell size and lipid contents under various combinations of nutrients under miniaturized continuous culture system. The results indicate that microalgal carbon conversion trend did not show similar results of conventional flask culture system. We assumed that unlike with bath culture system, there were not any variations of nutrient comes from consumption under continuous culture system. However, in batch culture system, nutrient concentration were constantly variable due to constant consumption from cells without any perfuse of medium. Due to this reason, previous researches only focused on "fully" deprived nutrients, so it could not guarantee promising strategy for economics of biodiesel with their different culture system. Our platform, μ-chemostat, is continuously perfused well defined combinations of nutrients, so it realizes miniaturized continuous culture system as same with mass culture system. We believe that this method could guarantee the most promising optimal condition for achieving economics of biodiesel with identical culture system. From sets of experiments, we concluded that half of nitrogen deprivation is the best

condition for maximizing lipid contents under continuous culture system. We also validated that trend of cell size was almost depended on nitrogen concentration.

We also describes a new method for enhancing microalgal growth and intracellular lipid accumulation using vibration. As previously mentioned, conventional microaglal biodiesel researches are only focused on the nutrient starvation that activates biosynthesis of lipid formation. However, these approaches slow down microalgal growth and development. Although these unfavorable conditions lead high lipid productivity at single cell level, their low growth rate are a major bottleneck considering commercial biodiesel production in the point of view at whole culture system. Due to this reason, we represent new concept for improving economics of biodiesel by realizing high growth rate and lipid productivity.

Here we described a vibration effect on *C. reinhardtii*, never discussed. Mechanical vibration enhanced proliferation and we assumed that the cell displacement is the crucial factor for maximizing growth and development. The most interest thing is mechanical vibration boosts proliferation *via* enhanced carbon conversion ability. Although mechanical vibration system cause stress on photosynthetic system, all frequencies enhances growth yield. In cases of sound system, except for 1000 Hz, all frequencies boosts proliferation as well as lipid production.

Throughout the thesis, we initiated the first step toward biodiesel research using microfluidic platform which ever not tried. We hope that our experimental techniques will opened a new paradigm in biodiesel research as

well as system biology. In this research, we only focused *C. reinhardtii*, the most widely studied model microalgae. For the advanced applications of developed platform in industrial system, we should explore other green microalgae species to identify their optimal condition for achieving economics of biodiesel.

Bibliography

[1] Ehrlich PR, Kareiva PM, Daily GC. Securing natural capital and expanding equity to rescale civilization. Nature. 2012;486:68-73.

[2] Agency IE. Resources to reserves 2013. World Energy outlook 2013. 2013:17-23.

[3] BPstats. BP Statistical Review of World Energy. 2014.

[4] Lashof DA, Ahuja DR. Relative contributions of greenhouse gas emissions to global warming. Nature. 1990;344:529-31.

[5] Houghton JR. The science of climate chang. Climate change 1995. 1996;2.

[6] Chisti Y. Biodiesel from microalgae. Biotechnol Adv. 2007;25:294-306.

[7] Koroneos C, Spachos T, Moussiopoulos N. Exergy analysis of renewable energy sources. Renew Energ. 2003;28:295-310.

[8] Dresselhaus MS, Thomas IL. Alternative energy technologies. Nature. 2001;414:332-7.

[9] Fischer M, Werber M, Schwartz PV. Batteries: Higher energy density than gasoline? Energ Policy. 2009;37:2639-41.

[10] Ma F, Hanna MA. Biodiesel production: a review. Bioresource Technol. 1999;70:1-15.

[11] Leathers HD, Foster P. The world food problem: tackling the causes of undernutrition in the Third World. 2004.

[12] Oswald WJ, Golueke CG. Biological transformation of solar energy. Adv Appl Microbiol. 1960;2:223-62.

[13] Ghirardi ML, Zhang L, Lee JW, Flynn T, Seibert M, Greenbaum E, et al. Microalgae: a green source of renewable H_2. Trends Biotechnol. 2000;18:506-11.

[14] Akkerman I, Janssen M, Rocha J, Wijffels RH. Photobiological hydrogen production: photochemical efficiency and bioreactor design. Int J Hydrogen Energy. 2002;27:1195-208.

[15] Banerjee A, Sharma R, Chisti Y, Banerjee UC. *Botryococcus braunii*: A Renewable Source of Hydrocarbons and Other Chemicals. Cri Rev Biotechnol. 2002;22:245-79.

[16] Melis A. Green alga hydrogen production: progress, challenges and prospects. Int J Hydrogen Energy. 2002;27:1217-28.

[17] Metzger P, Largeau C. *Botryococcus braunii*: a rich source for hydrocarbons and related ether lipids. Appl Microbiol Biotechnol. 2005;66:486-96.

[18] Kay RA, Barton LL. Microalgae as food and supplement. Cri Rev Food Sci Nutr. 1991;30:555-73.

[19] Spolaore P, Joannis-Cassan C, Duran E, Isambert A. Commercial applications of microalgae. J Biosci Bioeng. 2006;101:87-96.

[20] Metting B, Pyne JW. Biologically-active compounds from microalgae. Enzyme Microb Technol. 1986;8:386-94.

[21] Raja R, Hemaiswarya S, Kumar NA, Sridhar S, Rengasamy R. A Perspective on the Biotechnological Potential of Microalgae. Cri Rev Microbiol. 2008;34:77-88.

[22] Schwartz RE, Hirsch CF, Sesin DF, Flor JE, Chartrain M, Fromtling RE,

et al. Pharmaceuticals from cultured algae. J Ind Microbiol. 1990;5.

[23] Shimizu Y. Microalgal metabolites: a new perspective. Annu Rev Microbiol. 1996;50:431-65.

[24] Shimizu Y. Microalgal metabolites. Curr Opin Microbiol. 2003;6:236-43.

[25] Singh S, Kate BN, Banerjee UC. Bioactive Compounds from Cyanobacteria and Microalgae: An Overview. Cri Rev Biotechnol. 2005;25:73-95.

[26] Demirbas A. Importance of Biodiesel as Transportation Fuel. Energ Policy. 2007;35:4661-70.

[27] Walther TC, Jr. RVF. The life of lipid droplets. BBA-Mol Cell Biol L. 2009;1791:459-66.

[28] Ingham CJ, Vlieg JETvH. MEMS and the microbe. Lab Chip. 2008;8:1604-16.

[29] Cookson S, Ostroff N, Pang WL, Volfson D, Hasty J. Monitoring dynamics of single-cell gene expression over multiple cell cycles. Mol Syst Biol. 2005;1:0024.

[30] Ryley J, Pereira-Smith OM. Microfluidics device for single cell gene expression analysis in *Saccharomyces cerevisiae*. Yeast. 2006;23:1065-73.

[31] Paliwal S, Iglesias PA, Campbell K, Hilioti Z, Groisman A, Levchenko A. MAPK-mediated bimodal gene expression and adaptive gradient sensing in yeast. Nature. 2007;446:46-51.

[32] Moore TI, Chou C-S, Nie Q, Jeon NL, Yi T-M. Robust spatial sensing of mating pheromone gradients by yeast cells. PLoS One. 2008;3:e3865.

[33] Lee SS, Vizcarra IA, Huberts DHEW, Lee LP, Heinemann M. Whole

lifespan microscopic observation of budding yeast aging through a microfluidic dissection platform. Proc Natl Acad Sci. 2012;109:4916-20.

[34] Witman GB. *Chlamydomonas* phototaxis. Trends Cell Biol. 1993;3:403-8.

[35] Kim HS, Weiss TL, Devarenne TP, Han A. A high-throughput microfluidic light controlling platform for biofuel producing photosynthetic microalgae analysis. 14th International Conference on Miniaturized Systems for Chemistry and Life Sciences. 2010:295-7.

[36] Merchant SS, Prochnik SE, Vallon O, Harris EH, Karpowicz SJ, Witman GB, et al. The *Chlamydomonas* genome reveals the evolution of key animal and plant functions. Science. 2007;318:245-51.

[37] Dewan A, Kim J, McLean RH, Vanapalli SA, Karim MN. Growth kinetics of microalgae in microfluidic static droplet arrays. Biotechnol Bioeng. 2012;109:2987-96.

[38] Pan J, Stephenson AL, Kazamia E, Huck WTS, Dennis JS, Smith AG, et al. Quantitative tracking of the growth of individual algal cells in microdroplet compartments. Integr Biol. 2011;3:1043-51.

[39] Morimoto Y, Tan W, Tsuda Y, Takeuchi S. Monodisperse semi-permeable microcapsules for continuous observation of cells. Lab Chip. 2009;9:2217-23.

[40] Fukuda H, Kondo A, Noda H. Biodiesel fuel production by transesterification of oils. J Biosci Bioeng. 2001;92:405-16.

[41] Eltgroth ML, Watwood RL, Wolfe GV. Production and cellular localization of neutral long-chain lipids in the haptophyte algae *Isochrysis galbana* and *Emiliania huxleyi*. J Phycol. 2005;41:1000-9.

[42] Monteiro MR, Ambrozin ARP, Lião LM, Ferreira AG. Critical review on analytical methods for biodiesel characterization. Talanta. 2008;77:593-605.

[43] Elsey D, Jameson D, Raleigh B, Cooney MJ. Fluorescent measurement of microalgal neutral lipids. J Microbiol Methods. 2007;68:639-42.

[44] Cooper MS, Hardin WR, Petersen TW, Cattolico RA. Visualizing "green oil" in live algal cells. J Biosci Bioeng. 2010;109:198-201.

[45] Berthier E, Young EWK, Beebe D. Engineers are from PDMS-land, Biologists are from Polystyrenia. Lab Chip. 2012;12:1193-396.

[46] Kim E, Lee S, Park SB. A Seoul-Fluor-based bioprobe for lipid droplets and its application in image-based high throughput screening. Chem Commun. 2012;48:2331-3.

[47] Lee Y, Na SC, Lee S, Jeon NL, Park SB. Optimization of Seoul-Fluor-based Lipid Droplet Bioprobe and its Application in Microalgae for Bio-fuel Study. Mol Biosyst. 2013;9:952-6.

[48] Reers M, Smith TW, Chen LB. J-aggregate formation of a carbocyanine as a quantitative fluorescent indicator of membrane potential. Biochemistry. 1991;30:4480-6.

[49] Smiley ST, Reers M, Mottola-Hartshorn C, Lin M, Chen A, Smith TW, et al. Intracellular heterogeneity in mitochondrial membrane potentials revealed by a J-aggregate-forming lipophilic cation JC-1. Proc Natl Acad Sci USA. 1991;88:3671-5.

[50] Lee J-H, Lee I-H, Choe Y-J, Kang S, Kim HY, Gai W-P, et al. Real-time analysis of amyloid fibril formation of a-synuclein using a fibrillation-

state-specific fluorescent probe of JC-1. Biochem J. 2009;418:311-23.

[51] Wang ZT, Ullrich N, Joo S, Waffenschmidt S, Goodenough U. Algal lipid biodies: Stress induction, Purification, and Biochemical Characterization in Wild-Type and Starchless *Chlamydomonas reinhardtii*. Eukaryot Cell. 2009;8:1856-68.

[52] Bollig K, Lamshöft M, Schweimer K, Marner F-J, Budzikiewicz H, Waffenschmidt S. Structural analysis of linear hydroxyproline-bound O-glycans of *Chlamydomonas reinhardtii*—conservation of the inner core in Chlamydomonas and land plants. Carbohyd Res. 2007;342:2557-66.

[53] Chen W, Zhang C, Song L, Sommerfeld M, Hu Q. A high throughput Nile red method for quantitative measurement of neutral lipids in microalgae. J Microbiol Meth. 2009;77:41-7.

[54] Hell SW. Toward fluorescence nanoscopy. Nature Biotechnology. 2003;21:1347-55.

[55] Bollig K, ft ML, Schweimer K, Marner F-J, Budzikiewicz H, Waffenschmidt S. Structural analysis of linear hydroxyproline-bound O-glycans of *Chlamydomonas reinhardtii*—conservation of the inner core in *Chlamydomonas* and land plants. Carbohyd Res. 2007;342:2557-66.

[56] Stevens PV. Trace bio-organic constituents of gelatins: a review. Food Aust. 1992;44:320-4.

[57] Graham LE, Wilcox LW. Algae: Prentice-Hall, Inc.; 2000.

[58] Weibel DB, Garstecki P, Ryan D, DiLuzio WR, Mayer M, Seto JE, et al. Microoxen: Microorganisms to move microscale loads. Proc Natl Acad Sci. 2005;102:11963-7.

[59] Rhee SW, Taylor AM, Tu CH, Cribbs DH, Cotman CW, Jeon NL. Patterned cell culture inside microfluidic devices. Lab Chip. 2005;5:102-7.

[60] Ramachandran GN, Bansal M, Bhatnagar RS. A hypothesis on the role of hydroxyproline in stabilizing collagen structure. Biochim Biophys Acta. 1973;322:166-71.

[61] Hyams J, Davies DR. The induction and characterisation of cell wall mutants of *Chlamydomonas reinhardii*. Mut Res. 1972;14:381-9.

[62] Kim L, Toh Y-C, Voldman J, Yu H. A practical guide to microfluidic perfusion culture of adherent mammalian cells. Lab Chip. 2007;7:681-94.

[63] Matsumura K, Yagi T, Yasuda K. Role of timer and sizer in regulation of *Chlamydomonas* cell cycle. Biochem Bioph Res Co. 2003;306:1042-9.

[64] Cooper MS, D'Amico LA, Henry CA. Confocal microscopic analysis of morphogenetic movements. Methods Cell Biol. 1999;59:179-204.

[65] Lee SS, Horvath P, Pelet S, Hegemann B, Lee LP, Peter M. Quantitative and dynamic assay of single cell chemotaxis. Integr Biol. 2012;4:381-90.

[66] Breslauer DN, Lee PJ, Lee LP. Microfluidics-based systems biology. Mol BioSyst. 2006;2:97-112.

[67] Keenan TM, Folch A. Biomolecular gradients in cell culture systems. Lab Chip. 2008;8:34-57.

[68] Kim S, Kim HJ, Jeon NL. Biological applications of microfluidic gradient devices. Integr Biol. 2010;2:584-603.

[69] Sasaki H, Onoe H, Osaki T, Kawano R, Takeuchi S. Parylene-coating in PDMS microfluidic channels prevents the absorption of fluorescent dyes.

Sensor Actuat B- Chem. 2010;150:478-82.

[70] Ren K, Zhao Y, Su J, Ryan D, Wu H. Convenient Method for Modifying Poly(dimethylsiloxane) To Be Airtight and Resistive against Absorption of Small Molecules. Anal Chem. 2010;82:5965-71.

[71] Mays RL, Dickey MD, Genzer J. Microfluidic channels fabricated from poly(vinylmethylsiloxane) networks that resist swelling by organic solvents. Lab Chip. 2013;13:4317-20.

[72] Ren K, Dai W, Zhou J, Su J, Wu H. Whole-Teflon microfluidic chips. Proc Natl Acad Sci USA. 2011;108:8162-6.

[73] Unger MA, Chou HP, Thorsen T, Scherer A, Quake SR. Monolithic microfabricated valves and pumps by multilayer soft lithography. Science. 2000;288:113-6.

[74] Johnson ID, Kang HC, Haugland RP. Fluorescent membrane probes incorporating dipyrrometheneboron difluoride fluorophores. Anal Chem. 1991;198:228-37.

[75] Wang J, Ren L, Li L, Liu W, Zhou J, Yu W, et al. Microfluidics: A new cosset for neurobiology. Lab Chip. 2009;9:644-52.

[76] Whitesides GM. The origins and the future of microfluidics. Nature. 2006;442:368-73.

[77] Jr. RVF, Walther TC. Lipid Droplets Finally Get a Little R-E-S-P-E-C-T. Cell. 2009;139:855-60.

[78] Grima EM, Belarbi E-H, Fernández FGA, Medina AR, Chisti Y. Recovery of microalgal biomass and metabolites: process options and economics. Biotechnol Adv. 2003;20:491-515.

[79] Grima EM, Sevilla JMF, Fernández FGA. Microalgae, mass culture methods: Wiley; 1999.

[80] Fernández FGA, Camacho FG, Chisti Y. Photobioreactors: light regime, mass transfer, and scaleup: Wiley; 1999.

[81] Molina E, Fernández FGA, Camacho FG, Rubio FC, Chisti Y. Scale-up of tubular photobioreactors. J Appl Phycol. 2000;12:355-68.

[82] Molina E, Fernández J, Acién FG, Chisti Y. Tubular photobioreactor design for algal cultures. J Biotechnol. 2001;92:113-31.

[83] Roessler PG, Brown LM, Dunahay TG, Heacox DA, Jarvis EE, Schneider JC, et al. Genetic Engineering Approaches for Enhanced Production of Biodiesel Fuel from Microalgae. Enzymatic Conversion of Biomass for Fuels Production: American Chemical Society; 1994. p. 255-70.

[84] Dunahay TG, Jarvis EE, Dais SS, Roessler PG. Manipulation of Microalgal Lipid Production Using Genetic Engineering. In: Wyman C, Davison B, editors. Seventeenth Symposium on Biotechnology for Fuels and Chemicals: Humana Press; 1996. p. 223-31.

[85] Radakovits R, Jinkerson RE, Darzins A, Posewitz MC. Genetic engineering of algae for enhanced biofuel production. Eukaryot Cell. 2010;9:486-501.

[86] Sharma KK, Schuhmann H, Schenk PM. High lipid induction in microalgae for biodiesel production. Energies. 2012;5:1532-53.

[87] Titmarsh D, Cooper-White J. Microbioreactor Array for Full-Factorial Analysis of Provision of Multiple Soluble Factors in Cellular Microenvironments. Biotechnol Bioeng. 2009;104:1240-4.

[88] Wang L, Liu W, Wang Y, Wang J, Tu Q, Liu R, et al. Construction of oxygen and chemical concentration gradients in a single microfluidic device for studying tumor cell–drug interactions in a dynamic hypoxia microenvironment. Lab Chip. 2013;13:695-705.

[89] Jeon NL, Dertinger SKW, Chiu DT, Choi IS, Stroock AD, Whitesides GM. Generation of solution and surface gradients using microfluidic systems. Langmuir. 2000;16:8311-6.

[90] Park J, Wu J, Polymenis M, Han A. Microchemostat array with small-volume fraction replenishment for steady-state microbial culture. Lab Chip. 2013;13:4217-24.

[91] Lien T, Knutsen G. Synchronous growth of *Chlamydomonas reinhardtii* (*Chlorophyceae*): a review of optimal conditions. J Phycol. 1979;15:191-200.

[92] Jaalouk DE, Lammerding J. Mechanotransduction gone awry. Nat Rev Mol Cell Bio. 2009;10:63-73.

[93] Wang N, Butler JP, Ingber DE. Mechanotransduction across the cell surface and through the cytoskeleton. Science. 1993;260:1124-7.

[94] Lee CH, Shin HJ, Cho IH, Kang Y-M, Kim. IA, Park K-D, et al. Nanofiber alignment and direction of mechanical strain affect the ECM production of human ACL fibroblast. Biomaterials. 2005;26:1261-70.

[95] Wang Y, Maciejewski BS, Soto-Reyes D, Lee H-S, Warburton D, Sanchez-Esteban J. Mechanical stretch promotes fetal type II epithelial cell differentiation via shedding of HB-EGF and TGF-α. J Physiol. 2009;587:1739-53.

[96] Han M-J, Seo Y-K, Yoon H-H, Song K-Y, Park J-K. Effect of mechanical tension on the human dental pulp cells. Biotechnol Bioprocess Eng. 2008;13:410-7.

[97] Matheson LA, Maksym GN, Santerre JP, Labow RS. Differential effects of uniaxial and biaxial strain on U937 macrophage-like cell morphology: Influence of extracellular matrix type proteins. J Biomed Mater Res A. 2007;81A:971-81.

[98] Sambajon VV, Jr. JEC, Gassner RJ, Buckley MJ. The effects of mechanical strain on synovial fibroblasts. J Oral Maxil Surg. 2003;61:707-12.

[99] Judex S, S.Gupta, Rubin C. Regulation of mechanical signals in bone. Orthod Craniofac Res. 2009;23:94-104.

[100] Liao X, Lu S, Zhuo Y, Winter C, Xu W, Li B, et al. Bone Physiology, Biomaterial and the Effect of Mechanical/Physical Microenvironment on Mesenchymal Stem Cell Osteogenesis. Cell Mol Bioeng. 2011;4:579-90.

[101] Nava MM, Raimondi MT, Pietrabissa R. Controlling Self-Renewal and Differentiation of Stem Cells via Mechanical Cues. J Biomed Biotechnol. 2012;2012:12.

[102] Riehl BD, Park J-H, Kwon IK, Lim JY. Mechanical Stretching for Tissue Engineering: Two-Dimensional and Three-Dimensional Constructs. Tissue Eng Part B. 2012;18:288-300.

[103] Su FC, Wu C-C, Chien S. Review: roles of microenvironment and mechanical forces in cell and tissue remodeling. J Med Biol Eng. 2011;31:233-44.

초 록

본 논문에서는 미세조류의 생물학적 탄소전환 연구에 있어서 새로 방식의 미세유체 기반 연구에 대해서 설명한다. 미세유체 기술은 시공간적으로 제어된 세포 주변의 미세환경의 제어를 가능하게 하며, 이러한 이유로 항상 생물학자들의 관심을 받아왔다. 이러한 시스템은 층류와 확산 현상을 장점으로 하여 농도 구배, 영양조건 그리고 물리화학적 영향을 포함하는 생물 관련 자극을 형성할 수 있다. 게다가, 미세유체 기술은 그 작은 부피와 고속분석을 기반으로 하는 새로운 패러다임을 제시한다. 그러나 불행하게도, 미세조류를 미세유체 시스템에 적용하기 위해서는 몇 가지 고려할 사항이 존재한다. 본 연구에서는 미세조류를 미세유체 플랫폼에 적용하기 위한 몇 가지 제한된 사항에 대해서 해결책을 제시한다. 첫째, 미세조류에 있어서 생물 공정을 최적화 하거나 개발함에 있어서 주요 탄소 전환 물질로 알려진 지질의 정량화가 필요하다. 본 논문에서는 지질을 염색하기 위한 새로운 형광 표지자로서 SF44와 JC-1을 제시한다. 우리는 질소친화적인 형광 표지자가 지질과 특이적인 결합을 보이는 것을 확인 하였으며, 세포 도입에 있어서 물리화학적인 조건을 변화하면서 최적의 도입 조건을 찾아내었다. 형광분광계를

이용하여 *Chlamydomonas reinhardtii*에서의 지질 생성 동력학의 정량적 측정을 위한 실험 방식을 개발하였으며, 이는 전자현미경을 통한 지질 크기 측정법과의 비교 분석을 통해서 확인하였다. 둘째, 동물 세포와는 다르게, 미세조류 연구에 있어서 그들의 상대적으로 작은 크기와 운동성은 미세유체 시스템으로의 적용에 제한사항으로 작용한다. 이에, 우리는 젤라틴을 생물학적 접착제로 사용하여 단순한 방식으로 미세조류를 고정화 하는 방식을 제시한다. 우리는 6일 동안 세포를 지속적으로 모니터링을 하였다. 표면 고정화 기법은 고해상도 및 세포 분열에 대한 실시간 세포 이미징을 가능하게 하였으며, 세포배양에 따른 지질 축적 관찰을 가능하게 하였다. 셋째, 미세유체 시스템을 구성하는 주요 물질인 PDMS는 소수성 형광 표지자의 흡착에 다른 세포 이미징 및 처리가 어려운 점이 존재한다. 이에, 우리는 테플론 코팅을 사용하는 새로운 방법을 통하여 PDMS에서 원하지 않는 소수성 분자의 흡착을 방지하는 방법을 제시한다.

제한된 사항의 해결을 종합하여, 우리는 이전에 논의 되지 않았던 바이오 디젤의 경제성을 달성하기 위한 가장 유망한 방법을 찾는 새로운 패러다임을 제안한다. 소형화된 연속 배양 시스템을 기반으로 하여, 우리는 단일 세포의 거동을 측정하기 위한 다양한 탄소와 질소원의 조합을 생성해 내었다. 연속 배양 시스템 하에서의 연구 결과는 이전의 플라스크 배양조건에서의 결과와 다른 경향을

보여주었다. 연구 결과를 종합하면, 세포 크기는 질소 농도에 영향 받을 뿐 아니라, 정상 배양 조건 대비 절반의 질소 농도에서 극대화 된 세포 내 지질 생성이 이루어졌다. 특히, 대량 연속 배양 공정에 있어 바이오 디젤의 경제성을 고려한다면, 절반의 질소 농도가 좋음을 알 수 있었다. 우리는 개발된 플랫폼이 고속 분석과 생물 관련 자극의 도움을 통해서 바이오 디젤 연구에서뿐만 아니라 시스템 생물학에 있어서 유용한 도구로서 적용하리라 판단한다.

본 논문에서는 또한 진동을 이용하여 미세조류의 생장과 세포 내 지질 생성을 촉진하는 새로운 방법을 제안한다. 이전에 논의한 것처럼, 기존의 미세조류 유래 바이오디젤 연구는 지질 생합성을 촉진하는 영양분의 결핍을 통해서만 이루어져 왔다. 그러나 이러한 방법은 미세조류의 생장과 발달을 저해한다. 비록 단일 세포 수준에서는 제한된 생장 조건하에서 높은 지질 생산성을 보여주나, 그들의 낮은 생장률은 전체 배양 시스템의 관점에서 보자면 바이오디젤의 상업화에 있어서 병목으로 작용한다. 이러한 이유에 기인하여, 우리는 바이오디젤의 경제성을 향상시키기 위한 일환으로 높은 생장률과 지질 생산을 구현하는 새로운 개념을 제시한다.

*Chlamydomonas reinhardtii*를 기계적 진동과 소리를 이용하여 다양한 주파수에서 처리하였다. 기계적 진동은 세포 생장을 촉진하였고 이는 세포의 변위가 주요인자로 작용하였다고 생각한다. 흥미

로운 점은, 기계적 진동이 탄소전환을 통한 생장을 촉진하는 것을 확인하였다. 비록 기계진동이 광합성 시스템에 스트레스를 주었음에도 불구하고, 전 주파수 대역에서 세포생장이 촉진되었다. 소리의 경우에는 1000 Hz를 제외하고 모든 주파수 대역에서 세포의 생장을 촉진하였을 뿐 아니라, 지질의 합성도 증가하였다. 이러한 결과는 진동이 세포 내 지질 합성을 가속화할 뿐만 아니라 정상 배양 조건 하 에서 세포 생장도 촉진하였음을 확인하였다. 우리는 이러한 배양 조건이 미세조류를 이용한 바이오디젤 생산에 있어서 적합한 배양 조건이 되길 희망한다.

주요어: 미세조류, 바이오디젤, 미세유체, 고속분석, 미세키모스탯, 진동
학 번: 2009-31246